Addis Ababa University
School of Graduate Studies
Institute of Technology
Department of Civil and Environmental Engineering

Actual evapotranspiration estimation using remotely sensed data and hydrological model: a case study of Gilgelabay catchment

Genet Abdi
2015

Actual evapotranspiration estimation using remotely sensed data and hydrological model: a case study of Gilgelabay catchment

Genet Abdi Tolla

A thesis submitted to School of Graduate Studies, Addis Ababa University in partial fulfillment of the Requirements for the Degree of Masters of Science in Civil and Environmental Engineering

July 2015

Actual evapotranspiration estimation using remotely sensed data and hydrological model: a case study of Gilgelabay catchment

Thesis submitted to School of Graduate Studies, Addis Ababa Institute of Technology for partial fulfillment of requirements for the Degree of Masters of Science in Civil Engineering (Hydraulics Engineering)

Genet Abdi Tolla

APPROVED BY BOARD OF EXAMINERS

Name	Signature	Date
1. Dr. Daniel F/Selasie (External Examiner)	_____	/___/___/_____/
2. Dr. Yenesew Mengiste (Internal Examiner)	_____	/___/___/_____/
3. Dr.Ing Dereje Hailu (Advisor)	_____	/___/___/_____/
4. Dr. Esayas G/Yohannes (Chairman)	_____	/___/___/_____/

Acknowledgments

I praise and thank God, the Almighty for giving me this opportunity and the power to complete this research work successfully.

Very Special thanks go to the Ethiopian National Meteorology Agency and the Ministry of Water Resources Hydrology department for their cooperation in providing me with the necessary data for this research work.

I would like to extend my sincere gratitude to my advisor Dr. Ing. Dereje Hailu for his patience, understanding and valuable comments which helped me to organize the thesis and prepare myself how to answer the questions that will be raised.

I would like to express my deepest gratitude to my co-advisor Phd candidate Mr. Yared Ashenafi Bayissa, whose expertise, understanding and advice greatly broaden my knowledge. He devoted his time to guide, assist and encourage me in the process of the research work. During these times, I have learnt a lot from him which includes how to analyze problems that leads to solutions, to cite one, how to run different models. Above all without his unreserved assistance, this research work would not have been completed. I owe my deepest gratitude to him. Furthermore, I would like to thank my friends and colleague for their valuable suggestions and help.

Last but not least, I wish to express my deepest gratitude to all my family members for their continuous support and encouragement in the course of this research work.

Genet Abdi

Table of contents

List of figures

List of tables

Appendices

Appendix 1	Python script for converting MODIS HDF data to raster and PCRaster formats
Appendix 2	Python script for running the SEBS model
Appendix 3	Weather Generator Parameter

List of Acronyms

ABL	Atmospheric Boundary Layer
CCLM	COSMO-Climate Limited Area Modelling
BCEOM	Le Bureau Central d'Etudes pour les Equip ements d'Outre-Mer
CGIAR	Consultative Group on International Agricultural Research
COSMO	Consortium for Small-scale Modelling
csf	content sealed format
CSI	Consortium for Spatial Information
DEM	Digital Elevation Model
DOY	Day of the year
ECMWF	European Center for Medium Range Weather Forecasting
EOS	Earth Observation System
ET	Evapotranspiration
GDAL	Geospatial Data Abstraction Library
GeoFiff	Geographical Tag Image Format
GMT	Greenwich Mean Time
GUI	Graphical User Interface
HDF-EOS	Hierarchical Data Format-Earth Observing System
HRU	Homogeneous Hydrological Response Units
IDW	Inverse Distance Weighting
ITCZ	Inter-Tropical Convergence Zone
LAI	Leaf Area Index
LPDAAC	Land Processes Distributed Active Archive Center
LST	Land Surface Temperature
masl	Meters above sea level
MODIS	Moderate Imaginary Spectroradiometer
MSG	Meteosat Second Generation
NASA	National Aeronautics and Space Administration
NDVI	Normalized Difference Vegetation Index
NMA	National Meteorological Agency
NTSG	Numerical Terradynamic Simulation Group
POTRAD	Potential Radiation Model
SEBS	Surface Energy Balance System
SEBAL	Surface Energy Balance Algorithm for Land
SMEC	Snowy Mountains Engineering Corporation
SLURP	Semi distributed Land Use based Runoff Process
SRTM	Shuttle Radar Topography Mission
SWAP	Soil, Water, Atmosphere, Plant
SWAT	Soil and Water Assessment Tool
TOA	Top of the Atmosphere
UTC	Coordinated Universal Time
UTM	Universal Time Mercator
WGS	World Geodetic System

ABSTRACT

In order to get reliable qualitative and quantitative information about a potential of water resource in a catchment it is important to assess and evaluate the spatial and temporal variation of actual evapotranspiration by applying SEBS algorithm and SWAT hydrological model and eventually compare with MODIS ET. This is one of the motivations for evaluating the spatial and seasonal dynamics of actual ET for the Gilgel Abay catchment using energy balance algorithm and hydrological model.

Spatially distributed actual evapotranspiration (ETa) values were estimated using Surface Energy Balance System (SEBS) approach and the Soil and Water Assessment Tool (SWAT). The input data for SEBS and SWAT were acquired from different sources with different spatial and temporal resolutions. The dynamics of ETa was assessed only for the selected dry years (2009) and wet year (2005 and 2007). Moreover, the analysis was based on the nine selected days of those years having a cloud cover less than 30%. The estimated ETa values were also compared with MOD16 ET at sub-catchment scale.

SEBS based estimated daily actual ET eventually were compared with MODIS ET and SWAT actual ET estimates to assess the temporal and spatial variability in the catchment. The result showed that the mean value of SEBS daily actual ET during those days reached up to 5.9 mm/d (Jan-01-2005), 5.5mm/d (January 10, 2007) and 5.1 mm/d (March 12, 2007). In distinction as it observed from the results during wet season days the SEBS estimated actual ET is relatively lower and highly variable spatially. The mean actual ET for day of the year [DOY] 253- 2009 is 8.8 mm/d, DOY 336 - 2007 is 5.8 mm/d and DOY 330- 2009 5.1 mm/d which shows the spatial variability resulted due to heterogeneity of the vegetation cover during the wet season. Similarly, the long-term mean annual actual ET derived from previous hydrological studies using SWAT compared well with MODIS ET over the terrestrial part of the catchment. The evaluation of the wet season actual ET from 2000-2010 from MODIS and SEBS was compared with SWAT and the result showed that a good correlation. Thus, overall MODIS ET product showed good agreement with results from the SWAT models both in magnitude and spatial variability

Key words: Gilgel Abay, ET, ETa, Remote Sensing, MODIS, SEBS and SWAT

1. Introduction

1.1 Background

The distribution of water resource on earth is quite wide-ranging where many locations have abundance while others have very little. Water exists on earth as solid (ice), liquid or gas (water vapor) in oceans, rivers, clouds and rain, all of which are in a frequent state of change (surface water evaporates, cloud water precipitates, rainfall infiltrates the ground, etc.). However, the total amount of the earth's water does not change (*Chow et al., 1988*). Water covers 70% of the earth's surface, but most water resources available for human consumption and the ecosystem are contained in lakes and rivers.

The transfer of liquid water from soil to vapor in the atmosphere (Evapotranspiration) is one of the most profound and consequential processes on Earth. Evapotranspiration is the second largest term in the terrestrial water budget after precipitation. Evapotranspiration (ET), along with evaporation from open water, supplies vapor to the atmosphere to replace that condensed as precipitation. Thus, information on the spatial distribution of actual evapotranspiration (ETa) is crucial for water management in river basins. Thus, accurate estimation of global evapotranspiration is considered to be of great importance due to its key role in the terrestrial and atmospheric water budget. Also a comprehensive understanding on the spatial and seasonal dynamics of actual ET is important with regard to water resources planning, development and management in a river basin.

Given the heterogeneity of the landscape and the large number of complex controlling factors, including climate, plant biophysics, soil properties, and topography, the precise estimation of actual ET is one of the most problematic components of the water cycle (Bastiaanssen et al. 1998; Mu et al. 2007). Estimation of evapotranspiration by using satellite remote sensing technique has become popular and is applied to various places. ET is also an important component in surface energy balance which has a significant effect on the water balance of catchment. Nowadays remote sensing is probably the only feasible means of projecting ET over large scale area. Satellite sensors with different spatial and temporal resolution for the observation of the atmospheric and hydrologic parameters are available and are used for the estimation of ET. Remote sensing is a tool providing advanced ways of retrieving data and

information and enabling spatial, 'grid based', analysis techniques. Satellite sensors with different spatial and temporal resolution for the observation of atmospheric and hydrological variables are used for the estimation of actual ET. In addition, Kalma et al. (2008) mentioned the advantage of using remote sensing to monitor the land surface temperature and reflectivity (using different spectral regions) in connection with its ability to spatially integrate over heterogeneous surfaces at a range of resolutions.

The SEBS (Surface Energy Balance models) compute the latent heat flux by evaluating the net radiation, soil heat flux and sensible heat flux and solve for latent heat flux as the residual term from the surface energy budget. The key issue of this approach is to estimate accurately the sensible heat flux, as estimation (or measurement) of net radiation and soil heat flux is considered relatively easy (Kalma et al. 2008; Su 2002). Li et al. (2009) mentioned that energy balance models are theoretically verified and physically based and require less ground-based measurements.

The SEBS algorithm which was implemented in the PCRaster Python library by Van der Kwast (2009) were modified and adapted to this study area. Additionally Soil and Water Assessment Tool (SWAT) hydrological model using the required data will be used to estimate the actual ET and the result will be compared with MODIS ET .Thus, this study intends to assess the spatial and seasonal dynamics of actual ET for the Gilgel Abay catchment using actual ET derived from different sources.

1.2 Problem Statement

Due to the lack of basic understanding of the spatial and temporal variability of hydrological parameters, water resource management is becoming a major challenge in most countries. Enhanced understanding on the hydrological cycle components such as the spatial and seasonal characteristics of actual ET for the Gilgelabay catchment has a huge importance in order to assess the water resource potential in the surrounding. Furthermore, this catchment is the headwater of the Nile River, which is shared by a number of countries and sustains the livelihoods of many people.

In this aspect, quantification of the components of hydrologic cycle is vital. ET is one of the most important hydrologic components in several respects; the difference between precipitation and evapotranspiration over the long term is the water available for direct use (Dingman, 2002). Despite of its significance, ET is often treated as a lumped residual flux from the hydrologic budget, or estimated indirectly from local weather station data, which has a lack of uniformity in the quality and distribution of weather and flow observation points. In areas with heterogeneous vegetation cover like cropland, grassland, forests and other kind of plant species may coexist naturally within $1km^2$. Each vegetation species will have its own physiological nature.

However, actual ET estimation at field and river basin scale is constrained by data availability. The use of remote sensing is the recent development to resolve the challenge of the spatial distribution. Its capability of observing a number of physical characteristics of the earth's surface has been found useful for the parameterization of models for regional ET estimation using this technique (Peters, 1995).

Thus, an effort to quantify and assess the spatial and temporal variability of the actual ET flux is important information for water management in the current and future situations. Thus, for this thesis actual ET estimates will be obtained from the following:

- Estimates of actual ET by hydrological SWAT model for Gilgelabay catchment using meteorological data from 1998- 2010.
- The MODIS terrestrial ET was acquired for various temporal resolutions from Numerical Terra dynamic Simulation Group (NTSG), University of Montana (NTSG 2012)

In addition to these, the SEBS algorithm (Su 2002) will be used for daily actual ET estimations at a relatively higher spatial resolution compared to the hydrological and regional climate models. SEBS was selected because it:

i) minimizes the uncertainty from input data, such as the radiance surface temperature and ground meteorological variables by considering the energy balance at the limiting cases;
ii) computes explicitly the roughness height for heat transfer instead of using fixed values;
iii) is an open source algorithm which makes it easy to adapt.

Basically, this approach is based on the principle of the surface energy balance, which dictates the partition of the surface turbulent fluxes into latent and sensible heat flux in

the soil-vegetation-atmosphere continuum. Su (2002) showed the potential and reliability of SEBS to evaluate actual ET at various temporal and spatial scales.

Overall, the purpose of this thesis research is to thoroughly assess the temporal and spatial variation of actual ET in the terrestrial part of the Gilgelabay catchment using estimates from the processed based SEBS, MODIS ET product and actual ET outputs of SWAT hydrological model.

1.3 Objective of the Study

The objective of this study is to assess and evaluate the spatial and temporal variation of actual evapotranspiration by applying SEBS algorithm and SWAT hydrological model and eventually compare with MODIS ET.

1.3.1 Specific Objective

I. To estimate daily actual ET for number of cloud free represented days in the dry and wet seasons of year 2005, 2007 and 2009
II. To evaluate and compare qualitatively the SEBS daily actual ET estimate and MODIS 8 days aggregated actual ET products for the selected dry and wet season days.
III. To model the catchment using the SWAT hydrological model and to estimate the daily actual ET.
IV. To compare SEBS daily actual ET estimate with SWAT hydrological model at Gilgel Abay catchment.
V. To compare mean annual actual ET resulted from SEBS, SWAT hydrological model and MODIS ET of the catchment

Research questions

- How is the spatial and temporal variation of daily ET in the study area?
- Is there significant difference in the result of ET using SEBS and MODIS ET MOD16A2?
- Is there significant difference in the result of ET using SEBS and SWAT models?
- Can SEBS accurately estimate the daily actual ET for Gilgelabay Catchment for the selected days in the wet and dry seasons?
- Could SEBS daily actual ET estimates compare well with SWAT model estimates?

1.4 Organization of the Thesis

The content of the thesis is outlined briefly in this section as follows:

Chapter 1**:** includes general introduction, problem statement and objective of the study. It raises a research question which the research tries to answer with the available data and methodology applied.

Chapter 2: presents general literature reviews mainly focusing on remote sensing approaches for actual ET estimation and description of the SEBS algorithm and a brief introduction about SWAT hydrological model are presented.

Chapter 3: gives description of the study area based on topographic, climate and land use information.

Chapter 4: describes in detail the materials that have been used for the daily actual ET estimation using SEBS as well as the secondary actual ET data obtained from various sources for Gilgel Abay catchment.

Chapter 5: presents detailed description of all the methodologies that have been set for the research work in addition it explains about the pre-processing of the images including preliminary assessment of the acquired images.

Chapter 6: will illustrate the analysis and discuss the result of actual evapotranspiration estimation using different methods. It includes the output map of spatially distributed ET of the study area.

Chapter 7: Conclusion and recommendations will be mentioned.

2. Literature Review

2.1 Concept of Evapotranspiration

In order to properly state the available water resource potential of a certain river basin it is first essential to determine the amount of water available in that system. Accordingly, it requires the understanding of the hydro-system and its interaction with the environment and to be able to properly describe the water flow, 'in and out', of the basin. Information and data regarding the basin such as runoff, evaporation and rainfall, for example, are some of the components that would be necessary in describing the water movement or circulation. A scientific approach to that is to carry out a hydrologic analysis of the basin.

Evapotranspiration is a portion of the hydrologic cycle that is derived from the summation of the evaporation and transpiration from a vegetated surface. Evaporation consists of any water that is returned to the atmosphere from the soil surface, depression storage, or intercepted storage and Transpiration consists of any water that leaves through the vegetated surface via plant stomata.

In practice, evaporation and transpiration are combined into one term: evapotranspiration (ET), because of both evaporation and transpiration occur simultaneously and there difficulty in distinguishing between the two processes.

Evaporation from soil surfaces makes up a significant portion of the total ET occurring from a given land surface. The process of evaporation requires energy and is the process of changing the state of liquid water to a gaseous state. The amount of evaporation occurring from a land surface or water body is governed mainly by the amount of energy available at the surface to facilitate the change of state coupled with ability of the surrounding air to transfer the wet air to the atmosphere. Actual ET and related processes are responsible for 70 percent of the lateral global energy transport through latent heat, and therefore play an important role in the redistribution of water on the Earth's surface (Mauser and Schädlich 1998).

2.2 Method of Estimating Evapotranspiration

Accurate knowledge of temporal and spatial variations in precipitation and ET is critical for improved understanding of the interactions between land surfaces and the atmosphere (Mu et al., 2007), and owing to increasing human consumption, climate impacts and decreasing availability, methods for monitoring the water balance at both fine and regional scales are important in order

to preserve and manage water resources (Melesse et al., 2006). However, precipitation and ET are the most problematic components of the water cycle to estimate accurately because of the heterogeneity of the landscape and the large number of controlling factors involved, including climate, plant biophysics, soil properties, and topography (Mu et al., 2007).

ET can be measured or estimated using empirical formulae from taking measurements in the field or more indirectly rather than as a result of a specific evapotranspiration experiment.

Therefore, a qualitative understanding of evapotranspiration has a great importance in water balance study of the river basin in such a way that in a longer period of time the difference between precipitation and evapotranspiration is the available water for use and most of the food supply is grown in irrigated lands and knowledge of actual ET help on the use of efficient water without loss required for the plant growth.

There exist several methods for estimating ET, among these methods:

1. Direct Measurement

   The classical direct measurement techniques include Pan-measurement, Bowen ratio, eddy correlation system, and weighing lysi-meter and scintillo-meter. These methods are mainly based on site(field) measurements and are costly, time consuming, and require elaborate and sensitive instrumentations and are insufficient to measure characteristics of heterogeneous surfaces (Jia et al. 2009).
2. Water Balance and Hydrologic Modeling

   The modeling method includes water balance model and hydrological models such as SWAP, SLURP and SWAT which simulate the transformation of precipitation into stream flow taking into account all the intermediate process such as evapotranspiration, interception, infiltration, runoff and ground water flow including all the artificial effect of dams, reservoirs, diversions and irrigation schemes. All these methods have some limitation and strength.
3. Remote Sensing

   Unlike point estimates, spatial ET mapping at various scales has been conducted using thermal infrared imageries (Anderson et al. 2011; Jia et al. 2009; Mu et al. 2007; Mu et al. 2011). Li et al.(2009) outlined the advantages of remote sensing techniques for ET

estimation over the conventional "point" measurements as: i) provision of large and continuous spatial coverage within a few minutes; ii) less costs when the same spatial information is required; iii) applicability in un-gauged areas where man-made measurements are difficult to conduct or unavailable. Thus, for this study using Remote Sensing technique and SWAT hydrologic modeling will be used.

2.3 Remote Sensing Technique

Concept of Remote Sensing

Remote sensing is the science and art of obtaining information about an object, area or phenomena that is not in contact with the object, area or phenomena under investigation (S.Kumar, 2005). It can be useful to a hydrologist in terms of providing advanced ways of retrieving data and information and enabling spatial analysis techniques.

Remote Sensing can be defined as the science and technology by which the characteristics of objects of interest can be identified, measured or analyzed through the information obtained by a device that records reflected, emitted, or diffracted electromagnetic energy without direct contact.

Remote-sensing systems, mainly the once deployed on satellites, provide a continuous and consistent view of Earth transmitting the information to ground station facilitating the ability to monitor Land surface and the atmosphere surrounding the earth.

In much of remote sensing, the process involves an interaction between incident radiation and the targets of interest. This is exemplified by the use of imaging systems where the following seven elements are involved.

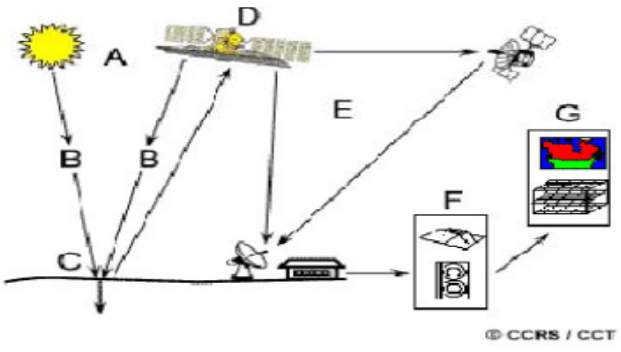

Figure 2-1: Process that illustrate Remote Sensing

1. Energy Source or Illumination (A) – the first requirement for remote sensing is to have an energy source which illuminates or provides electromagnetic energy to the target of interest.
2. Radiation and the Atmosphere (B) – as the energy travels from its source to the target, it will come in contact with and interact with the atmosphere it passes through. This interaction may take place a second time as the energy travels from the target to the sensor.
3. Interaction with the Target (C) - once the energy makes its way to the target through the atmosphere, it interacts with the target depending on the properties of both the target and the radiation.
4. Recording of Energy by the Sensor (D) - after the energy has been scattered by, or emitted from the target, we require a sensor (remote - not in contact with the target) to collect and record the electromagnetic radiation.
5. Transmission, Reception, and Processing (E) - the energy recorded by the sensor has to be transmitted, often in electronic form, to a receiving and processing station where the data are processed into an image (hardcopy and/or digital).
6. Interpretation and Analysis (F) - the processed image is interpreted, visually and/or digitally or electronically, to extract information about the target that was illuminated.
7. Application (G) - the final element of the remote sensing process is achieved when we apply the information we have been able to extract from the imagery about the target in order to better understand it, reveal some new information, or assist in solving a particular problem.

Nowadays many researchers have been done to derive spatially distributed evapotranspiration over large scale using surface energy balance and remote sensing data. This technique provides spatial information from the earth's surface by measuring reflected and emitted electromagnetic radiation. The measurements of thermal infrared, infrared and visible band or remote sensing data are inputs for the parameterization of the energy balance component of ET estimation. It has

an advantage of measuring repeatedly the same area with large coverage and on a pixel based discreitization.

2.4 MODIS land surface products

MODIS (Moderate Resolution Imaging Spectroradiometer) is one of the five scientific instruments onboard the satellite platform Terra, part of NASA's Earth Observation System (EOS)(detail of the instruments are listed in Table 2.1). It was launched on December 18, 1999 and began collecting data on February 24, 2000 (NASA 2012). These satellites provide unprecedented information regarding vegetation and surface energy (Justice et al. 2002). These are essential for actual ET estimation in near real time basis for regional and global scale applications. Its detectors measure 36 spectral bands and it acquires data at three spatial resolutions: 250 m, 500 m, and 1,000 m with almost daily coverage of the entire earth (LPDAAC 2012). MODIS provide a variety of land surface products with different levels of processing such as land surface temperature, reflectance, and vegetation indices, LAI and actual ET, among others (Table 2-1).

Table 2-1: List of MODIS land surface products pertinent to this study

MODIS product	Product Name	Temporal Resolution	Spatial resolution	Parameter derived
MOD09A1	Land surface reflectance	8 days	500m	Broadband Albedo
MOD11A1	Land surface temperature	Daily	1000m	Radiance Temperature
MOD13A1	Vegetation Index(NDVI)	16 days	500m	Emissivity, LAI, canopy height
MOD16A2	Terrestrial evapotranspiration	8 days & monthly	1000m	Evapotranspiration

MODIS global evapotranspiration products by Mu et al. (2011) are the first regular 1 km^2 land surface ET dataset for 109.03 Million km^2 global vegetated land area at an 8 day interval (NTSG 2012). The development of this global evapotranspiration algorithm is based on MODIS and global meteorology data using the Penman–Monteith logic (Mu et al. 2011).

2.5 The Surface Energy Balance System

The Surface Energy Balance System (SEBS) is a single-source model, which estimates atmospheric turbulent fluxes and surface evaporative fraction from remote sensing data. It is available as part of the free open-source software. It is proposed by Su (2002) for the estimation of atmospheric turbulent fluxes and evaporative fractions using satellite earth observation data, in combination with meteorological information.

The satellite remote sensing approach for estimation of actual ET is an alternative and only feasible means for projecting actual ET over large scale area and is important to account the spatial variability and heterogeneity in the area.

Therefore, single-source schemes are more widely utilized for operational monitoring and forecasting (Timmermans et al., 2005a). In the current setup SEBS requires three sets of input data:

- Products derived from remote sensing data: albedo, emissivity, temperature and the Normalized Difference Vegetation Index (NDVI) to derive local surface roughness parameters;
- Meteorological parameters collected at a reference height (air pressure, temperature, relative humidity, wind speed);
- Radiation data (downward solar radiation and downward long wave radiation).

The main ultimate input to drive the complex interaction between the earth-atmosphere systems is the extraterrestrial radiation. Basically, surface energy budget governs the water exchange and partition of the surface turbulent fluxes into sensible and latent heat in the soil-vegetation-atmosphere complex. Owing to this fact, for computing actual ET, the surface energy balance equation is the primary boundary condition which needs to be satisfied:

$$Rn = Go + \lambda E + H \ (\mathrm{W/m^2}) \quad \text{.....(1)}$$

Where Rn is the net radiation, G_o is the soil heat, H is the sensible heat flux and λE is the latent heat flux, all in [W/m^2]. On smaller time scales, such as less than a year, the effects of seasonal and daily storage and release of heat energy in the soil and vegetation biomass can no longer be

ignored (van der Kwast 2009).By Convention, all fluxes away from the surface are negative and towards the surface are positive.

Net Radiation

The surface net radiation, Rn, is the balance among all the incoming and outgoing short and long wave radiation and can be given: Net Radiation in any point on earth is the result of net shortwave(incoming and outgoing) and long wave (incoming and outgoing) radiation. Mathematically it can be represented as

$Rn = (1 - \alpha) * R_s + \varepsilon\alpha . \sigma . T\alpha^4 - \varepsilon s . \sigma . Ts^4$ ……(2)

Where α denotes surface albedo, Rs is downward shortwave radiation [W/m^2] which is determined by combined factors of solar constant, solar inclination angle, geographical location and time of year, atmospheric transmissivity, ground elevation, etc. (Van Dam 2000), εα is effective atmospheric emissivity [-] and εs is emissivity of the earth surface [-]; Tα and Ts are temperature of the atmosphere and the earth surface, respectively [K] and σ is the Stefan–Boltzmann constant [J /sm^{-2} K^{-4}].

Soil Heat Flux (Go)

The soil heat flux (Go) is the rate of heat storage in a soil because of temperature gradient between soil surface and the underlying topmost soil layers. The temperature gradient varies with the fractional vegetation cover and the leaf area index, as light interception form and shadow formation on the bare soil determine radioactive heating of the bare soil surface. It is determined as an unfixed percentage of the total available energy, which is given by

$Go = Rn * (\Gamma + (1 - fc) * (\Gamma s - \Gamma c))$ ……(3)

Where, Γc and Γs are empirical coefficient. These values have been determined using exponential observations, but depend also on the soil and vegetation type. For most bare soil conditions Γs value of 0.315 is valid (Kustas et al., 1989), and for vegetation often Γc is assumed to be 0.05 (Choudhury and Monteith, 1973). An interpolation is then performed between these limiting cases using the fractional canopy coverage, which can be determined from remote sensing data.

Sensible Heat Flux

Sensible heat flux (H) is the rate at which energy loss from soil through convection and diffusion process because of temperature difference between the surface and lower most overlaying atmosphere. To determine the sensible heat flux, similarity theory is applied. The sensible heat flux is part of the solar energy consumed by rising warm air from the land surface. Similar theory and Monin- Obukhov stability correction is applied to calculate the sensible heat flux in the model. The relationships for the mean wind and temperature profiles are written in integral form as:

$$u = \frac{u_*}{k}\left[In\left(\frac{z-d_0}{z_{0m}}\right) + \psi_m\left(\frac{z-d_0}{L}\right) + \quad (-\psi_m)\left(\frac{z_{0m}}{L}\right)\right. \quad \text{..... (4)}$$

$$\emptyset_0 - \emptyset_a = \frac{H}{ku_* p_p^C}\left[In\left(\frac{z-d_0}{z_{0h}}\right) - \psi_m\left(\frac{z-d_u}{L}\right) - \psi_m \quad \left(\frac{z_{0h}}{L}\right)\right. \quad \text{..... (5)}$$

Su (2002) calculates the sensible heat flux by applying the similarity theory principle in the Atmospheric Surface Layer (ASL) for mean wind speed, u [m/s] and mean potential temperature, (θ_0-θa) [K].

Roughness length for heat transfer

The roughness length, one of the important land surface parameters that influence the heat transfer between the land surface and the atmosphere, is vital for estimation of heat transfer (Su et al. 2001). For the determination of the sensible heat flux by means of similarity theory, the roughness height for heat transfer must be precisely estimated. The scalar roughness height z_0h for heat transfer can be derived from the following relationship with the roughness length for momentum transfer (Su 2002; Su et al. 2001):

The roughness length for momentum transfer, or momentum roughness (*zom*), is an important parameter for the wind profile calculations contained within [4] & [5] and also for the calculation of roughness length for heat transfer, or heat roughness (*zoh*).

$$Zoh = \frac{Zom}{\exp(KB-1)} \quad \text{.....(6)}$$

Where B^{-1} is the inverse Stanton number, a dimensionless heat transfer coefficient. For vegetated areas, an extended model is used to estimate the kB^{-1} value (Su, 2002), while for bare soil the

model proposed by Brutseart (1982) is used. The earth's surface is usually rough and for a rough surface, *zom* is taken to equal the surface roughness length (*z0*) (Brutseart, 1982).

$$KB^{-1} = \frac{KC_d}{4Ct\frac{u}{u(h)}(1-e^{\frac{-n}{2}}} f_c^2 + 2f_c^2 f_s^2 \frac{K\frac{u}{u(h)}.\frac{Z_{om}}{h}}{C_t} + KBs^{-1} f_s^2 \quad \ldots\ldots(7)$$

Where fc and fs are the fractional canopy coverage and its complement, respectively [-]. Ct is the heat transfer coefficient of the leaf (0.01). Lhomme et al.(2000) noted that the excess resistance for heat transfer varies with all the structural characteristics of the vegetation, but LAI and the view angle of the radiometer appear as the main factors for variation.

Evaporative Fraction and Actual Evapotranspiration

The SEBS model estimates evaporative fraction by taking dry and wet limits of sensible heat flux. Since latent heat flux reaches minimum under dry limit condition and it can be neglected.

The basic consideration of energy balance at the limiting cases is the milestone for the determination of the evaporative fraction in SEBS (Su 2002). During the dry-limit condition, the latent heat flux (i.e. the evaporative component of the turbulent flux) goes down to zero due to soil moisture limitation whilst the sensible heat flux would attain its maximum value. For this case Eq. 1 reduced to:

$$\lambda E_{dry} = R_n - G_o - H_{dry} = 0 \quad \ldots\ldots (8)$$

Or, $H_{dry} = R_n - G_o$

At wet-limit, condition with unlimited soil moisture availability but only constrained by the available energy, the sensible heat flux (Hwet) takes its minimum limit, and evapotranspiration occurs at the potential rate, (λEwet). Consequently, this leads to:

$$\lambda E_{wet} = R_n - G_o - H_{wet} \text{ or } H_{wet} = R_n - G_o - \lambda E_{wet} \quad \ldots\ldots(9)$$

Then, the evaporative fraction, which is the portion of the available energy that is consumed during the evapotranspiration process divided by total available energy (Rn -G_0) is expressed as:

$$\Lambda = \frac{\lambda E}{R_n - G_o} \quad \ldots\ldots(10)$$

The latent heat flux is the total water vapour flux from the biophysical surface into the atmosphere expressed as energy. The actual evapotranspiration is proportional to this energy when expressed as depth of water.

Mohamed et al. (2005) applied remote sensing techniques to estimate the temporal evaporation flux from Sudd Wetland, the biggest wetland in the Nile River Basin. This study noted the importance of spatially distributed evaporation parameters from remote sensing for calibrating a regional climate model enclosing the Nile Basin. Similarly, Mituga et al.(2010) applied SEBAL to assess the spatio-temporal distribution of actual ET in the upper Ewaso Ng'iro North Basin, Kenya. This study found a correlation of about 70% between actual ET from SEBAL and water balance model.

In Su (2006), it is stated that from a remote sensing perspective, there are two principles which need to be considered when attempting to calculate ET: the conservation of energy, and the effect of turbulent transport. The conservation of energy states that ET is a change in state of water by demanding a supply of energy for vaporization and if all sources and sinks for energy can be determined, ET will remain the only unknown. The effect of turbulent transport acknowledges the role of the wind in transporting vapour away from an evaporating surface (Su, 2006). This is the basis of the energy balance approach in the estimation of evaporation using earth observation data.

Courault *et al*. (2005) provide an overview of work done in the international community over the last 25 years related to evapotranspiration estimation from earth observation data; Overgaard *et al*. (2006) review the different types of energy-based land-surface models and the potential of linking these to distributed hydrological models; Kalma *et al*. (2008) focus on the use of remotely sensed surface temperatures in *ET* estimation; Petropoulos *et al.* (2009) examine surface temperature/ vegetation indices methods in retrieving land surface energy fluxes; and Verstraeten *et al.* (2008) assess evaporation methods across different scales of observation, from leaf scale (e.g. porometry) or point scale (e.g. lysimetry), to field scale (e.g. eddy covariance and scintillometry), landscape/ catchment scale (e.g. mass water balance and energy balance) and finally continental scale where only the earth observation energy / mass water balance is possible.

Mu et al. (2011) developed a global remote sensing ET algorithm based on Cleugh et al. (2007) using the logic of Penman-Moneith which considers both the surface energy partitioning process and environmental constraints on evapotranspiration. The results from this study revealed that the spatial actual ET agrees well with that of the MODIS global gross and net primary production (MOD17), with the highest actual ET values over the tropical rainforest and the lowest actual ET values in dry areas with short growing seasons. In addition, based on the findings the authors concluded that the MODIS ET product can provide important information on the global and regional water cycle and the resulting environmental change. The globally estimated actual ET values at 1km spatial resolution are available at the NTSG portal for public access at various temporal scales (NTSG 2012).

J.van der Kwast and W.Timmermans(2009) tried to evaluate the SEBS model on land scape scale using tower based flux measurement at different land cover units during an overpass of ASTER sensor over the SPARCE 2004 in Barrax, Spain. In this study how SEBS estimated sensible heat flux relate to flux measurement. As a result SEBS estimated sensible heat fluxes well to measured fluxes. The contrasts between well irrigated pivots and other land cover types are observed in both the field measurements and the SEBS results. Standard deviations in field measurements of H are similar to standard deviations of H modeled by SEBS. Especially in well irrigated fields, sensible heat flux estimates by SEBS can deviate up to 70% with 0.5K difference in surface temperature.

Lal.P.Muthowatta (2010) estimated spatial distributed actual evapotranspiration value based on satellite data for the Karkhen River Basin, Iran. In the study total water evaporated from the basin during one year study period was estimated and the estimated water consumed by the different land use classes gave better in sight to water managers and planners about how the water is consumed this information is vital to make water allocation decision. Average actual ET is highest for the irrigated areas while the lowest values are found in bare land areas. Average actual ET per unit land area in rainfed agricultural is significantly lower than that in irrigated areas. Comparing the actual ET map with the land use map of the sub-basin reveal that high values of actual ET are found in the irrigated areas and low values are from bare land areas. In most of the rainfed agricultural areas in the sub-basin the actual ET is between 200 to 350 mm/year.

Lesely Gibson (2013) studied on the importance of selecting accurate vegetation parameters when estimating evapotranspiration using SEBS model in Eastern, Cape, South Africa. The study illustrate the sensitivity of SEBS model to Zom generated from NDVI and in the southern part of the study area the value is very low(0.034m) and then the difference in result when using two different approaches to derive Zom i.e using published values for specific crops or land cover and the second is deriving values for it empirically from satellite data(NDVI) .Thus, the result showed that no significant changes in the calculation of the sensitivity H were observed to calculate Zom.

Gibson *et al*. (2009) use the SEBS model to calculate annual *ET* for a quaternary catchment in the Western Cape, South Africa to assess the compliance of water users to water use legislation. The results of the study are inconclusive as the estimated annual catchment ET significantly exceeds the estimated annual catchment rainfall.

Tadesse A.Abitew (2012) uses SEBS and remote sensing data to estimate actual evapotranspiration of Lake Tana Basin in Ethiopia. The study illustrate the estimation of actual evapotranspiration over the basin applying SEBS model using remote sensing, meteorology and solar radiation data and the result obtained compared with other studies performed in the area using different model SWAT and CCLM (COSMO-Climate Limited Area Modelling). The evaluation shows that SEBS estimated a range of 3.5mm/d to 4.5mm/d daily actual ET. The result of SEBS model compared with daily actual ET estimates for the Rib and Gumara sub-basins derived from SWAT and MODIS ET and it showed good agreement at sub-basin level and the comparison further improved at a watershed scale. Similarly, the long-term mean annual actual ET derived from previous hydrological studies using SWAT compared well with MODIS ET over the terrestrial part of the Lake Tana basin, however, the CCLM estimates were by far underestimated when compared to any of the models due to the low spatial resolution and probably the ET processes are not well developed in this model. Despite the good agreement at a basin scale, the actual ET estimated at the sub-basin level was not corresponding among the different models, particularly in the Rib and Gumara sub-basins. The evaluation of daily actual ET from MODIS agreed well with the widely accepted elevation and potential ET correlation. It was concluded that the known actual ET difference for these two sub-basins based on SWAT

estimates is overestimated and unreliable. Therefore, future research that couples remote sensing and hydrological modeling could provide realistic actual ET estimates.

3. Description of the Study Area

3.1 Location

The Gilgelabbay catchment is located in the Northwest part of Ethiopia between $10^0$56' to $11^0$51' N Latitude and $36^0$44' to $37^0$23' E Longitude. The Gilgelabbay River originates from small springs located near Gishabbay 2750 m.a.s.l .and drains to the southern part of Lake Tana. The catchment area of Gilgelabbay River upstream of the out let of Lake Tana is around 5000km^2 and basin. The catchment contributes the largest inflow into the Lake and it covers an area of 3802 km^2. It is the largest tributary of the Lake Tana basin which accounts around 30% of the total area. The catchment has two gauged sub-catchments, Gauged Gilgelabbay and Koga that have size of 1656 km^2 and 299 km^2, respectively.

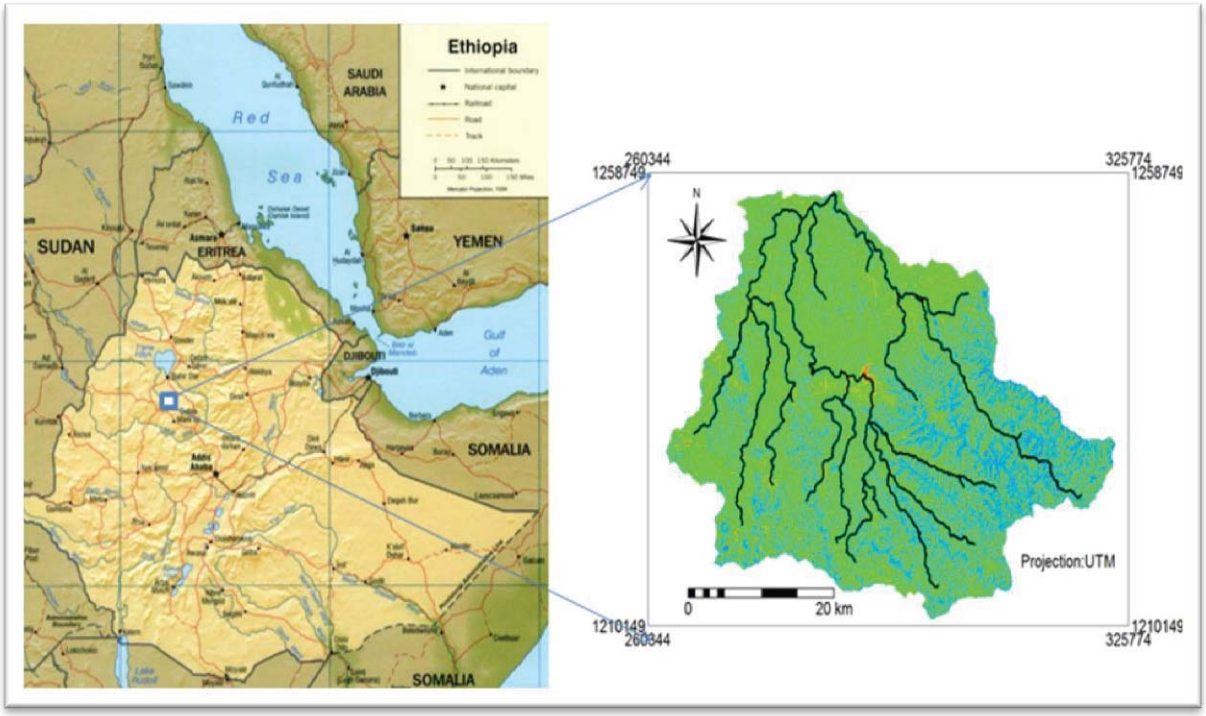

Figure 3-1: Location of the study area

3.2 Topography

The elevation of Gilgelabbay catchment varies from 1787 to 3518 ma.s.l. The higher elevation ranges are located at the Southeast corner while the remaining area is relatively uniform. From the slope map of the catchment area, around 70% of the catchment area falls in the slope ranges from 0-8% and 25% of the area falls in the slope range of 8-30%.

The remaining 5% of the area has slope greater than 30%. The largest flow path of the river towards the outlet is 163.2km.

3.3 Climate

The climate of Ethiopia is mainly controlled by seasonal movement of Intertropical Convergence Zone and its atmospheric circulation (Shaka, 2008) and topography. As the Gilgel Abay catchment is located in the highland part of Ethiopia and its climate is also affected by topography. The mean annual temperature of cool-semi humid is 17-20℃ while that of cool humid zone is 11.5 – 17℃.The dry and wet season occur between October and May and between June to September respectively. Generally the rainy season of the catchment is from June to September with its contribution of 70-90% of the annual rainfall (Abdo et l.,2009). The area has mean annual rainfall 1900mm in the Southern and 1200mm in the Northern part (Kebede,2009). As reviewed by (BCEOM,1999) the temperature variations throughout the year are minor in the study area. The humidity varies between 58% and 80% in May and August, respectively. During the period June to August the sunshine duration of the area is reduced to 3.6 to 5.2 hours daily.

3.4 Geology and Soil

Quaternary volcanic rocks overlay the older Tertiary volcanic over much of the Gilgelabbay catchment boundary. The Quaternary volcanic sequence comprises blocky and fractured vesicular basalt, some basaltic breccias and tuffs perhaps as much as 200-300m thick (SMEC,2007).

Soil textural data obtained from SEA shows that the textural class dominant soil of the study area are clay and clay loam. The soil of Gilgelabbay catchment is mostly covered by Haplic Luvisols with area coverage of around 2583km^2. Luvisol are generally fertile soils because of their mixed mineralogy, relatively high nutrients content and presence of weathered minerals. The cultivated areas are mostly located on this type of the soil throughout the catchment (Tesema, S.M, 2006).

3.5 Land use/Land cover

Rainfed agriculture is the main economic activity of the basin. The surrounding flood plains known as Alefa and Achefer are intensively cultivated areas for more than

centuries. One of the major natural forests covers a small part of the Gilgelabbay catchment at the north, which is known as Zege, the peninsula of the lake. Some marshes and wetlands occur at the floodplains, especially near the lake, with a dominant flora type of Papyrus (Cyperus papyrus). Bushes, shrubs and grassland including grazing land cover the rest of the basin. Many small urban areas are distributed throughout the whole basin of which biggest is Bahir Dar city, which is located on the south corner of the lake where the Blue Nile River starts. (Tessema 2006)

3.6 Hydrology and Drainage

Rainfall in the Gilgelabbay catchment originates from moist air coming from Atlantic and Indian oceans following the north-south movement of the Intertropical Convergence Zone (ITCZ). There is a high spatial and temporal variation of rainfall in the study area. The main rainfall season which accounts around 70-90% of the annual rainfall occurs from June to September. Small rains also occur sporadically during February/March to May.

According to Conway (1997) the climate of the high elevation areas can be considered as a temperate and that of the low elevation areas as tropical.

The source of the Gilgelabay River is a spring that emerges from Gish Abbay Mountain near Sekela town. Locally the name of the stream is Abbay which is considered as the Blue Nile River. On the way downstream, the river receives inflow from several rivers and stream and is named as Gilgelabbay near Wetet Abbay town. Many perennial rivers such as Guder, Dabola, Gugri, Libsi and Ashar drain in the river upstream of Wetet Abbay town and Koga, Kilti, Bered and Areb drain in the river downstream of Wetet Abbay town till it reaches to the out let at Lake Tana. Koga River is gauged since 1959 and its flow rate is measured before it joins Gilgelabay River.

4. Materials and Data Availability

4.1 General

For this study meteorological data as well as remotely sensed satellite data were acquired from different sources and used as an input for SEBS algorithms and SWAT model. Ground meteorological data were collected from National Meteorological Agency (NMA) of Ethiopian Addis Ababa and the Remotely Sensed Satellite data were downloaded from LPDAAC. According to NMA, there are four categorical classes for meteorological stations. Class I (principal) station that record a range of meteorological variables such as daily precipitation, daily minimum and maximum air temperature, three hours relative humidity, three hours wind speed and daily sunshine hours data. Adet, Bahir Dar, Dangila, Motta and Shahura meteorological stations are principal stations (two of them are within the catchment and the rest outside but very close to the catchment. Kidamaje, Wotetabay and Abayshelko stations are class III with three meteorological variables (rainfall, maximum and minimum temperature). Table 4-1 shows the stations and meteorological variables collected for the study.

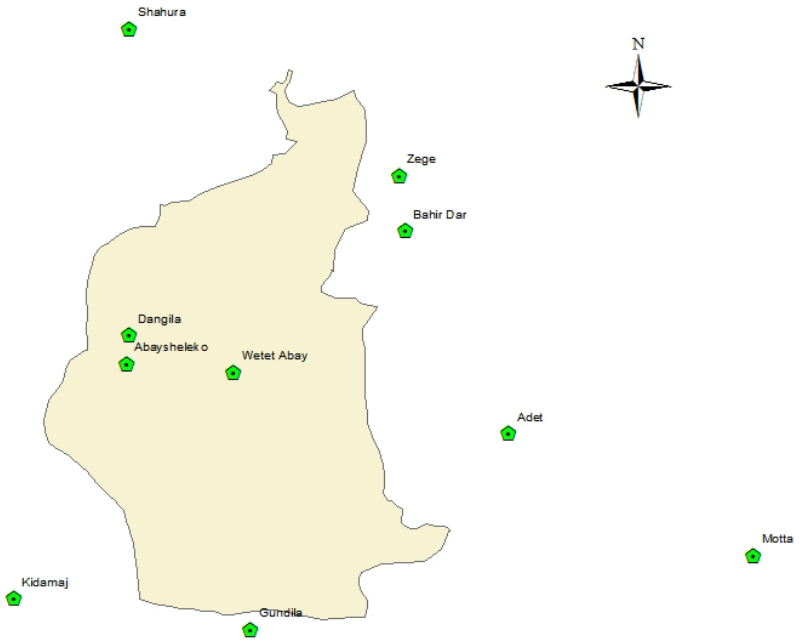

Figure 4-1: Meteorological stations and catchment area

4.2 MODIS land surface products

MODIS (Moderate Resolution Imaging Spectroradiometer) a key instrument operating on board of Terra (EOS AM) launched in December 1999 and Aqua (EOS PM) launched in May 2000. Terra's orbit around the earth is timed so that it passes from north to south across the equator in the morning while Aqua passes south to north over the equator in the afternoon.

MODIS is playing a vital role in the development of validated, global, interactive earth system models to predict global change to assist policy makers in making decision concerning of our environment (https://lpdaac.usgs.gov/). The MODIS land surface product are produced and distributed by the Land Process Distributed Active Archive Center (LP DAAC) which process, archive and distribute land data and product derived from the EOS sensor.

The MODIS HDF products are tiled in grids of 10^0 by $10^{0.}$ Each tile is assigned by horizontal (h) and vertical (v) contains 0 to 35 to horizontally and 0 to 17 vertically with its upper left corner assigned by (0,0) coordinates and it bottom is (35,17). The Gilgelabay catchment lies in the horizontal and vertical coordinate of (21,7) so that the MODIS products under this tile are downloaded for further processing. These tiled products are archived with sinusoidal projection.

In this study, MODIS Terra, preprocessed products are used for the estimation of actual evapotranspiration(ET). The MODIS products were collected from the MODIS ftp site (ftp://e4ftl01.cr.usgs.gov/MOLT/).

MODIS level 3 and 4 products, such as MOD11A1, MOD09A1, MOD13A1 and MOD16A2 were downloaded to retrieve the land surface biophysical parameters such as broadband albedo, emissivity, Normalized difference vegetation index (NDVI), Leaf Area Index LAI and radiance temperature, among others. The specification of each MODIS product used in this research is presented in Table 2-1 section 2.4 in this thesis. All the data at the LPDAAC portal are in Hierarchical Data Format-Earth Observing System (HDF-EOS) format, which is the standard archive format for EOS Data Information System (EOSDIS) products. The MODIS level 3 products are atmospherically corrected and spatially geo-located tiled map in a sinusoidal projection. MOD09A1 and MOD13A1 are available for 8 and 16 day temporal resolution throughout the year at the LPDAAC portal. Although the biophysical land surface characteristics are likely to change within the stated temporal resolution, the changes are believed not be

significant within such a short a period. For MOD11A1 only images with cloud cover less than 30% and 10% for wet and dry season days, respectively, were downloaded based on the data filtering options for cloud cover for grid location h21v7 (i.e. horizontal and vertical number for tile identification), which comprises the Gilgelabay Catchment. The search to spot cloud free images for the study area for MOD11A1 spans from 2000 to 2010.

MODIS data for terrestrial evapotranspiration (MOD16) were downloaded for the same period at 8 day temporal resolution. In addition, monthly and annual MOD16A2 for annual temporal resolution were also retrieved for the period of 2000-2010

4.3 Digital Elevation Model

Digital Elevation Model (DEM) was obtained from the Shuttle Radar Topography Mission(SRTM).SRTM is an international project lead by the National Geospatial Intelligence NGI & National Aeronautics and Space Administration(NASA), the Italian Apace Agency (ASI) and the German Aerospace Center. It provides three resolution outputs: 1Km and 90m resolution DEMs for the world and 30m resolution DEM for some part of the world *(http://www.cgiar-csi.org/data/elevation/item/45-srtm-90m-digital-elevation-database-v41*).

The (90m) spatial resolution dataset was selected because of its optimal resolution for the purpose of the current study. The vertical error of the DEM is reported to be less than 16 m. The MODIS products used for this study have 1 km pixel resolution; the DEM was re-sampled to 1 km spatial resolution. In this the study area the elevation ranges between 1791 and 3480 m.a.s.l. Figure 4-2 shows the resampled DEM that was used as an input to the POTRAD model which calculates the available global shortwave radiation at the surface. Further it was used to interpolate the surface atmospheric pressure and to extract elevations of different stations where daily average air temperature to be calculated.

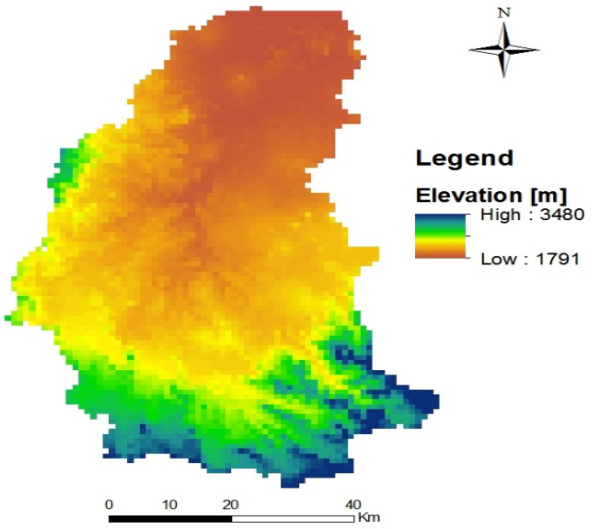

Figure 4-2: Digital Elevation Model of the Gilgelabay catchment (CGIAR-CSI 2012).

4.4 Meteorological Data

For estimation of actual ET using SEBS algorithm meteorological and radiation data were required. These data were obtained from the National Meteorological Agency (NMA) of Ethiopia for a period of 2000 - 2010 and the European Center for Medium Range Weather Forecast (ECMWF), respectively.

Table 4-1: List of first class meteorological stations and the weather parameters measured in the Lake Tana Basin. Tmax, Tmin, rh, u, sd, and Preci represents maximum temperature, minimum temperature, relative humidity, wind speed, sunshine duration and rainfall respectively.

Station	Lat.	Long.	Elev.	Weather Variables					
				Tmax	Tmin	RH	U(ws)	Sd	Prec.
Adet	11.27	37.49	2179	*	*	*	*	*	*
Bahir Dar	11.60	37.32	1827	*	*	*	*	*	*
Dangila	11.43	36.87	2116	*	*	*	*	*	*
Motta	11.07	37.89	2417	*	*	*	*	*	*
Shahura	11.93	36.87	2205	*	*	*	*	*	*
Kidamaj	11.00	36.68	1928	*	*				
Wetet Abay	11.37	37.04	1920	*	*				
Zege	11.69	37.31	1801	*	*				

4.5 Biophysical Data

The biophysical characteristics of the Gilgelabay catchment in Lake Tana basin were collected from both remote sensing products as well as literatures. In SEBS, the biophysical parameters such as canopy height and LAI play an important role in the determination of the turbulent fluxes.

The land-use/cover data used for this study was from the work of Kebede (2009) who performed a supervised land cover classification with the use of Landsat TM images. He used confusion matrix to validate the accuracy of the land classification of the area. This land cover map was further used by Gumindoga(2010) to cross validate the land cover classification map. Based on this classification there are about 6 land-cover types in the catchment (Table 4-2).The canopy height varies significantly for cultivation, wetland and grassland land use types which is attributed to the maturity stage for crops and the water availability(this is taken from Ahmed 2012; Wierngar 1993)

These crop heights were obtained from different studies from the study area. For instant during the dry season most agricultural lands have the minimum height and during wet season the area had the maximum height.

Table 4-2: Annual maximum and minimum canopy height corresponding to different land use.

Land-use type	Maximum height (m)	Minimum height (m)
Water &Marshy	0.2	0.05
Shrub Land	3.0	2.5
Agriculture	2.0	0.05
Grassland	0.5	0.1
Wetland	1.0	0.2
Natural forest	8	8

4.6 ECMWF downward solar radiation

SEBS also requires the downward solar radiation at the earth's surface. Thus, the top of the atmosphere (TOA) incident shortwave radiation and downward shortwave radiation at the surface with a spatial resolution of 0.75 degree for 12:00 pm local time (GMT+3), which is the closest time for the terra overpass time for the study area, were obtained from the European Center for Medium Range Weather Forecast (ECMWF ERA-interim data portal for a few selected days (ECMWF 2012) (http://data-portal.ecmwf.int/data/d/interim_daily/). ECMWF provides product of its operational forecast to publics with various level of restriction. The solar radiation data was considered to estimate transmissivity of the atmosphere over the study area. The NetCDF file tool was used to convert NetCDF format to the standard excel format for easy manipulation of the data.

4.7 SWAT and MODIS estimated actual ET

SWAT model is a widely used semi-distributed watershed hydrology and water quality model. In this model the water balance is the driving force behind the movement of pesticides, sediments and nutrients in a watershed. Therefore, it simulates the hydrological processes including evapotranspiration, precipitation, infiltration, surface runoff, lateral flow and percolation in a continuous time. In general, the SWAT model firstly partitioned a river basin into a number of sub-basins based on a threshold area, and the sub-basin in turn is further divided into one or several homogeneous hydrological response units (HRUs) representing unique combinations of soil and land use similar enough to affect the hydrological process. The subdivision of the watershed enables the model to represent the heterogeneity in the landscape, thereby showing the variability in actual ET for various land covers and soil types. Runoff is predicted separately for each HRU and routed to obtain the total runoff for the watershed, which increases accuracy and gives a much better physical description of the water balance.

The main reasons for the selection of SWAT model are that the model is physically based, spatially distributed, and it belongs to the public domain. SWAT simulates hydrological outputs based on a changed climate if the changes in the climate parameters are given as an input to the model. This makes the model suitable for the proposed task. Beyond that, the ArcGIS 10.2 integrated SWAT interface called the ArcSWAT model provides a user friendly Graphical User Interface (GUI) that ease the use of the model.

5. Methodology

5.1 General

Estimation of the actual ET using the surface energy balance system (SEBS) model will lead to estimation of atmospheric turbulent fluxes as a residue. As it is described earlier, the model needs three sets of stated data in the previous chapters; the remotely sensed data, ground based measured weather data and ECWMF data (the final data set includes downward solar radiation and downward long wave radiation that should either be measured or modeled). Besides they need a careful analysis of the quality of each dataset before its usage in the SEBS algorithm. For each processing step a computer code in the Python programming language was prepared (script attached in Appendix I of this thesis). The next sections of this paper will elaborate all the approaches and actions which were done on each set of the input data.

On the other hand, the major datasets required by the SWAT model include a digital elevation model, land-use map, meteorological data and observed flow, among others. The semi-distributed nature of the model could help to represent a watershed's varying characteristics to a reasonable level. Therefore, the accuracy of the actual ET amount of each sub-basin and their aggregated values for the whole watershed simulated by SWAT could be reliable because the semi-distributed model is based on the water balance that reflects the reality of hydrological processes, in which the actual ET amount is confined logically to the amount of primary hydrology elements such as precipitation and runoff, which can be measured directly and the actual ET amount can be restricted rationally to the water balance equation.

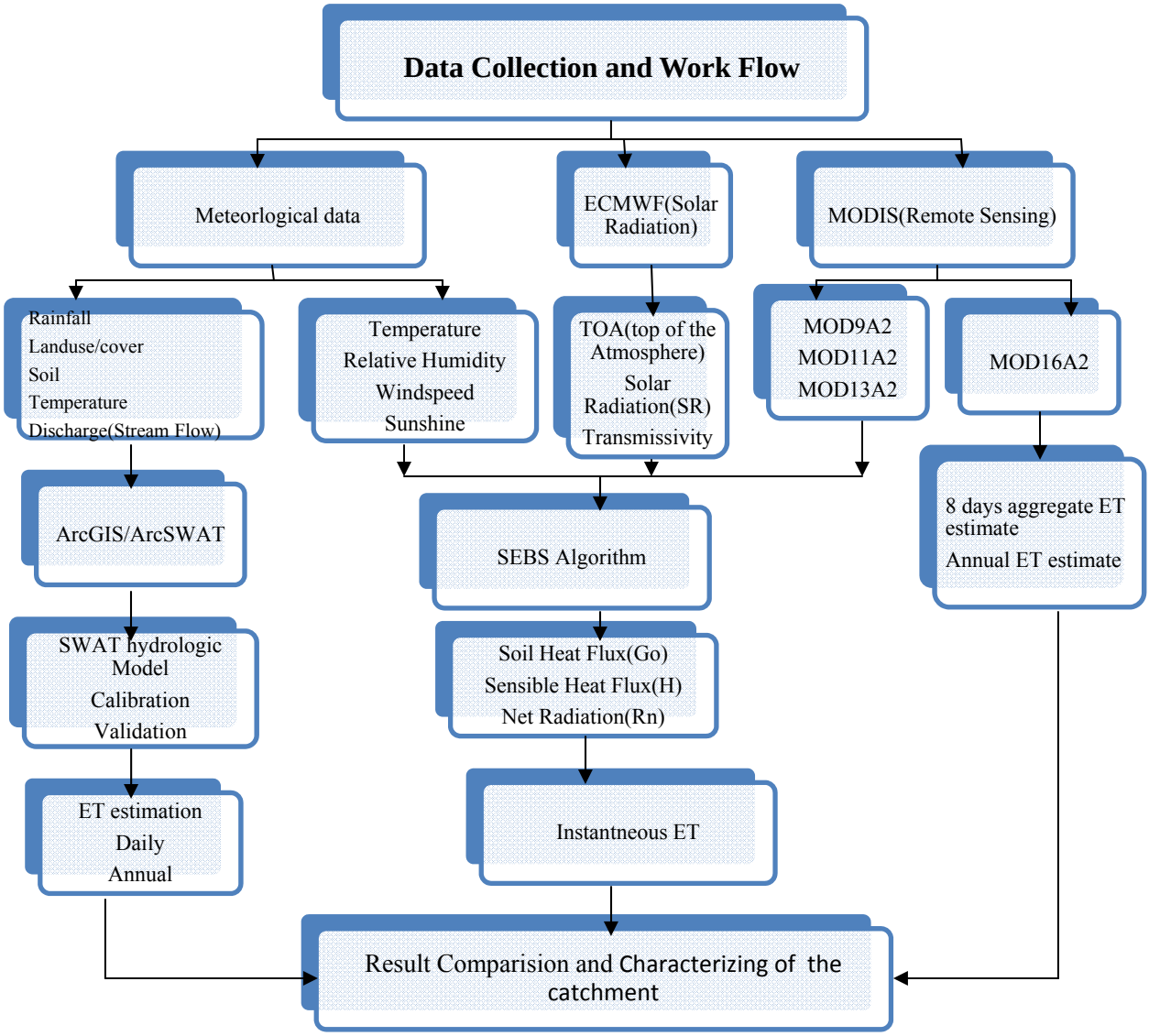

Figure 5-1: A general workflow showing the major task in this study

5.2 MODIS images pre-processing

MODIS re-projection Tool is software for reading data files in HDF-EOS format, specify a geographic subset or band subset as input to processing, perform geographic transformation to a different coordinate system and it also use to write the output to file formats other than HDF-EOS.

In this thesis, the initial task is to manipulate and convert the HDF formatted MODIS images to a PCRaster readable content sealed format (csf), which is the input dataset format to SEBS in PCRaster. Thus, a Python code were prepared using the open source Geospatial Data Abstraction Library (GDAL 2012), which allows the conversion of the Level 3 products from HDF to GeoTiff, GeoTiff to PCRaster format back-to-back for the four datasets: MOD9A1, MOD13A1, MOD11A1 and MOD16A2.

Second each image was re-projectected from MODIS sinusoidal projection system to WGS 1984 Universal Transverse Mercator (UTM) zone 37°N projection. MOD13A1 and MOD09A1 were re-sampled using the clone map to 1000 m resolution, which is the spatial resolution of the LST product. The clone map of the Gilgelabay catchment is an empty map that defines the geographical and cartographical location attributes. In most cases the MODIS data retrieved from the LPDAAC and NTSG portal does not contain the real data figure rather the data value multiplied with a certain factor, which is basically for storage purpose and hence, it needs to be corrected using the appropriate scale factor as listed below.

LST [K] = MOD11A1× 0.02
Surface Reflectance [-] = MOD09A1 × 0.0001
NDVI [-] = MOD13A1 × 0.0001
ET [mm] = MOD16A2 × 0.1

The main purpose of this study was to assess the seasonal variability of actual ET over the Gilgelabay catchment. Accordingly, sufficient number of satellite images should be acquired for each season representation. However, data availability depends on both the overpass frequency and the cloud cover conditions. After the image processing completed, the next step was to select best quality daily images in different seasons. In image selection processes the initial step was done qualitatively using visualization tools such as Aguila (de Jong 2009) and OpenEV 1.8 (OpenEV 2012). MOD11A1 is available on a daily basis, the presence of persistent cloud cover in this region made the availability of cloud free images quite limited for wet season, thus for MOD09A1 and MOD13A1 only those days very close to the available MOD11A1 date were selected and the Python script was prepared accordingly. The final selections of the LST images were done after checking the physical plausibility of the values for the study area. Therefore, LST temperature below 290 K was assumed to be contaminated with clouds.

5.2.1 Land surface temperature (LST)

The MODIS/Terra Land Surface Temperature and Emissivity (LST/E) products provide per-pixel temperature and emissivity values in a sequence of swath-based to grid-based global products with sinusoidal projection and produced daily at 1 km spatial resolution.

The poor quality images for the study area are the presence of LST below freezing temperature, which mostly is not the case for most parts of the study area. For the selected good quality LST images (Table 5-1), their pixel values range from 290 K - 325 K (Figure 5-1).

Table 5-1: List of selected cloud free days in Gilgelabay catchment for LST images with the satellite overpass time at Bahir Dar station. DOY is day of the year and UTC is Coordinated Universal Time.

Acquisition date	DOY	Overpass time
January 1,2005	DOY 1- 2005	10:55
Feb 11,2005	DOY 42- 2005	10:55
April 1,2005	DOY 91-2005	10:55
January 10,2007	DOY 10 - 2007	10:55
March 12,2007	DOY 71- 2007	10:55
December 2,2007	DOY 336 - 2007	10:55
March 30,2009	DOY 89 - 2009	10:55
September10 ,2009	DOY 253 - 2009	10:55
November 27,2009	DOY 330 - 2009	10:55

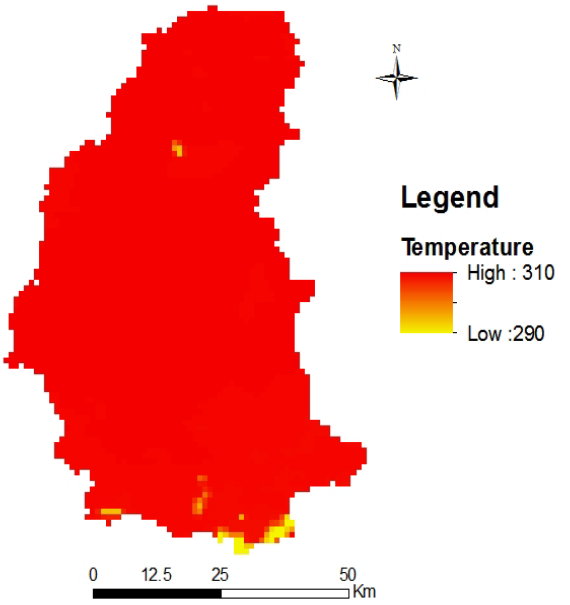

a)

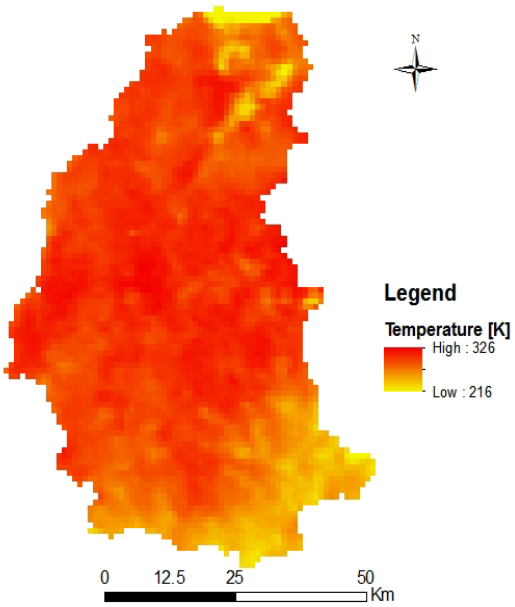

b)

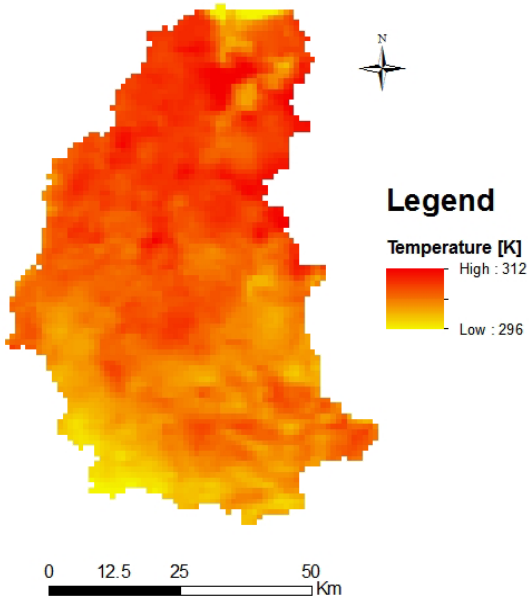

c)

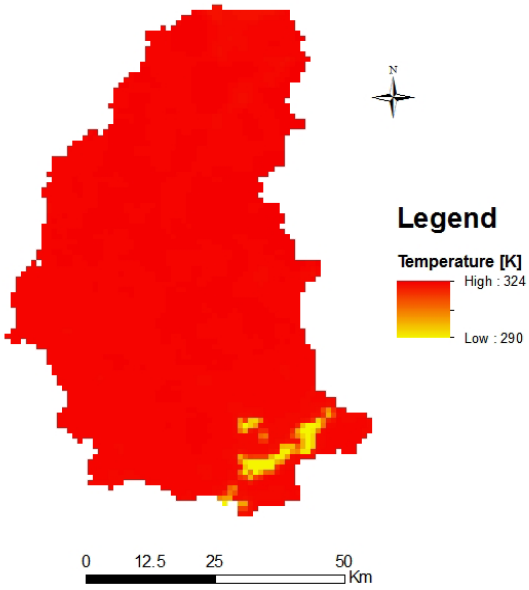

d)

Figure 5-2: Land surface temperature for Gilgelabay catchment on: a) Mar-28-2005 and b) Sept-11-2009 c)March 12,2007 and d) December 2,2007

5.2.2 Albedo

Albedo is important parameter for the estimation of the energy flux in SEBS algorithm, and it is computed from the processed MOD09A1 reflectance images. The broadband surface albedo is calculated using Liang (2001):

$$\alpha w=0.160\alpha_1+0.291\alpha_2+ 0.243\alpha_3+0.116\alpha_4+0.112\alpha_5+0.081\alpha_7 - 0.0015 \quad (11)$$

Where αn is the reflectance band n. Where αn, is simulated total shortwave albedo, *(i = 1~7)* is the narrow bands albedo of MODIS shortwave bands.

From the computed values of Albedo lower values were observed for wet season i.e. September 11, 2009 and relatively higher values found from images of dry season days, especially in April 1, 2005 and March 12, 2007 (Table 5-2)

Table 5-2: Mean and standard deviation of the estimated land surface albedo over Gilgelabay catchment

Date	Mean	STD
January 1,2005	0.18	0.03
Feb 11,2005	0.19	0.04
April 1,2005	0.23	0.036
January 10,2007	0.17	0.038
March 12,2007	0.20	0.035
December 2,2007	0.15	0.04
March 30,2009	0.18	0.039
September10 ,2009	0.09	0.02
November 27,2009	0.15	0.04

5.2.3 Broadband Surface Emissivity

Emissivity (Ɛs) is an important parameter in SEBS for the estimation of the long wave radiation from the heterogeneous terrestrial land surface. It is essential in determining the net available radiation which is the primary driver for the soil heat flux and turbulent fluxes. The land surface emissivity and the emissivity difference are calculated by considering the NDVI value for

individual pixels. The NDVI value is used to distinguish between bare soil pixels, mixed pixels and vegetated pixels and emissivity is calculated accordingly (Sobrino & El Kharraz, 2003).

$$\varepsilon_s = \varepsilon_v f_s + \varepsilon_g(1-f_c) + 4 < d_\varepsilon > f_c(1 - f_c) \quad \text{..... (12)}$$

Where $\varepsilon v = 0.985$ and $\varepsilon g = 0.960$ are emissivity for full vegetation cover and bare soil, respectively. Given the sparse vegetation cover in the study area, the vegetation structure parameter dε is vegetation structure parameter. According to Valor and Caselles (1996), was assumed to be 0.015 and *f*c [-] is the fractional vegetation cover which is determined based on Carlson and Ripley (1997):

$$fc = \left(\frac{NDVI - NDVI\,min}{NDVImax - NDVI\,min}\right)\text{^}2 \quad \text{..... (13)}$$

Where NDVImin and NDVImax are the minimum and maximum NDVI values in the study area, respectively. In the study area NDVImax reaches up to 0.88 in wet season days while the NDVImin is about 0.01 and occurs in dry season.

The spatial land surface emissivity values were derived from MOD13A1 NDVI data selected for this study after treated with the procedures mentioned in section 5.1 of this thesis. As would be expected, higher NDVI values associated with the rainy season and somehow after the offset of the rainy season. As shown in Figure 5-2 the emissivity from the catchment is relatively higher on September 11, 2009 compared to the other days selected from the dry season months.

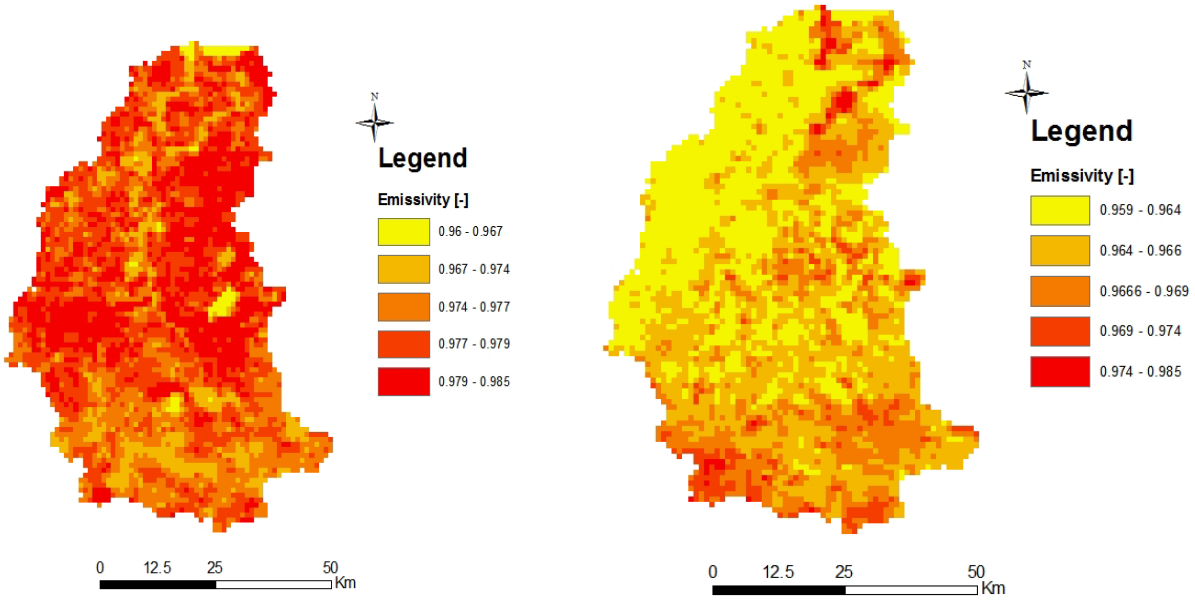

a) b)

Figure 5-3: Land surface emissivity derived from MOD13A1 NDVI product over Gilgelabay catchment on a) Sept-11-2009 and b) Mar-30-2007

5.3 Meteorological data processing for SEBS

Meteorological data such as (Wind speed, Temperature at surface, Reference and surface Pressure, Sunshine hours, Specific humidity and downward solar radiation) for the period of 2000-2010 will be considered in this study. In the following subsection the analysis done to get the input meteorological data ready for the SEBS algorithm is explained briefly.

5.3.1. Air temperature

The daily maximum and minimum air temperature at screen height (i.e. 2 meters) was collected from 6 stations. Even though at each station measurements are conducted at every synoptic hour, only daily maximum and minimum temperatures are accessible for public use. Despite the fact that ET estimation using SEBS is instantaneous meaning at the time of the Terra overpass over the study area, thus using the daily average temperature was assumed to be sufficient.

Given the size of the study area and the presence of higher variability in elevation, a temperature estimated at one station cannot be used to represent the entire catchment. Therefore, the average

daily temperatures for the selected days were interpolated spatially by considering the effect of altitude (Figure 5-3). Conway (2000) estimated 5.8 °C decrease for every 1000 meters increase in elevation and this lapse rate is considered while interpolating temperature spatially using the SRTM DEM. Since Bahir Dar meteorological station is considered to be the most reliable data source in the Lake Tana basin, the following relation was devised to get the spatial temperature.

$$Tp = TBahir\ Dar + (DEM - Elevation) * x \quad \text{.....(14)}$$

Where Tp is the temperature at the point of interpolation [°C], is the temperature at Bahir Dar station [°C], Elevation Bahir Dar is the elevation at Bahir Dar station [m] and = -0.0058 °C m-1 is the lapse rate (Conway 2000).

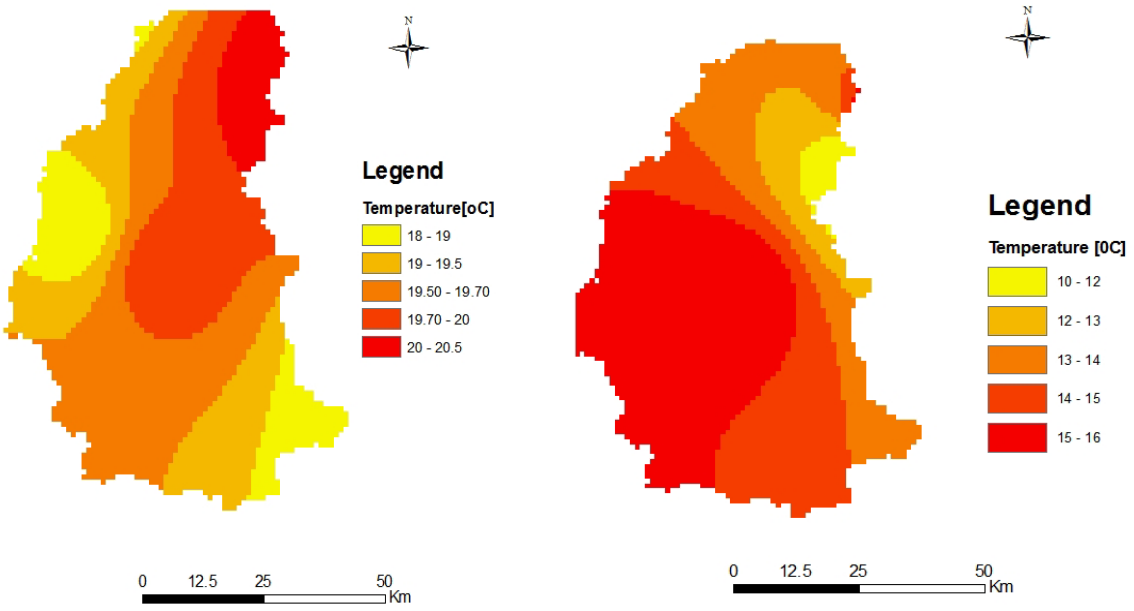

Figure 5-4: Spatially interpolated daily average air temperature over Gilgelabay catchment for Jan-1-2005 (left) and Sept-11-2009 (right).

5.3.2. Relative humidity and wind speed

The available energy at the surface is the dominant driving force for the vapor flux at the surface, the difference between the water vapor pressure at the evapotranspiring surface and the surrounding air is the determining factor for the vapor removal. The process of water vapor

removal from the evaporating surface to the overlying ambient atmosphere depends to a large extent on wind and air turbulence. The availability of daily average wind speed data from weather stations in the study area, wind speed is highly variable both spatially and temporally. SMEC (2008) mentioned that the wind speed data in the current study area is the most unreliable compared to other weather data. Apparently, this influences the accuracy of the actual ET estimation by SEBS.

The spatial daily average relative humidity and wind speed map was produced using the point measurement from five stations by the Inverse Distance Weighing (IDW) interpolation techniques with a power of 2 (Figure 5-4). No assessment was carried out to evaluate the performance of this IDW over the other methods for the study area; however, IDW is selected because of the smooth transition of values between each observing station with distance and its simplicity. For most of the days selected data is available; nonetheless, whenever there is missing data the long term average of the data for the same day was used.

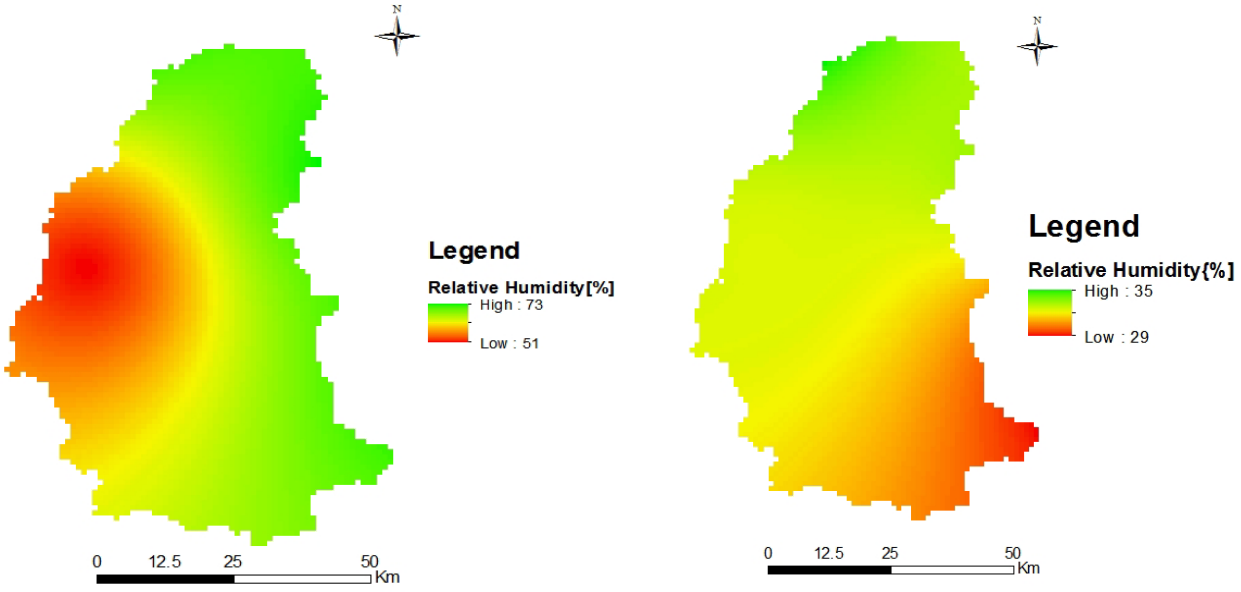

a) b)

Figure.5-5: The spatially interpolated daily average relative humidity over Gilgelabay catchment for a) Jan-1-2005 (left) and b) Sept-11-2009 (right).

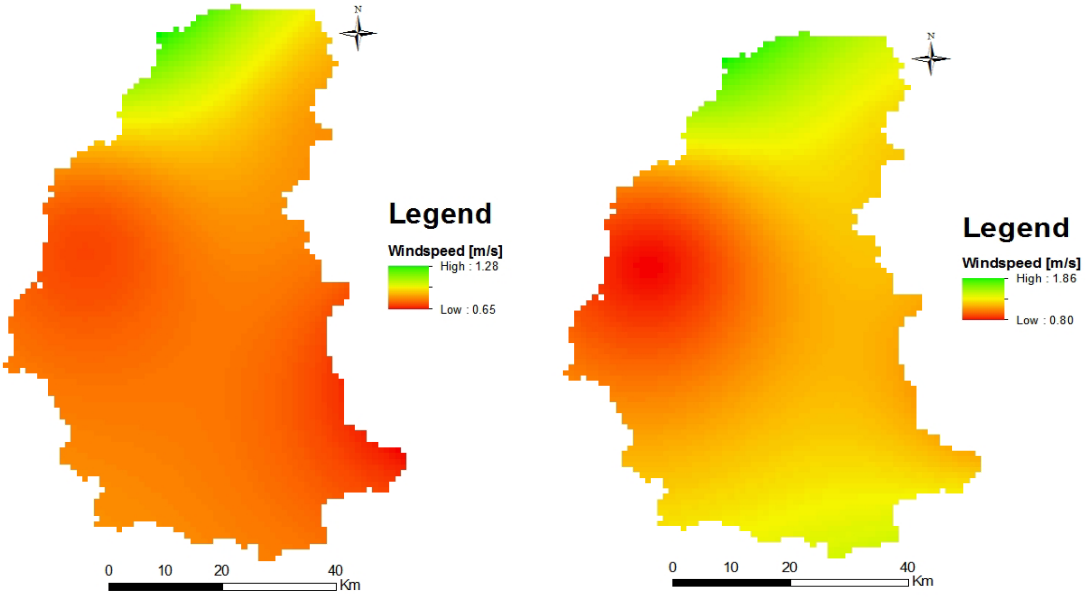

Figure 5-6: The spatially interpolated daily average wind speed over Gielgelabay catchment for Jan-1-2005 (left) and Sept-11-2009 (right).

5.3.3. Atmospheric surface pressure and Psychrometeric constant

The atmospheric pressure is an important parameter in SEBS for the estimation of sensible heat flux. Consequently, the surface pressure was extrapolated horizontally using its relationship with elevation from the DEM. Figure 5-6 shows the spatially interpolated surface atmospheric pressure ranging from 66 kPa to 82 kPa. Therefore, the pressure at the reference and measurement height was given by a simple ideal gas law:

$$\boldsymbol{P = 101.3 * \left(\frac{293 - 0.0065 * Z}{293}\right)^{5.26}} \quad \text{.....(15)}$$

where P is the pressure at the surface [kPa] and Z is the elevation above sea level [m].

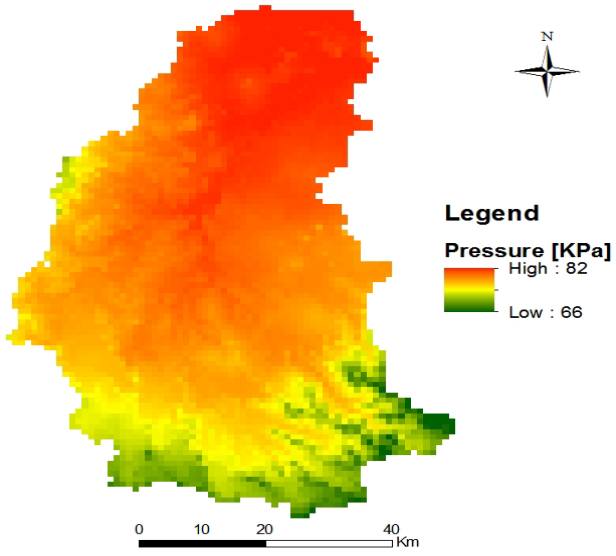

Figure 5-7: Estimated surface pressure map from digital elevation map for the Gilgelabay catchment

Since psychrometric constant is a function of atmospheric pressure, in this study it was calculated using the areal surface pressure computed above. Mostly the psychrometric constant is assumed to be 0.067 kPa °C^{-1}.

$$\gamma = 0.665 * 10^3 * P(Z) \quad (16)$$

Where γ is psychrometric constant [kPa °C^{-1}]

The computed psychrometric constant for the study area ranges from 0.042 to 0.055 kPa °C-1 following the air pressure variations.

5.4 Downward solar radiation

The available downward solar radiation at the earth surface were downloaded at ECMWF ERA interim database; however, it is not wise to use these data directly given its coarse spatial resolution and the fact that the available solar radiation at the surface is influenced by a number of factors such as elevation and zenith angle, among others. Therefore, it was decided to derive a less spatially varying atmospheric variable the so called transmissivity (t) using the TOA incident solar radiation (Ri) in [W m^2] and downward solar radiation (Rs) in [W m^2] at the surface,

$$t = R_s / R_i \quad (17)$$

Where t is transmissivity, R_i is incident solar radiation and R_s is downward solar radiation.

Overall, the higher transmissivity values of the atmosphere are also an indirect way to confirm the cloud free condition for the selected images in the study area.

Table 5-3: Transmissivity values computed using TOA and surface downward solar radiation data from ECMWF.

DOY	Transmissivity Value
January 1,2005	0.75
Feb 11,2005	0.73
April 1,2005	0.74
January 10,2007	0.75
March 12,2007	0.73
December 2,2007	0.76
March 30,2009	0.72
September11 ,2009	0.65
November 27,2009	0.76

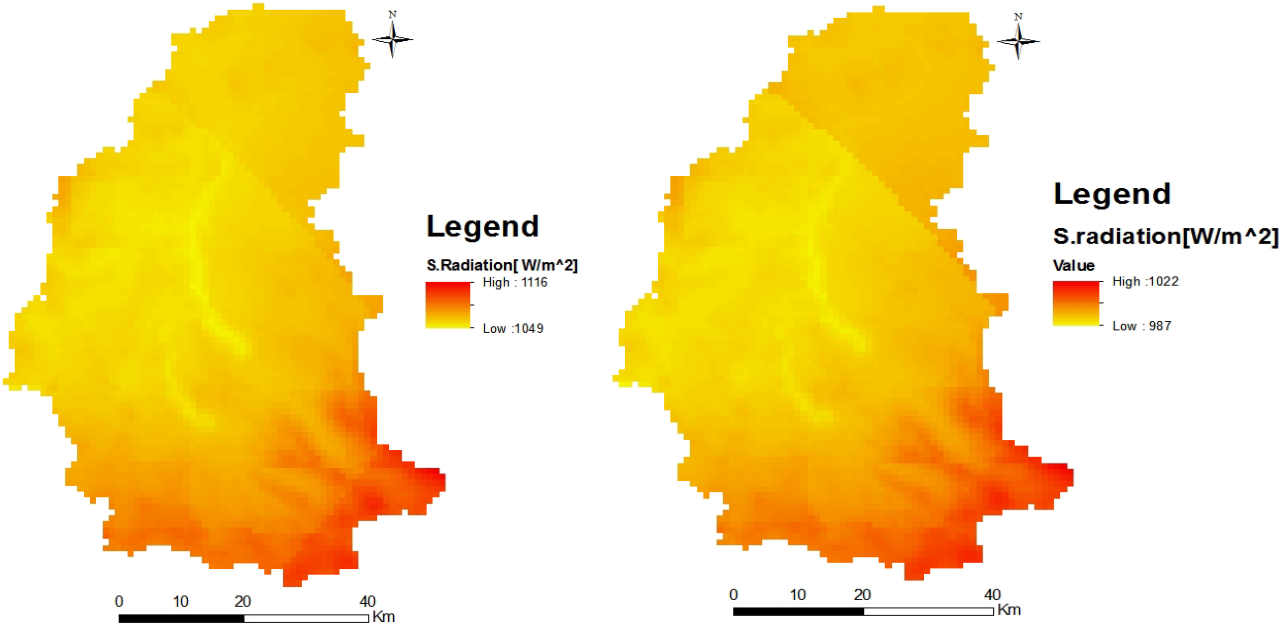

Figure 5-8: Estimated shortwave solar radiation at the earth surface over the study area for Jan-01-2005 (left) and Sept-11-2009 (right).

The computed solar radiations for all the selected days were higher than 1000 W m-2 except September 11, 2009 (Figure 5-7). The likely reason for a lower short wave radiation at the surface is a lower atmospheric transmissivity but in general all the computed radiation values were higher which is attributed to the proximity of the study area to the equator.

5.5 Biophysical Characteristics

5.5.1 Fraction of vegetation cover (FC)

The fraction of vegetation cover is a compulsory input in SEBS since it will directly be used in the calculation Stanton number, KB^{-1}(a dimensionless heat transfer coefficient), the soil heat flux and other important variables.

$$fc = (\frac{NDVI - NDVI\ min}{NDVImax - NDVI\ min})\text{^}2 \quad \text{.....(18)}$$

Where, $NDVI_{min}$ and $NDVI_{max}$ are the minimum and maximum NDVI respectively during the study period. In this study area the maximum and minimum NDVI were 0.83 and 0.18 respectively.

5.5.2 Leaf area index (LAI) estimation

LAI is one of the factors that are used to determine the excess resistance for sensible heat transfer. It can be estimated using the NDVI values from MOD13A1 based on Su (2000)

$$\text{LAI} = NDVI * \frac{(1+NDVI)^2}{(1-NDVI)} \quad \text{.....(19)}$$

van der Kwast (2009) suggested that Eq.19 is only valid for low vegetation covers because NDVI saturates at high LAI values. For high vegetation covers LAI is underestimated. In this case this approach is deemed to be valid for the current study area since there is no significant forest cover.

The estimated LAI values were found to be higher for September 11, 2009 (Figure 5-8) that is, obviously, associated with the higher NDVI values during the rainy season in catchment. However the LAI values were found to be lower for the remaining selected days with a spatially low LAI for March 12, 2007 which lies in the dry period in the region.

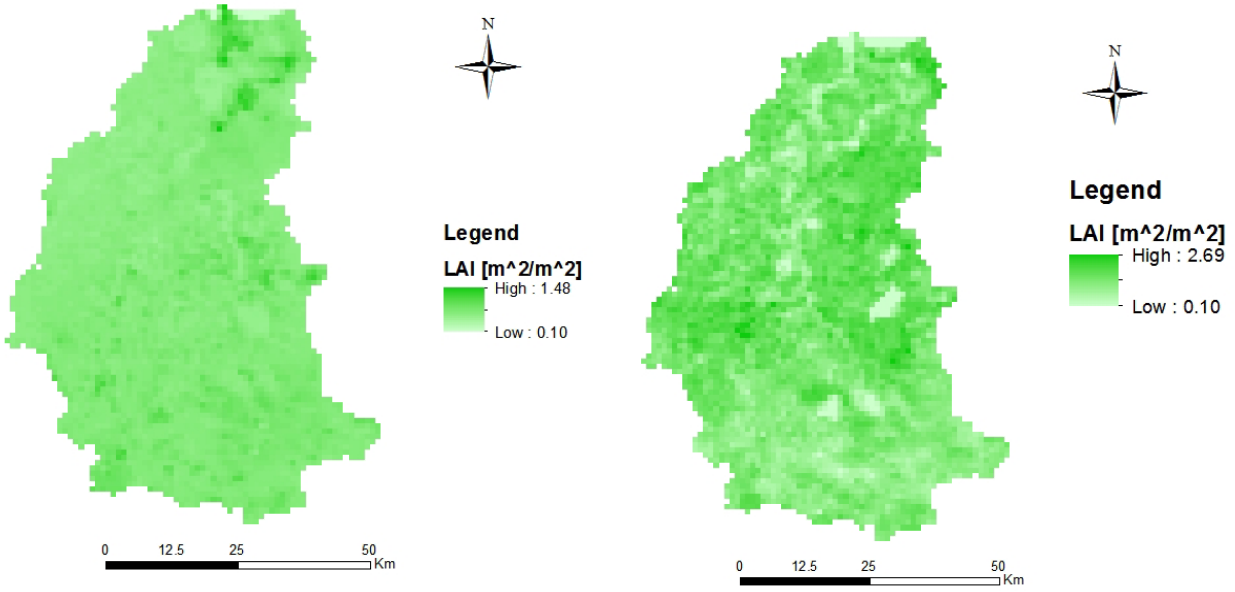

Figure 5-9: Leaf Area Index values over Gilgelabay catchment estimated using NDVI products from MOD13A1 for: a) March 12, 2007 and b) September 11, 2009.

5.5.3 Canopy height and Aerodynamic roughness length

Aerodynamic roughness height (Zom) is important vegetation parameter which has influence on the transfer of momentum in the surface energy balance system. It is the height above the displacement height (d) at which mean wind speed becomes zero (Brustsaret, 2005). In this study the Aerodynamic roughness height (Zom) was calculated using the land cover map of the study area.

Van der Kwast (2009) outlined the challenges in SEBS is to precisely estimate the aerodynamic roughness length that either NDVI values or look-up tables based on literature values and field measurements can be used for the determination of roughness height and zero plane displacement height. In the current study the canopy height for each land-use type was estimated based on literature values on the possible maximum and minimum canopy height together with NDVI values (see Eq.23).The NDVI values were used in order to take into account the growing stage of crops and vegetations in different seasons.

In the SEBS model the roughness lengths for momentum transfer (Zom) were determined using the following empirical relationship (Su et al. 2001)

$$Zom = 0.005 + 0.5\left(\frac{NDVI}{max\ (NDVI)}\right)^{2.5} \quad \text{.....(20)}$$

where max (NDVI) is the maximum NDVI in the study area

Brutsaert (1982) formulated the empirical relation of the roughness length for momentum with canopy height as well as canopy height with the zero plane displacement (d_0)

$$hc = \frac{Zom}{0.136} \quad \text{.....(21)}$$

$$do = \frac{2}{3}\text{hc} \quad \text{.....(22)}$$

$$\text{hc} = hmin + \left(\frac{hmax - hmin}{NDVImax - NDVImin}\right)(NDVI - NDVImin) \quad \text{.....(23)}$$

Where hc is average crop height [m] and Zom is Aerodynamic roughness height[m]

where hmin and hmax is the minimum and maximum canopy height for each land-use type [m] and NDVImax and NDVImin is the maximum and minimum NDVI value for each land-use type.

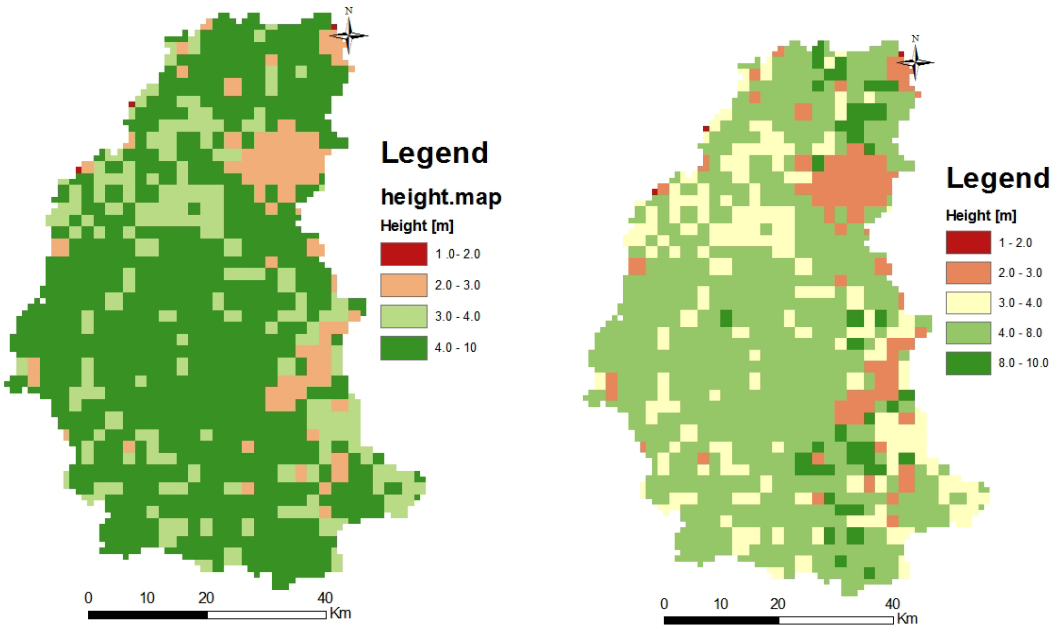

Figure 5-10: Estimated canopy height based on the maximum and minimum height of Gilgelabay catchment for March 12 2007 (left) and September 11, 2009 (right).

5.6. SEBS Instantaneous actual ET estimations and Daily Average ET

In SEBS it is assumed that the daily value of evaporative fraction is approximately equal to the instantaneous. The instantaneous remotely sensed measurements could be used to derive daily total ET by assuming the partitioning of available energy into the various surface fluxes diurnally constant. Therefore, the daily average ET can be determined as:

$$\text{ETdaily} = \sum_{n=0}^{24} 8.64 * 10\text{^}7 * \left(\Lambda * \frac{Rndaily - Godaily}{\lambda \rho w}\right) \quad \text{.....(24)}$$

Where ETdaily is the daily average ET [mm d^{-1}], Rndaily is the daily mean net radiation, G_0daily is the daily mean soil surface heat flux, ρw is the density of water [kg m^{-3}]; λ is the latent heat of water taken as 2.47×106 [J kg^{-1}].

Table 5-4: Summary of all computed primary input spatial dataset to SEBS with their source

Variables and parameters	Data source/Method
Air temperature [°C]	Met. station
Wind speed [ms-1]	Met. station
Relative humidity [kg kg-1]	Met. station
Surface temperature [K]	MODIS
Atmospheric pressure [kPa]	Empirical
Surface shortwave radiation [Wm-2]	ECMWF
Emissivity [-]	MODIS
Albedo [-]	MODIS
NDVI [-]	MODIS
Canopy height [m]	MODIS /Literature

5.7 SWAT (Soil and Water Assessment Tool) Model

5.7.1. Model Input

The spatially distributed data (GIS input) needed for the ArcSWAT interface include the Digital Elevation Model (DEM), soil data, land use and stream network layers. Data on weather and river discharge were also used for prediction of stream flow and calibration purposes.

5.7.1.1 Meteorological Data

Weather data such as rainfall for all stations, temperature from class III and principal stations; relative humidity, wind speed and sunshine hour from principal stations were collected from National meteorological Service Agency. Thirteen years (1998-2010) daily and monthly meteorological data were collected from the agency.

The meteorological stations have different class according to the national meteorological service agency. On the principal stations all the data type are available. Among the stations Bahirdar and Dangila are the principal stations and the data obtained from these stations is used for completing the monthly statistical parameters during the preparation of the weather generator for SWAT model. The geographical location of the stations and their class is summarized and tabulated below.

5.7.1.2 Hydrological Data

The river flow data which will be used for calibrating the simulated flow were collected from Ministry of Water Resource, Hydrology department. There are two river gauging stations in the catchment. Even though there are two stations which are located just upstream, Gilgelabay and Koga are Confluence Rivers but for this studies only one of the river stations, Gilgelabay River is considered. Thirteen years daily flow data at the gauging stations were collected.

5.7.1.3 Land use and Soil Data

The information contained in the landuse map tells how the different uses of the surface are distributed inside the area under study. Spatial distribution and a list of specific land use parameters were required. SWAT has predefined land uses identified by four letter codes and it uses these codes to link land use maps to SWAT land use databases in the GIS interfaces. Hence, while preparing the lookup table, the land use types were made compatible with the input needs

of the model. Hence the classified land use map and its attribute were adjusted to the SWAT model requirement format and database. SWAT model also requires different soil textural and physicochemical properties such as soil texture, available water content, hydraulic conductivity, bulk density and organic carbon content for different layers of each soil type.

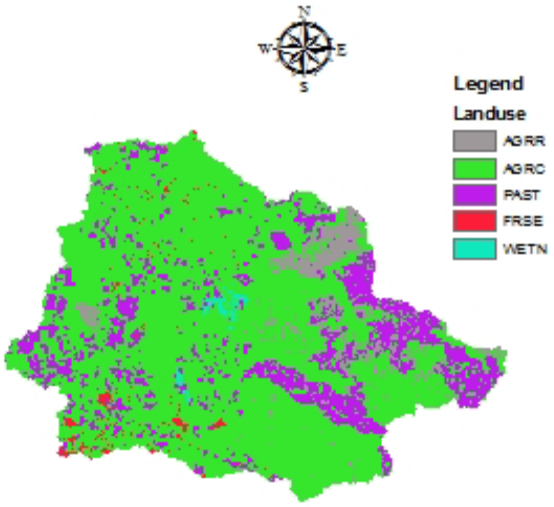

Figure 5-11: Land use map of the catchment

5.7.2 Model Setup

The model setup involved five steps: (1) data preparation ;(2) sub basin discretization: (3) HRU definition; (4) parameter sensitivity analysis; (5) calibration and uncertainty analysis.

5.7.2.1 Watershed delineation

5.7.2.1.1 Digitized Elevation Model

Topography was defined by a DEM that describes the elevation of any point in a given area at a specific spatial resolution. A 90 m by 90 m resolution DEM expressed in section 4.3 is also used for SWAT simulation. This DEM was used to delineate the watershed and to analyze the drainage patterns of the land surface terrain. Subbasin parameters such as slope gradient, slope length of the terrain, and the stream network characteristics such as channel slope, length, and width were derived from the DEM.

5.7.2.1.2 Stream Definition

Based on the aim of the study, the required detail of the stream network, the size and number of

sub basins were determined during processing DEM by defining the threshold area of 3000 hectare.

5.7.2.1.3 Outlet and Inlet Definition

In this section one outlet point was added at the place where measured stream flow data are available near Merawi station where flow is monitored. This outlet enables finally to calibrate and validate the model output. Finally, after sub basin parameter calculation the whole catchment is sub divided in to 25sub-basins.

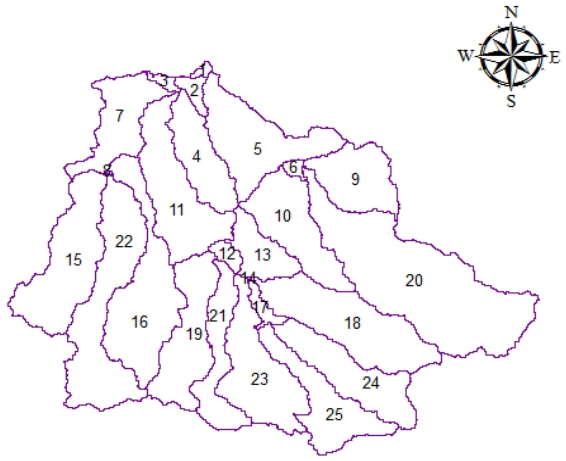

Figure 5-12: Sub basin classifications

5.7.3 Hydrologic Response Units Distribution (HRU)

The watershed were divided into areas having unique land use and soil combinations enables the model to reveal differences in evapotranspiration and other hydrologic conditions for different land cover/ crops and soils (Neitsch, 2002).HRU represents a sub-division in the sub-basin that is characterized by a unique combination land use and soil type. The HRU has no location in the sub-basin model, but is only defined as a fraction of the sub-basin that can be represented by a unique combination of soil and land use. HRUs are used in SWAT runs since they simplify a run by lumping all similar soil and land use areas into a single response unit.

5.7.4 Weather Data Definition

SWAT requires daily meteorological data that can either be read from a measured data set or be generated by a weather generator model. The important input data is meteorological data which

includes rainfall, discharge, temperature, relative humidity, solar radiation, wind speed and potential evaporation (optional). If any of these data is not available, which is very likely, SWAT can generate data using a weather generator. Daily precipitation and temperature data are available for each of the sub basins. The rest of the required data were generated from daily data included in userwgn.dbf database. For this study the meteorological data were collected from NMA and Ministry of Water Resources.

5.7.5 Sensitivity analysis and Auto calibration

The ability of a watershed model to sufficiently predict constituent yields and stream flow for a specific application is evaluated through sensitivity analysis, model calibration, and model validation. Due to spatial variability, budget constraints or access difficulties model input parameters always contain uncertainty to some extent. However, a model user has to assign values to each parameter. The model is then calibrated against measured data to adjust the parameter values according to certain criteria. This implies that the modeler has a clear understanding of all the parameters used as input to the model and of the processes represented in the model. Parameters that are not well understood may be left unchanged even though they are sensitive or are adjusted to implausible values. Not knowing the sensitivity of parameters can also result in time being uselessly spent on non-sensitive ones. Focus on sensitive parameters can lead to a better understanding and to better estimated values and thus reduced uncertainty.

5.7.6 Simulation

The simulation were carried out from 1st January 1998 to 31st December 2010. The first six years data were used for warming and validation up the model while the next seven years data were used for calibration. SWAT has three options for estimating potential ET – Hargreaves (Hargreaves and Samani 1985), Priestley-Taylor (Priestley and Taylor 1972), and Penman-Monteith (Monteith 1965).The Penman-Monteith method was used in this study. SWAT computes evaporation from soils and plants separately as described in Ritchie (1972). Soil water evaporation is estimated as an exponential function of soil depth and water content based on potential ET and a soil cover index based on above ground biomass.

Previous studies have proved Penman-Montheith to be the most appropriate equation to calculate the evapotranspiration when the limiting factor is the water and not the energy, therefore

Penman-Montheid method will be used. The routing method to be selected to route the water through the channel network will be Muskingum routing method.

5.7.7 Data for model calibration and Calibration

Several calibration techniques have been developed for SWAT, including manual calibration procedures and automated procedures. The calibration and uncertainty analysis for this study performed using SWAT-CUP Soil Water Assessment Tool-Calibration Utilization Program. SWAT-CUP was recently developed and provides a decision-making framework that incorporates different semi-automated approaches. Among these algorithms Sequential Uncertainty Fitting (SUFI2), using both manual and automated calibration incorporating sensitivity and uncertainty analysis above. In SWAT-CUP, users can manually adjust parameters and ranges iteratively between auto calibration runs. Parameter sensitivity analysis helps focus the calibration and uncertainty analysis and is used to provide statistics for goodness-of-fit. The user interaction or manual component of the SWAT-CUP calibration forces the user to obtain a better understanding of the overall hydrologic processes (e.g., baseflow ratios, ET, sediment sources and sinks, crop yields, and nutrient balances) and of parameter sensitivity. It is important for future calibration developments to spatially account for hydrologic processes; improve model run time efficiency; include the impact of uncertainty in the conceptual model, model parameters, and measured variables used in calibration; and assist users in checking for model errors. When calibrating a physically based model like SWAT, it is important to remember that all model input parameters must be kept within a realistic uncertainty range and that no automatic procedure can substitute for actual physical knowledge of the watershed.

The curve number (CN2), Deep aquifer percolation fraction (Rchrg_dp), Threshold water depth in the shallow aquifer for return flow to occur (GWQMN) and Ground water “revap’ (GW_REVAP) are the most sensitive among the parameters used in the surface runoff calibration, then followed by that of the base-flow. The same approach was followed as above being the adjustment made to the most sensitive parameters affecting the baseflow: the threshold water depth in the shallow aquifer for flow (GWQMN), the deep aquifer percolation fraction (rchrg_dp), and the groundwater revap coefficient (GW_REVAP). Each time the baseflow calibration is finalized, the surface runoff volume was also checked as adjustment of the

baseflow parameters can also affect the surface runoff volume. The same procedure was also followed to calibrate the water balance of the daily flows too.

Table 5-5: List of parameters considered for Sensitivity Analysis for calibration

SWAT Parameter Name	Description
CN2	Moisture condition II curve number
Sol_K	Saturated hydraulic conductivity (mm/h)
RCHRG_DP	Deep Aquifer percolation fraction
Sol_AWC	Available water capacity (mm/mm soil)
GWQMN	Threshold water depth in the shallow aquifer for return flow to occur (mm)
Sol_Z	Soil depth
ALPHA_BF	Baseflow alpha factor (days)
ESCO	Plant evaporation compensation factor
GW_DELAY	Ground water Delay
GW_REVAP	Ground water "revap'
REVAPMN	Threshold depth of water in the shallow aquifer for "revap" to occur
Sol_ALB	Soil Albedo
CANMX	Maximum Canopy Storage(mm)
CH_K2	Effective Hydraulic conductivity in main channel alluvium

5.7.8 Model validation

The Model validation was performed at one station similar to that of the calibration-using stream flow data. Calibration and validation of the model is a key factor in reducing uncertainty and increasing user confidence in its predictive abilities, which makes the application of the model effective. Information on calibration and validation of multisite, multivariable SWAT models has been provided to assist watershed modelers in developing their models to achieve watershed management goals. Validation result at station is very important since the model used observed climate data input mainly: rainfall, minimum and maximum temperature. As a result it evaluates

the compatibility of measured climate data and global data in the catchment at least for the purpose of this study.

5.7.9 Model Evaluation

Model simulations were evaluated by using mean, standard deviation, regression coefficient (R2), and the Nash and Suttcliffe simulation efficiency (ENS) (Nash and Suttcliffe 1970). The regression coefficient (R^2) is the square of the Pearson product–moment correlation coefficient and describes the proportion of the total variance in the observed data that can be explained by the model. The closer the value of R^2 to1, the higher is the agreement between the simulated and the measured flows. It is calculated using the following equation:

$$R^2 = \left(\frac{\sum_{i=1}^{n}(Q_o - Q'_o)(Q_s - Q''_s)}{\left(\sqrt{\sum_{i=1}^{n}(Q_o - Q'_o)^2}\sqrt{\sum_{i=1}^{n}(Q_s - Q''_s)}\right)}\right)\text{^}2 \quad \text{.....(25)}$$

Where: -*N*: Number of compared values

Q is observed flow, Q_s' is observed mean flow

Qs is simulated flow and Q" is simulated mean flow

Nash and Sutcliffe simulation efficiency, ENS, indicates the degree of fitness of the observed and simulated plots with the 1:1 line (Santhi *et al.* 2002). It is calculated as follows with the same variables defined above

$$E_{NS} = 1 - \frac{\sum_{i=1}^{N}(Q_{obs}\ \ Q_{sim})\text{^}2}{\sum_{i=1}^{N}(Q_{obs}\ \ Q_{obs})\text{^}2} \quad \text{.....(26)}$$

ENS can have values ranging from -∞ to 1. If the simulation is accurate, ENS is equal to one.

If the accuracy of the simulation results is smaller than the average value of the measured variables, then ENS will have a negative value. The disadvantage of this evaluation tool appears in cases of extreme events; as such events have strong weights (Sintondji 2005).

6. Results and Discussion

This chapter is designed to analyze the findings and discuss the results of estimation of actual ET of the study area using SEBS, SWAT and MODIS ET. The result of the SEBS model for terrestrial part of the Gilgelabay Catchment for the spatio-temporal variability of actual ET for the year 2005, 2007 and 2009 incorporated with the input datasets are presented in different subsections accompanied with discussions. The outputs of the SEBS model simulations include the estimates for the energy balance components, Evaporation Fraction and actual ET over the study area, (net radiation, soil heat flux and sensible heat flux). The comparison of SEBS estimated actual ET with the SWAT model and MODIS ET data derived from satellite using remote sensing were also discussed. Besides, comparisons of mean annual actual ET for the whole catchment derived from MODIS ET and SWAT are presented. In the last part of this section a comprehensive reflections on the overall observations in this study are noted.

6.1. Estimated energy budget components

The estimated energy budget components discussed in section 5 by the SEBS algorithm were mapped for the selected nine days for the entire catchment will be presented.

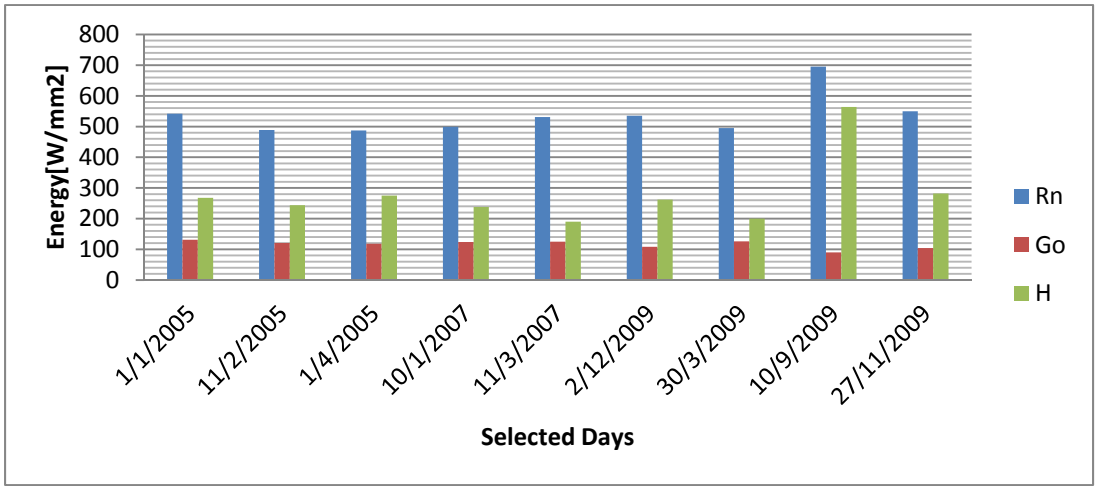

Figure 6-1: Mean of the estimated energy budget components over Gilgelabay catchment: H= sensible heat flux (Green), G0 = soil heat flux (Red) and Rn = net radiation (Blue).

Figure 6-2 shows, the mean net available energy for the selected days over the entire catchment ranges from 694.7 W/m2 (Sep-11-2009) to 495.3 W/m2 (Mar-29-2009). Higher net radiation during wet season days is mainly attributed as a result of low albedo values (see Table 5-2 section

5.2.2) during the wet season period, this in turn is due to high soil moisture availability and dense vegetation cover during wet season days. Kustas et al. (1994) outlined the effect of albedo and soil moisture content on the net available radiation at the surface.

From Figure 6.2, Figure 6.2b and Figure 6-2c, it was observed that the estimated soil heat fluxes over the study area are, generally, less spatially variable, especially for the days in the dry season. The soil heat flux at the surface is largely controlled by the surface vegetation cover (see in section 2.5, Eq.3). Therefore the mean soil flux is larger for those selected in dry season days with a maximum of 130.7 W/m2 (Jan-01-2005) and a minimum 89.40 W/m2 (Sep-11-2009).

On the other hand net radiation and soil heat flux, as shown clearly in Figure 6-2a and b, the estimated turbulent fluxes are significantly variable. The highest mean sensible heat flux were found on Sep-11-2009 (mean 564.1 W/m-2 ; STD ± 46.1 W/m2) and the lowest on January-10-2007 (mean 189.2 W/m2 ; STD ± 53.42 W m-2). Thus, from the study it was noted that the estimated sensible heat fluxes were relatively larger for days in the wet season and lower for days in the dry season. Figure 6.2b also reveals that for the major part of the study area the estimated per pixel sensible heat flux is higher than 281.6 W/m2 on Sep-11-2009 while on Jan-01-2005 it is less than 267.2 W m-2 (Figure 6.3b).

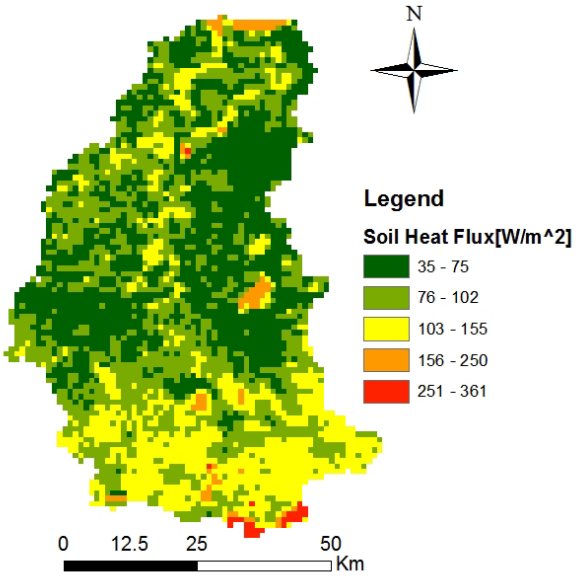

a)

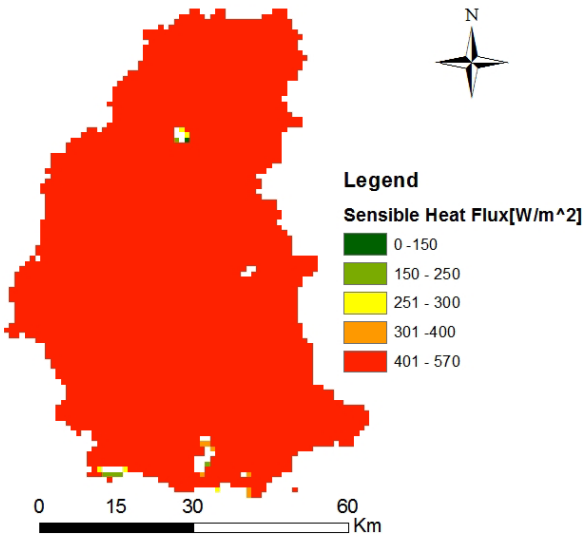

b)

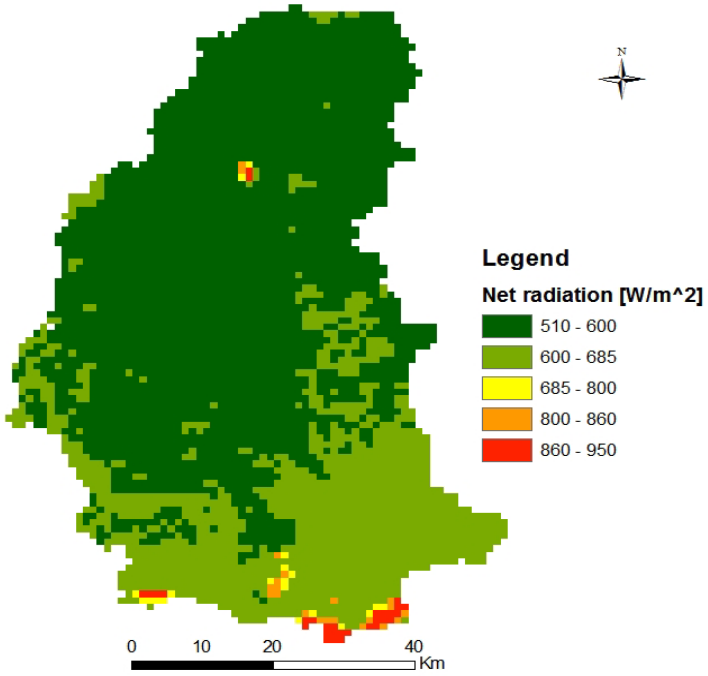

c)

Figure 6-2: SEBS estimated net radiation (a), sensible heat (b), and soil heat (c) of Gilgelabay catchment for September11, 2009.

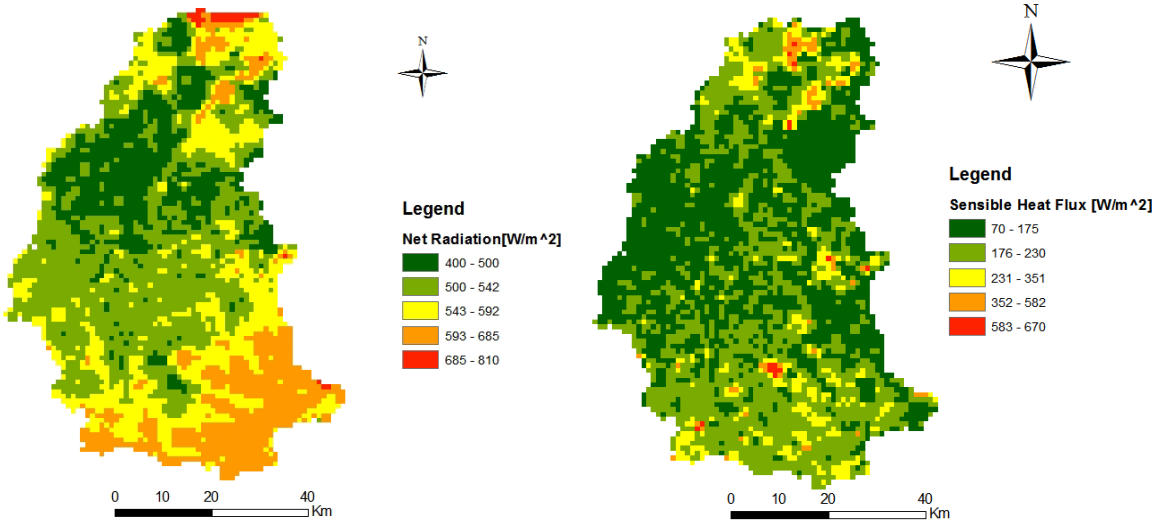

a) b)

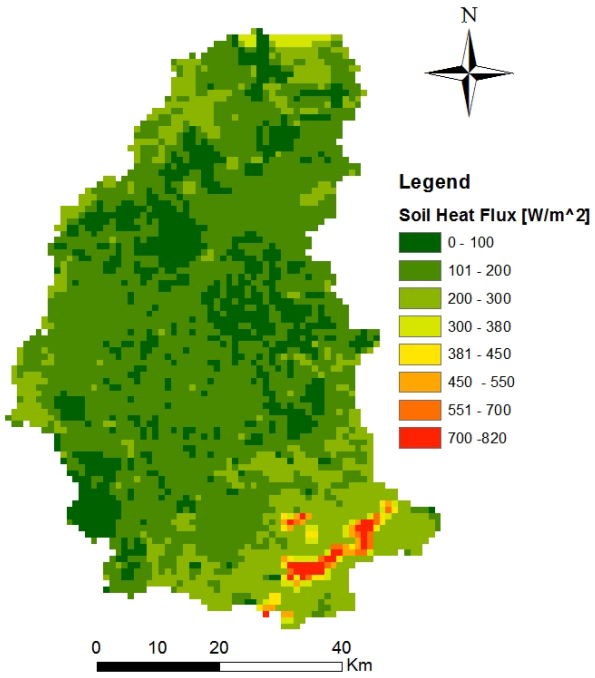

c)

Figure 6-3: SEBS estimated net radiation (a), sensible heat (b), and soil heat (c) of Gilgelabay catchment for January 1, 2005.

Here the SEBS model simulations showed relatively lower values of sensible heat flux over the entire catchment, particularly for surfaces with sparse vegetation and lower canopy during dry season. Several studies mentioned the lager uncertainties associated with the estimation of turbulent fluxes for surfaces covered with sparse vegetation using remotely sensed radiance temperature as an input to surface energy balance components (Chehbouni et al. 1997; Lhomme et al. 2000; Su et al. 2001; Su 2002; Su et al. 2005). Su et al.(2001) outlined that heat and momentum transfer between the surface and atmosphere are controlled by molecular diffusion, and form drag and pressure forces, respectively which is the underlying rationale for the difference between the roughness length for heat and momentum transfer. Over sparsed vegetation, kB^{-1} can be very large and variable (Lhomme et al. 2000). In SEBS this variable is usually higher than 8.0; the roughness height for momentum is always higher than the roughness height for heat (i.e. $kB^{-1} > 0$), except for bare soils for which negative values of kB^{-1} have been found (see Verhoef et al., 1997b). Small negative values have also been found for tall, dense canopies (Liu et al., 2007; Jia, 2004). Timmermans et al. (2011) mentioned values for closed

canopies are usually around 2, but kB^{-1} increases for sparse canopies (up to 15 for very sparse canopies), values of $kB^{-1} > 8$ are therefore deemed too large.

In this study, SEBS estimated relatively larger kB^{-1} for most land-cover types during the dry season and the mean values range from 9.6 to 13.1, and thus, a consequent significant reduction in the SEBS estimated sensible heat flux from the available surface net radiation. Therefore, although it could not be verified with a measured dataset, the sensible heat flux estimations for the dry season days were seemingly overestimated and unrealistic, particularly with cover classes with lower canopy height.

6.2. Spatio-temporal distribution of actual evapotranspiration

In section 6.1 the spatial and seasonal variability of the energy balance components were evaluated for the catchment. Obviously, the actual ET is derived from the SEBS estimated latent heat flux which is discussed in the previous section. The spatial distribution of actual ET for the selected nine days image is displayed in Figure 6-4.

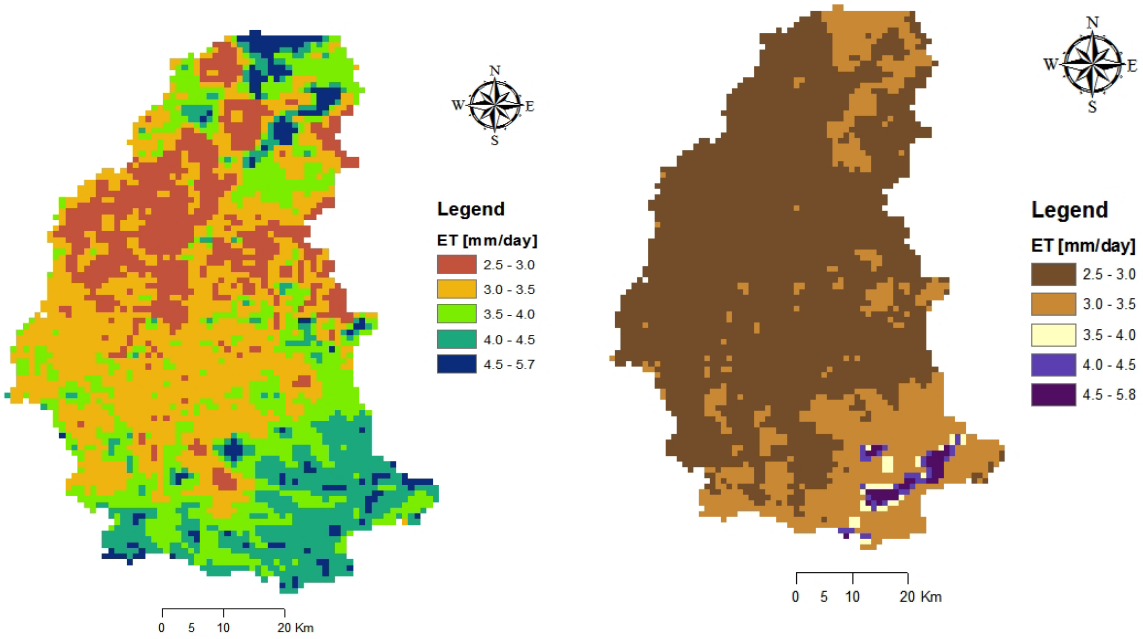

a) DOY 1-2005 b)DOY 71-2007

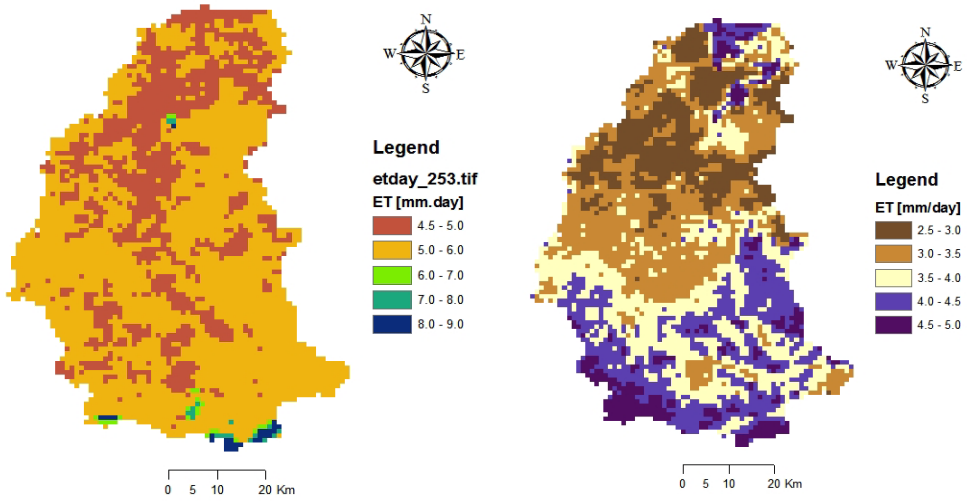

c) DOY-336-2007 d) DOY 253-2009

Figure 6-4: SEBS estimated spatial actual ET values over the study area

Generally, Figure 6-4 represented higher actual ET estimates with less spatial variability for days in the dry season considered for the three years. During these days the mean actual ET reaches up to 5.9 mm/d (Jan-01-2005), 5.6mm/d (January 10, 2007) and 4.7 mm/d (March 12, 2007). In distinction as it observed from the results during wet season days the SEBS estimated actual ET is relatively lower and highly variable spatially. The mean actual ET for DOY 253- 2009 is 8.7 mm/d, DOY 336 - 2007 is 4.9 mm/d and DOY 330- 2009 6.4 mm/d which shows the spatial variability resulted due to heterogeneity of the vegetation cover during the wet season. From the results it was learnt that the estimated actual ET values for days in the dry season and wet season seems reasonable.

6.3. SWAT model and Flow simulation for gauged Gilgelabbay sub-catchment

6.3.1 Sensitivity Analysis

Sensitivity is measured as the response of an output variable to a change in an input parameter with the greater the change in output response corresponding to a greater sensitivity. Parameters identified in sensitivity analysis that influence predicted outputs are often used to calibrate a model.

For this study the sensitivity analysis was carried out for a period of thirteen years, which included both the calibration period (from January 1st 2004 to December 31st 2010) and the

warm-up period (from January 1st , 1998 to December 31, 1999) and validation period (from January 1st 2000 to December 31st 2010). Even though 16 parameters with ten intervals of Latin Hypercube (LH) sampling (totally 500 iterations) were used for the sensitivity analysis, only 14 of them revealed meaningful effect on the daily flow simulation of the gauge Gilgelabbay Sub-catchment. As shown in table 6-2, the first eight parameters showed a relatively high sensitivity, being the curve number (CN2) is the most sensitive of all. The four most sensitive parameters controlling the surface runoff in the sub-catchment are curve number (CN2), deep aquifer percolation fraction (Rchrg_dp), Threshold water depth in the shallow aquifer for return flow to occur (GWQMN) and Ground water "revap' (GW_REVAP). With respect to the base flow, the deep aquifer percolation fraction (rchrg_dp), the threshold water depth in the shallow aquifer for flow (GWQMN) and Ground water "revap' (GW_REVAP) have the highest influence in controlling the base flow.

6.3.2 Flow calibration

Flow calibration was performed on daily bases for a period of seven years from January 1st 2004 to December 31, 2010 using the sensitive parameters identified this period was selected due to that the considered dry and wet years wanted to be included in the calibration period. However, flow was simulated for six years from January 1st 1998 to December 31, 2003 for validation purpose, within which the first two years were considered as a warm up period. As discussed previously in the methodology section, the flow was calibrated manually using the observed flow gauged at the outlet of the sub catchment. First of all, both the surface runoff and base flow components of the gauged flow were balanced with that of the simulated flow. Here the model was adjusted to calculate the potential evapotranspiration of this catchment by using the penman-Montieth Method. The adjusted flow was further calibrated temporally by making delicate adjustments to ensure best fitting of the simulated flow curves with the gauged flow curves. Manipulation of the parameter values were carried out within the allowable ranges recommended by SWAT developers.

Table 6-1: Results of the sensitivity analysis for gauged Gilgelabbay catchment

S.N	Parameters	Description	Lower Limit	Upper Limit	Final Fitted Values
1	CN2	Initial SCS CN II value	-0.25	0.25	-0.233
2	RCHRG_DP	Deep aquifer percolation fraction	0.05	0.95	0.4037
3	GWQMN	Threshold water depth in the shallow aquifer for return flow to occur (mm)	0	100	84.70
4	GW_REVAP	Ground water "revap'	0.05	0.4	0.1683
5	Canmx	Maximum Canopy storage(mm)	0	20	16.10
6	Sol_Z	Soil depth	-0.3	0.3	-0.2514
7	Sol_ALB	Soil Albedo	-0.3	0.3	0.1458
8	Sol_K	Saturated hydraulic conductivity[mm/hr]	-0.5	0.5	-0.077
9	Sol_AWC	Available water capacity	-0.3	0.3	0.2622
10	ESCO	Soil evaporation compensation	0	1	0.819
11	Alpha_BF	Base flow alpha factor	0	0.8	0.633
12	GW_DELAY	Ground water delay	0	100	8.10
13	REVAPMN	Threshold depth of water in the shallow aquifer for "revap" to occur	0	100	27.10
14	CH_K2	Effective Hydraulic conductivity in main channel alluvium	0	50	46.65

Table 6-2: Initial/default and finally adjusted parameter values

S.No.	Parameters	Description	Lower and upper bound Limit	Final Fitted Values
1	CN2	Initial SCS CN II value	-0.25 – 0.25	-0.233
2	RCHRG_DP	Deep aquifer percolation fraction	0.05 - 0.95	0.4037
3	GWQMN	Threshold water depth in the shallow aquifer for return flow to occur (mm)	0-100	84.70
4	GW_REVAP	Ground water "revap'	0.05-0.4	0.1683
5	Alpha_BF	Base flow alpha factor	0 - 1.0	0.633
6	GW_DELAY	Ground water delay	0 - 100	8.10
7	REVAPMN	Threshold depth of water in the shallow aquifer for "revap" to occur	0 - 100	27.10
8	CH_K2	Effective Hydraulic conductivity in main channel alluvium	0 - 50	46.65

Afterwards the adjusted flow was further calibrated temporally by making delicate adjustments to ensure best fitting of the simulated flow curves with the gauged flow curves. Manipulation of the parameter values were carried out within the allowable ranges recommended by SWAT developers. The initial/default and finally adjusted parameter values are shown in table 6-2.

The comparison between the observed and calibrated flow discharge values for the seven years of calibration indicated that there is a good agreement between the observed and simulated flows using SUFI-2 algorithms with higher values of coefficient of determination and Nash Sutcliffe efficiency (NSE) for Gilgel Abay rivers.

The daily calibration results in table 6-3 shows that there is a good agreement between the simulated and gauged daily flows. This is demonstrated by the correlation coefficient (R^2=0.78) and the Nash-Suttcliffe (1970) simulation efficiency (ENS=0.75) values for Gilgelabbay catchment. Similarly, the daily calibration result showed that correlation coefficient (R^2=78) and the Nash-Suttcliffe (1970) simulation efficiency (ENS=75) values for Gilgelabbay catchment,

this can be represented in Figure 6-6 . The results fulfilled the requirements suggested by Santhi *et al.* (2001) for R^2 greater than 0.6 and ENS greater than 0.5. Hence our results agree reasonably well with these values.

The p-factor, which is the percentage of observations bracketed by the 95% prediction uncertainty (95PPU) brackets, equals 0.76 and r-factor equals 0.91 for Gilgelabay River.

Table 6-3: Calibration statistics of average daily and monthly simulated and gauged flows at Gilgelabay River

Period	Total flow (m3/sec)		Average flow (m/sec)	
	Observed	Simulated	Observed	Simulated
Daily(2004-2010)	138172.97	136397.27	54.04	53.34

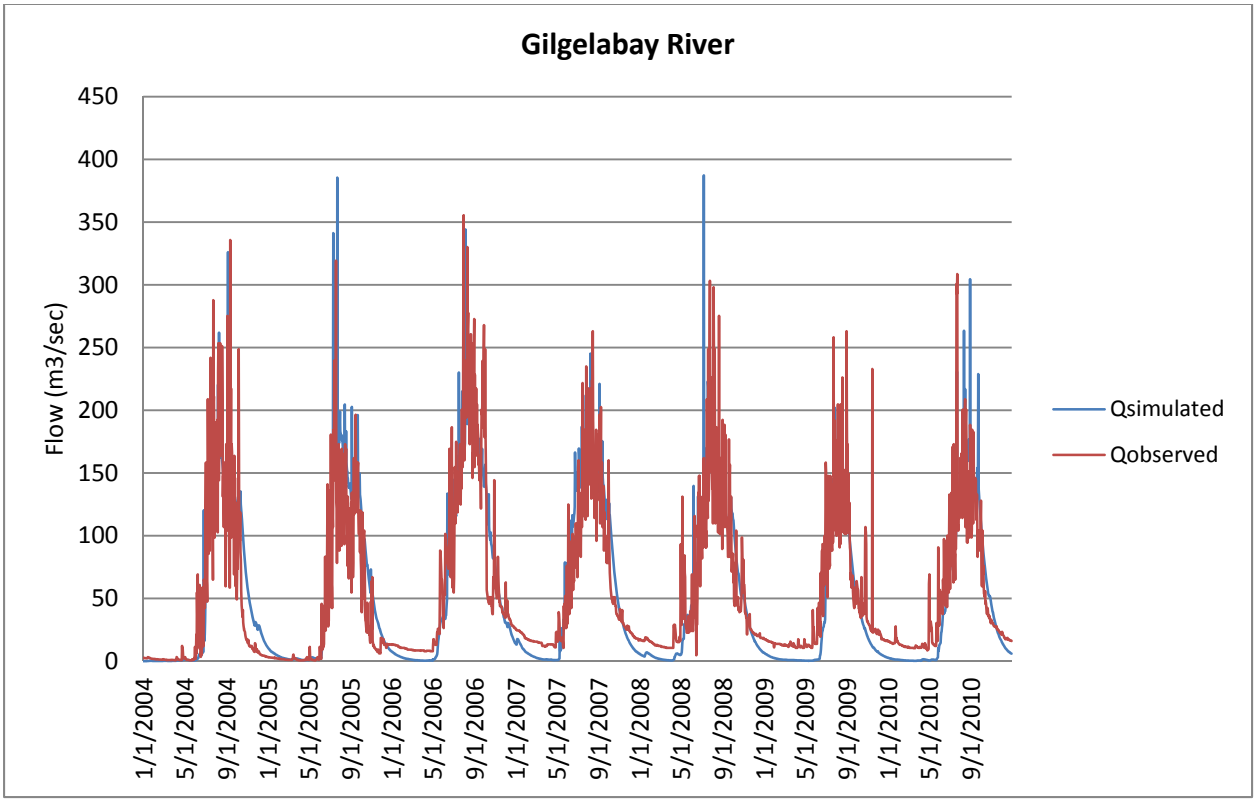

Figure: 6-5: Observed and simulated flow (discharge) in Gilgelabay during calibration [2004-2010]

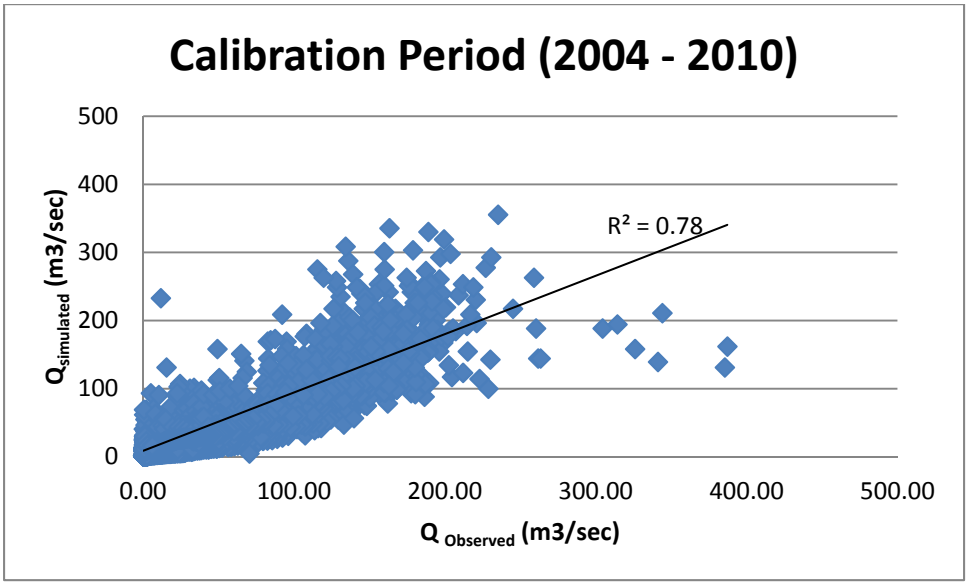

Figure 6-6: Graphical representation of regression coefficient R^2 for calibration period

6.3.3 Flow Validation

Validation proves the performance of the model for simulated flows in periods different than the calibration periods, but without any further adjustment in the calibrated parameters. Consequently, validation was performed for four years period from January 1st 2000 to December 31st 2003.

The validation results in Table 6-4 shows also that there is a good agreement between the simulated and observed flows. Also the p-factor, which is the percentage of observations bracketed by the 95% prediction uncertainty (95PPU), brackets 81% of the observation and r-factor equals 0.84 for Gilgelabay river for the validation period. The value of the regression coefficient is shown in Figure 6-7.

Table 6-4: Validation statistics of average daily and monthly simulated and gauged flows at Gilgelabay River

Period	Total flow (m3/sec)		Average flow (m/sec)	
	Observed	Simulated	Observed	Simulated
Daily(2000-2003)	76240.1	80420.41	52.18	55.04

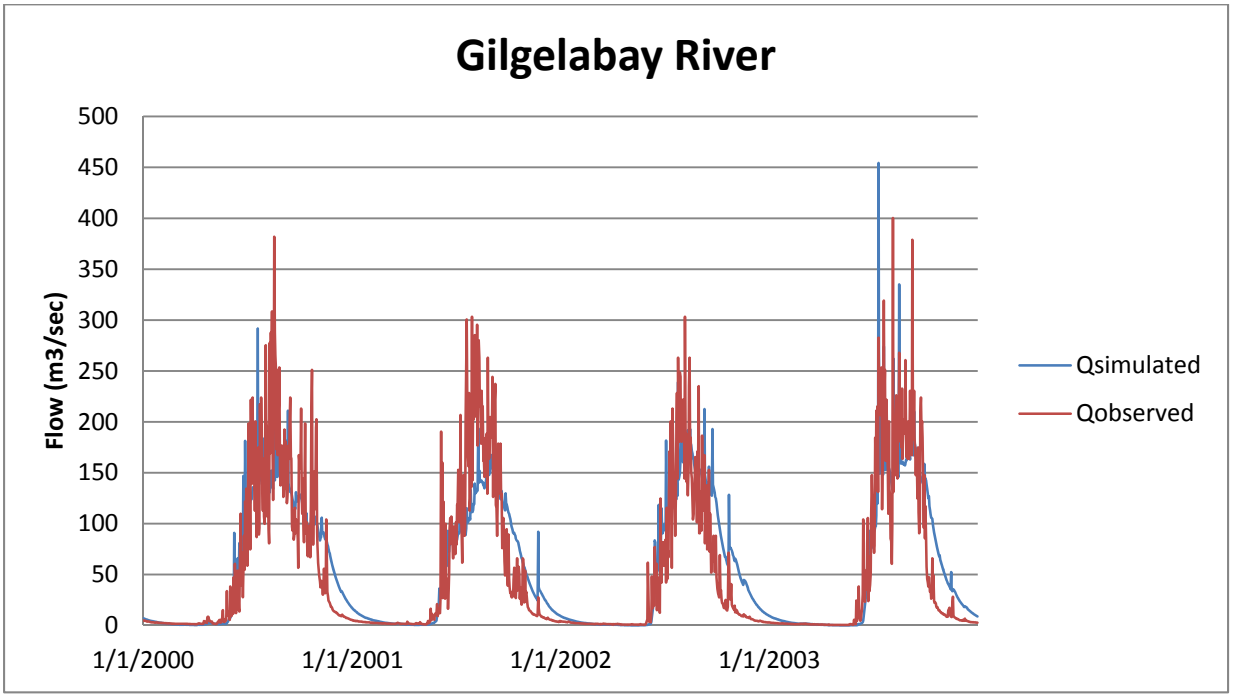

Figure: 6-7: Observed and simulated flow (discharge) in Gilgelabay during validation [2000-2003]

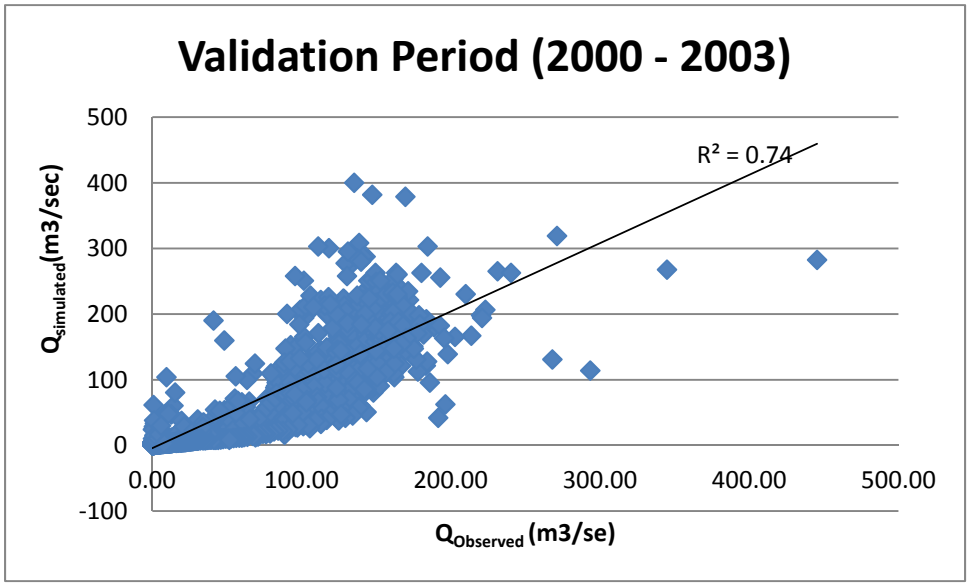

Figure 6-8: Graphical representation of regression coefficient R2 for validation period

Table 6-5: Stream Flow Calibration and Validation Result for GilgelAbay River Using SUFI-2

Objective Function		Gilgelabay River	
		Calibration Period (2004-2010)in %	Validation Period (1998-2003) in %
R2	SUFI-2	78	74
NSE	SUFI-3	75	73
p-factor	SUFI-4	76	81
r-factor	SUFI-5	91	84

Water balance is mainly based on the law of conservation of mass and can be computed for any soil volume. It is mainly the root zone water balance. Water balance modeling is necessary to understand the change of water availability, distribution of glacial availability and water and food security. Hence the main water balance components of this study included: the total amount of precipitation falling on the subbasin during the time step, actual evapotranspiration from the basin and the net amount of water that leaves the basin and contributes to streamflow in the reach (water yield). The water yield includes surface runoff contribution to streamflow,lateral flow contribution to streamflow (water flowing laterally within the soil profile that enters the main channel), groundwater contribution to streamflow (water from the shallow aquifer that returns to the reach) minus the transmission losses (water lost from tributary channels in the HRU via transmission through the bed and becomes recharge for the shallow aquifer during the time step). Table 6-6 lists of the simulated water balance components on an annual average basis for Gilgelabay catchment over the calibration and validation period.

Table 6-6: Different mean Hydrological water balance components for GilgelAbay catchment for calibration and validation period

Period	Rainfall (mm)	ET (mm)	SW (mm)	PERC (mm)	SURQ (mm)	GW_Q (mm)	LAT_Q (mm)	WYLD (mm)
Calibration(2004-2010)	2058.99	563.36	45.56	1338.42	47.52	850.92	112.95	1008.40
	100.00	27.40	2.20	65.00	2.30	41.30	5.50	48.90
Validation(1998-2003)	1891.32	533.49	59.42	1215.15	42.62	771.56	101.45	913.15
	100.00	28.20	3.10	64.20	2.20	40.80	5.30	48.30

ET = evapotranspiration, SURQ = surface runoff, LATQ = lateral flow into stream, GW_Q =Ground water contribution to stream flow, WYLD = SURQ +LATQ + GW_Q - LOSSES, SW = soil water, PERC = percolation below root zone (groundwater recharge).

Table 6-7: Comparison table for the water balance component from studies conducted in the research area by different researcher.

Period	Period	Rainfall (mm)	ET (mm)	PERC (mm)	SURQ (mm)	GW_Q (mm)	LAT_Q (mm)
D.T Mengistu(Sensitivity of SWAT simulated stream flow to climate change within the eastern Nile River Basin)	calibration/validation	100/100	58/57	20/21	22/26	19/20	0.1/0.1
Shimelis G. Setegn(Hydrological Modeling in Lake Tana Basin using SWAT)	calibration/validation	100/100	65/56	21/29	8/8.6	11/20	6.2/7.2
Current study	calibration/validation	100/100	27/28	65/64	2.3/2.2	41/40	5.5/5.3

6.4. Comparison of daily actual evapotranspiration estimates of SEBS, MODIS and SWAT

The actual ET estimated in this study from SEBS could also compared with the ET obtained from the hydrological SWAT model which is resulted by validating the measured data in the study area and also with MODIS ET. However, studies suggested that actual ET derived from remote sensing data could be evaluated with regionally calibrated water balances (Bastiaanssen et al. 1998; Gao and Long 2008; Kite and Droogers 2000). In general, hydrological models are calibrated against time series of observed surface runoff at gauging stations and it is assumed that the actual ET estimate can be realistic after simulation of hydrological processes for a rational period.

The SEBS estimated actual ET over the Gilgelabay catchment is compared with estimates of actual ET derived from SWAT hydrological modeling for the same place. Since SEBS estimated actual ET values for days in the dry season were not realistic, the comparisons were made only

for actual ET estimates for November 27, 2005(DOY330), Dec-02-2007(DOY336) and Nov-27-2009(DOY 330). The actual ET from SEBS for the selected days was compared with the ET of the whole catchment using SWAT model and MOD16A2. The area of catchment covers about 1662Km^2. Table 6-8 presents the daily actual ET estimates for the selected wet season days from the SEBS, MOD16A2 and SWAT models for the Gilgelabay catchment based on SWAT delineation.

Table 6-8: Comparison of daily actual ET estimated by SEBS and SWAT models with 8 days MODIS aggregate MOD16 of the catchments for Nov 27-2005, Dec 2, 2007 and Nov 27, 2009.

Nov 27,2005			Dec 02-2007			Nov 27,2009		
SWAT [mm/d]	SEBS [mm/d]	MOD16 [mm/d]	SWAT [mm/d]	SEBS [mm/d]	MOD16 [mm/d]	SWAT [mm/d]	SEBS [mm/d]	MOD16A [mm/d]
1.08	7.2	1.14	2.08	5.8	1.2	2.03	5.1	1.2

The SEBS estimates which are changed to the instantaneous daily ET will be compared with the SWAT model ET estimate and also the SWAT estimated actual ET running from 2000-2010 were compared with MODIS ET. Due to limited availability of cloud free images for the study area, the MODIS terrestrial actual ET products, MODIS ET (MOD16A2) data, are used to assess the seasonal dynamics and long-term mean annual actual ET at the basin scale. Since global products like MODIS ET use general empirical relations as well as global meteorological data, it sometimes might not represent specific cases in specific locations. Therefore, first, the 8 day aggregated MODIS ET data were used to evaluate the spatial and temporal variability of the catchment to assess if it could show the same pattern with SEBS estimations. Following the mean monthly estimates from 2000-2010 were compared with SWAT for the catchment to evaluate if the estimates are comparable. The comparison will show the actual ET estimates from global dataset which could provide a comparable estimates with the hydrological model results for the study area in order to use the product directly for the catchment spatial and temporal actual ET variability evaluation.

Generally by comparing the 8 days aggregate actual ET from MODIS with the SEBS estimated daily actual ET summed over 8 days for the study area. The actual daily ET estimated by the

SEBS seems higher as compared to the 8days MODIS aggregate and also by the SWAT model estimate. Consequently this will lead us showing the compared actual ET value by SWAT and MODIS ET of the study area seems comparable but the actual ET by SEBS seems higher.

Therefore, the MODIS ET estimates which are aggregated 8 days are more or less comparable to SWAT model estimate as it can be shown below but SEBS ET estimate seems a bit higher. This will lead us further to compare SWAT ET estimate with the SEBS in order to use it for seasonal and mean annual evaluations over the study area.

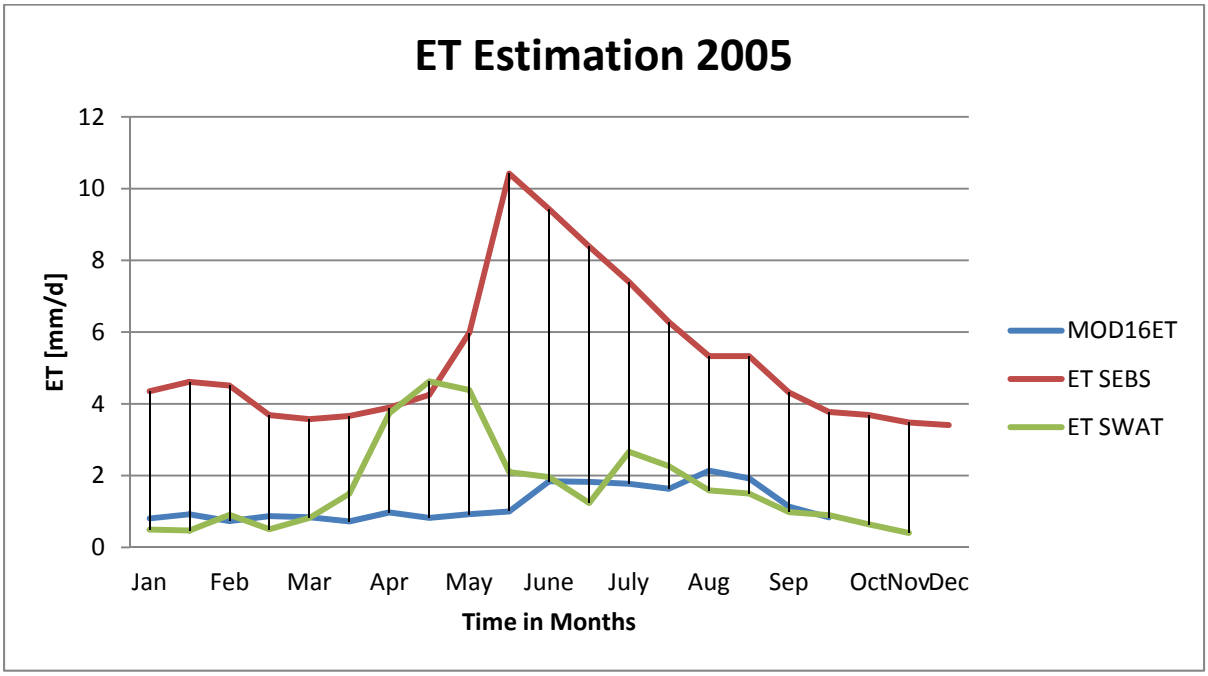

Figure 6-9: The scatter plot of mean monthly actual ET derived from MODIS and SEBS for the year2005

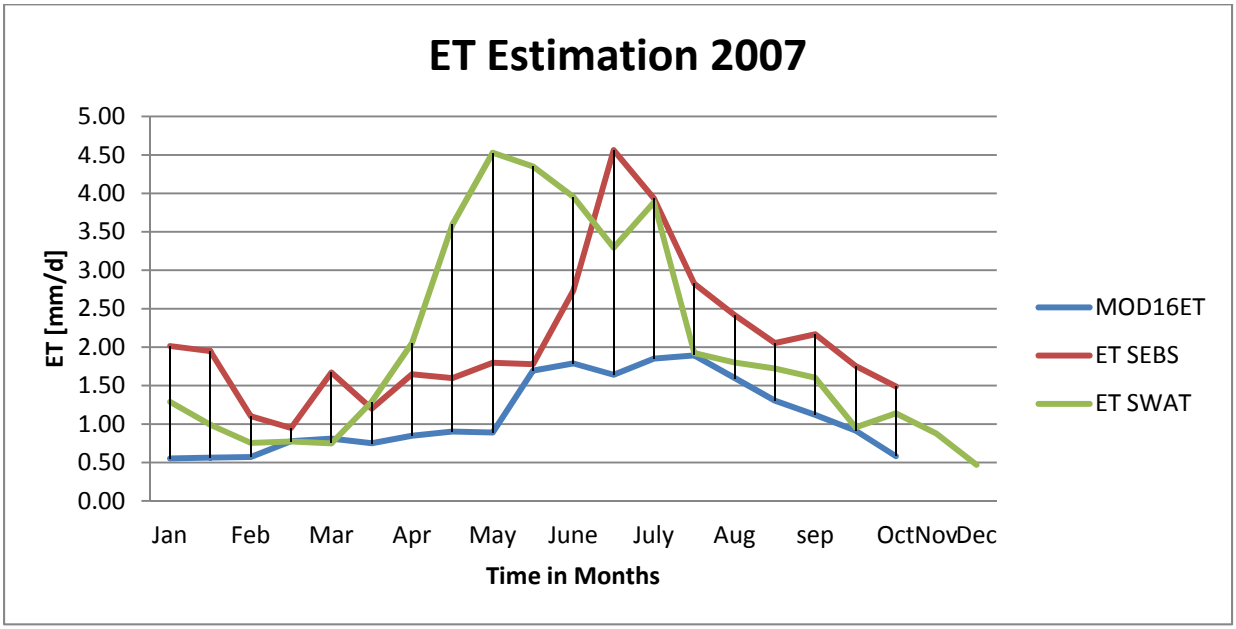

Figure 6-10: The scatter plot of mean monthly actual ET derived from MODIS and SEBS for the year 2007

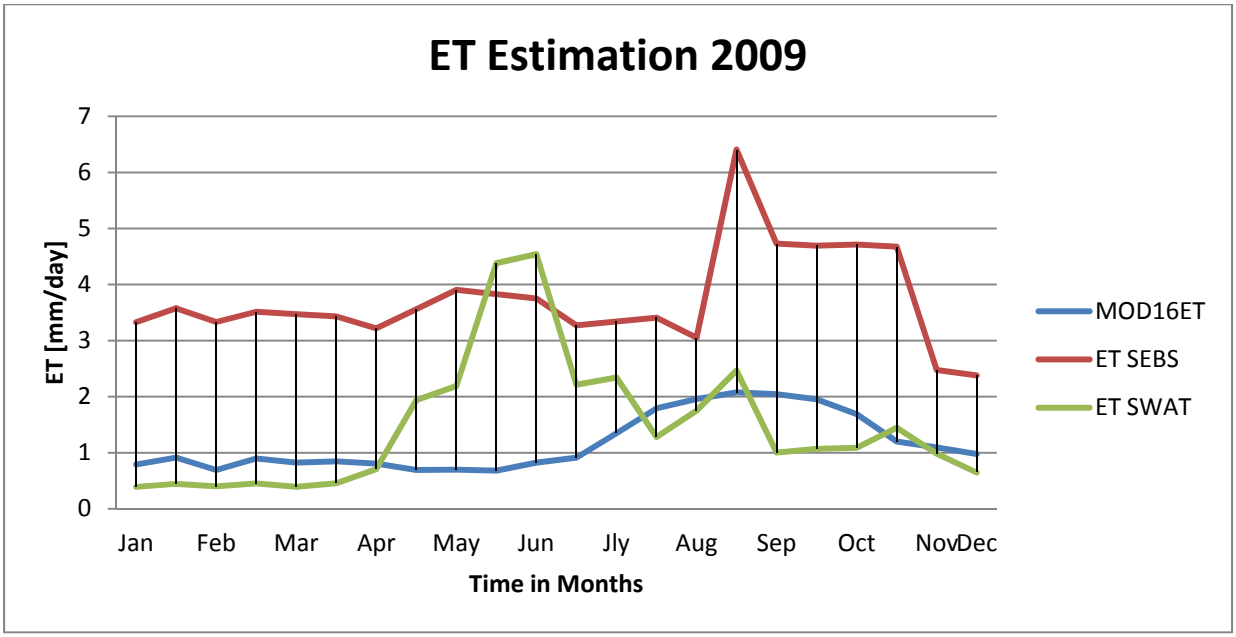

Figure 6-11: The scatter plot of mean monthly actual ET derived from MODIS and SEBS 2009

6.4. Comparison of annual actual evapotranspiration estimates from MODIS and SWAT

In this study the basin wide actual annual ET estimates from hydrological model SWAT studies with MODIS ET compared to investigate if actual ET derived from remote sensing data could show comparable estimates regionally. Setegn et al. (2008) applied SWAT to study the

hydrological balance of the Lake Tana basin. This study used measured weather and river discharge data from 1978 -2004.

Table 6-9: Summary of mean annual actual ET estimates over the Lake Tana basin estimated in different approaches: remote sensing, hydrological and SEBS as it represented in Tadesse A. (2012). Please note that the current study shows the actual ET estimate of the Gilgelabay catchment and the remote sensing approach covers only the vegetated land surface.

Duration	Mean annual actual ET [mm/ year]	Method/Model	Source
1981-1992	758(508)*2	SWAT	Setegn et al. 2008
1993-2004	782(532)*2	SWAT	Setegn et al. 2008
1991-1995	688(438)*2	SWAT	Demessie 2010
1978-2004	1248*1	SWAT	Setegn et al. 2008
2000-2009	491(607)	SWAT	Hiben,2012
2000-2010	460	MODIS	(http://www.ntsg.umt.edu/project/mod16)
2000-2010	389-411(366-370)	MODIS	Tadesse A,2012
2000-2010	594-622(660-725)	MODIS,SWAT	Current study

*1 refers to evaporation at the Lake Tana surface only.

*2 the values in bracket represents actual ET excluding the lake.

Setegn et al. (2008) estimated the mean annual evaporation from the lake to be 1248 mm year^{-1} and the lake water body accounts 20% of the total basin area (SMEC, 2008). So, the contribution from the lake is approximately 250 mm year^{-1}. The long-term mean annual actual ET from SWAT model for both periods compares well with MODIS estimates basin scale. The computed absolute differences between these estimates were 48 mm year^{-1} (1981-1992), 72 mm/ year (1993-2004) and 22 mm year^{-1} (1985-1995).

In MODIS ET, as noticed in the seasonal actual ET distribution, a higher mean annual actual ET were also observed in the southern part of the basin, where the largest tributary to the Lake Tana originates. On the other hand, the actual ET estimated by SWAT by Demissie (2010) shows

higher values in the central part of the Lake Tana basin. Overall the actual ET estimates of MODIS and SWAT for the Lake Tana Basin seem comparable (Tadesse, 2012).

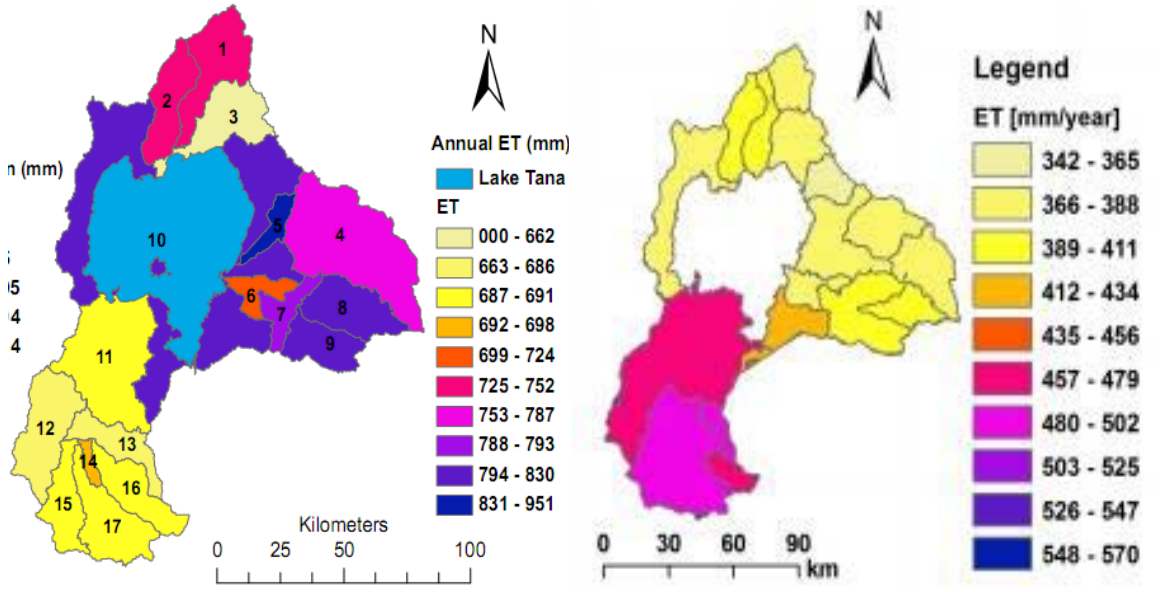

Figure 6-12: Mean annual ET of 1991-1995 from SWAT and MODIS (a) (Demissie 2010) and 2000-2010 from MODIS (b) for each sub-basin in the Lake Tana basin by (Tadesse A.2012)

It is clearly seen that actual evapotranspiration is observed in September is high. During this time most of the agricultural area is covered by different crops with their developing stage and the surface soil moisture content is also high in most of the area. Since rainy season in the area starts in June and ends around October, the high moisture content and ground water level is expected during this times so that the ET gets potential to be maximum.

Generally the actual ET estimated by SEBS and SWAT shows a visible difference and SEBS estimate shows us higher values and compare with seasonal variations of the study area. From field data the observed discharge is low in December to May. Since the season (with little rainfall in April) is dry and most of the agricultural fields are not covered by crops so that ET is expected to be low in this time. When the rainy season starts on June ET gradually increases up to September and then starts to decline again.

Table 6-10: Comparison table showing Mean annual MOD16A2 SWAT actual ET estimation

Period(Year)	MOD16A2 Mean annual actual ET [mm/ year]	SWAT annual actual ET[mm/year]
2005	622	725.6
2007	625	696.9
2009	594	660.4

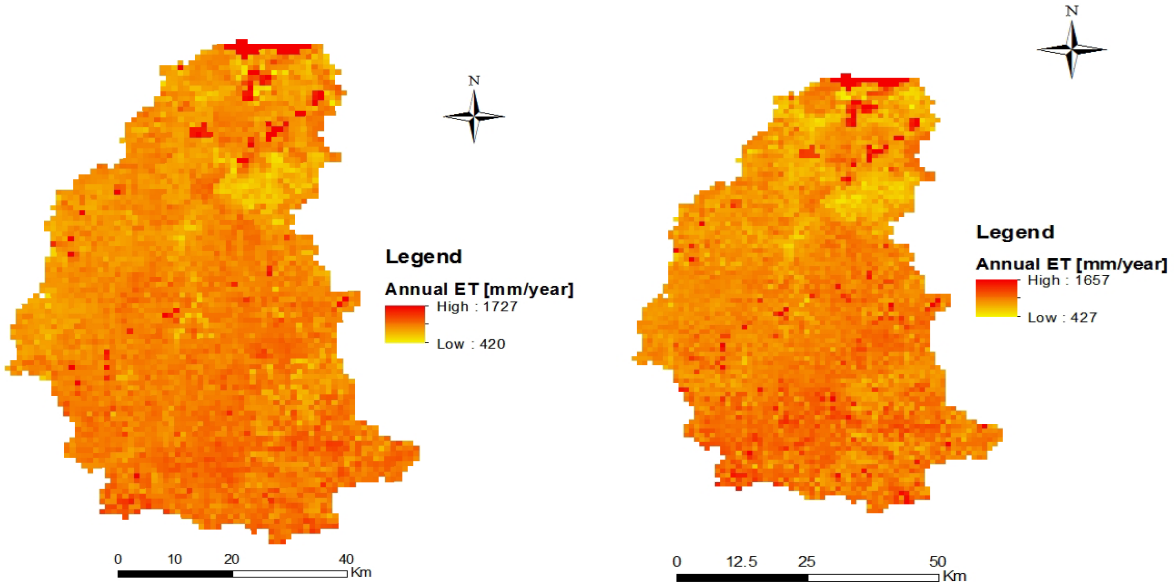

a) b)

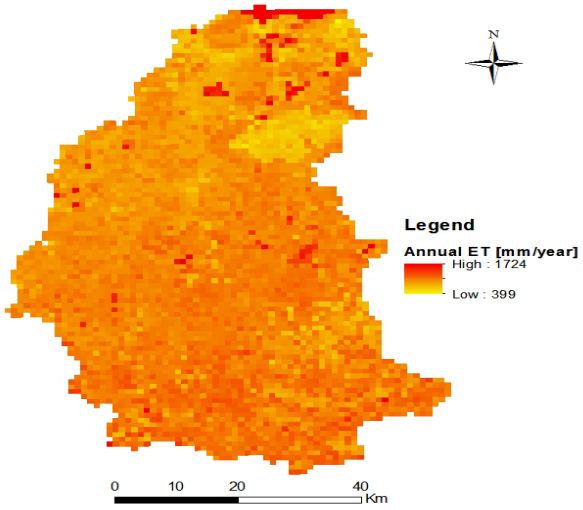

c)

Figure 6-13: Mean annual ET resulted from MOD16A2 for the year a)2005, b) 2007 and c)2009

6.6. Discussion

In this study the SEBS algorithm has been used to estimate the actual ET of a catchment for nine selected cloud free days that are assumed to represent wet and dry season conditions. These estimates are also compared with SWAT hydrological model and MODIS ET estimate resulted from remote sensing. The spatially variable land surface parameters collected from MODIS were enhanced with ground meteorological and solar radiation data.

Spatially, the land surface parameters such as land surface temperature and NDVI do not vary significantly within a season which is attributed to the fact that about 70% of the terrestrial part of the basin is used for rain fed agriculture. Therefore, as shown in Table 6.11, the statistics for the parameters at 1km spatial resolution revealed lower standard deviations from the mean. However, it was noted that the biophysical characteristics of the catchment varies significantly between seasons. For the selected wet season days the surface temperature is relatively lower and dominant part of the landscape is covered by crops and grasses with mean NDVI value up to 0.67 (Sept-11-2009) while during the dry season days the mean land surface temperature reaches up to 314 K (Mar-21-2007) and as expected the vegetation cover declines significantly; the lowest mean NDVI observed was 0.29 in Mar-12-2007. Generally, it was noted that the seasonal land surface characteristics were reflected well from the remotely sensed MODIS data of the catchment.

The SEBS actual ET estimates were realistic for January 01-2005, January 10, 2007 and Sept-11-2009 but a bit exaggerated on the other days. Though there is no measured data to directly compare these results, the SEBS ET results were compared with SWAT hydrological model estimated for the catchment. The comparative results were presented below. Given the fact that distributed hydrological model simulation is basically constrained based on measured precipitation and runoff and other spatially detailed information such as soil and land-use type, the actual ET estimations could be reliable and can be used as an option for validation (Bastiaanssen et al. 1998).

Table 6-11: Summary statistics of important land surface parameters of Gilgelabay Catchment.

	LST[k]		LAI[-]		NDVI[m2/m2]		KB-1[-]	
	Mean	STD	Mean	STD	Mean	STD	Mean	STD
January 1,2005	308.9	2.27	0.83	0.14	0.34	0.06	12.7	2.2
Feb 11,2005	313.2	2.38	0.73	0.11	0.29	0.05	10.7	1.8
April 1,2005	310.3	4.1	0.74	0.13	0.29	0.06	11.4	3.1
January 10,2007	307.1	2.06	0.91	0.18	0.37	0.07	11.4	2.5
March 12,2007	312.3	3.56	0.72	0.12	0.29	0.05	11.5	2.8
December 2,2007	305.8	2.5	1.10	0.18	0.44	0.07	9.6	2.7
March 30,2009	313.7	4.9	0.69	0.12	0.27	0.06	11.6	2.0
September11 ,2009	291.6	2.56	1.87	0.29	0.67	0.08	12.1	2.6
November 27,2009	304.2	5.6	1.08	0.21	0.44	0.08	9.8	3.2
April 1,2009	310.3	4.7	0.74	0.13	0.29	0.06	11.4	3.1

Based on the observation from this research the SEBS model showed a more or less a good performance at the basin scale, nevertheless, its actual ET estimates for the four dry season days (i.e. Jan-01-2005, Feb-12-2005, Mar-12-2007, Nov 27,2009 and Dec-2-2007) were found to be overestimated. As observed in this study and also mentioned in many studies the most sensitive parameter in surface energy balance models is surface radiance temperature. Therefore, a qualitative plausibility and consistency checking on the primary input remotely sensed LST together with NDVI and reflectance were carried out and noted to be reliable. The other important variable for the precise estimation of sensible heat flux is the roughness length for heat transfer (Su et al. 2001). As mentioned in many literatures the empirical formulation for the estimation of excess resistance for heat transfer, kB^{-1}, and in turn z_0h is noted to be highly uncertain in sparse vegetation cover in single-source models (Su et al. 2001). For the dry season days, it was observed that in the study area, the surface vegetation cover declines significantly which is linked to the lower NDVI values related to lower crop cover (Table 6-8). In fact this is a common trend for a region where rain fed agriculture is the dominant land-cover type because

the farming practice is only following the rainy season and hence there is no much crop cover during dry season.

The SEBS model estimated higher kB^{-1} for dry season days with mean values ranging from 12.70 (Jan-01-2005) and 9.6 (Dec-2-2007). Furthermore, it was noticed that kB^{-1} values are relatively higher for areas with lower canopy height. Therefore, it could be concluded that the overestimation of the kB^{-1} values in the current SEBS model resulted in underestimation in the estimated sensible heat flux and thus, higher actual ET during dry season. Even though, the LST data was assumed to be reliable, perhaps, the larger uncertainty in kB^{-1} could be also partly correlated with this parameter.

The daily actual ET estimated by SEBS was also observed to be comparable with the MODIS ET. Since the MODIS ET is available on 8 day temporal resolution, the comparison with SEBS daily estimates was done using simple but reasonable assumptions.

In theory, the amount of actual ET flux from the land surface to the atmosphere is governed by the amount of soil moisture available at the surface; and this in turn is mainly affected by the climatic condition, specifically the rainfall distribution. The analysis of the MODIS monthly ET from 2000-2010 showed the marked seasonal change of actual ET with the lowest actual ET occurring just before the rainy season, and the peak was observed to be at the end of the rainy season. The higher actual ET during the wet season is associated with the availability of ample soil moisture at the surface. The irregular rainfall distribution in March, April and May in the study area could not be reflected in the MODIS ET this could be because of the vegetation response to small amount of rainfall distribution is insignificant during these months. Therefore, the actual ET estimated in SWAT could better account soil moisture contribution to actual ET than the MODIS ET.

7. Conclusions and recommendations

7.1 Conclusion

The main objective of this study is to use SEBS technique and SWAT hydrological model for the spatial and temporal evaluation of daily actual ET using remote sensing and ground meteorlogical data for Gilgelabay catchment. Comparisons with actual ET estimates derived from MODIS, SWAT and SEBS models were also made and the seasonal dynamics and the mean annual ET over the study area were evaluated using these data. The estimations of daily actual ET for a few selected representative wet and dry season days using the SEBS algorithm were mainly dependent on remotely sensed data obtained from MODIS land surface products and ancillary ground data. Therefore, the results presented provided an insight on the variation of actual ET at 1 km, sub-basin and basin spatial scale and temporally at daily, seasonal and annual scale. However the study findings provide useful result into the spatial and temporal variability of actual ET in the catchment and the following conclusions can be drawn:

- The SEBS model was highly sensitive to changes in LST and atmospheric pressure. This is due to the higher dependence of surface energy balance models on the LST to estimate the sensible heat flux as well as outgoing long wave radiation from the surface.
- For the selected days in the dry season the daily actual ET estimates by the SEBS model were exaggerated and over estimated. Thus, the model showed unreliable performance in the study area. This lead the SEBS model to underestimates the sensible heat flux and allocates a higher latent heat flux.
- The MODIS ET product showed good agreement with results from the SWAT models both in magnitude and spatial variability. It probably gives better spatial results than SWAT; therefore, this product could be a valuable resource to hydrological studies in this region.
- The mean annual actual ET estimates from pervious hydrological studies using SWAT and MODIS ET showed a good agreement at the basin scale. Spatially, based on the remote sensing MODIS ET data the southern part of the basin showed a slightly higher actual ET flux while the north eastern part observed to have lowest mean annual values. These observations are consistent with rainfall distribution as well as the land-cover types in the basin.

- The SWAT hydrological model was calibrated for stream flow manually by using 7 years data. The model performance result showed that R^2 and ENS value during the calibration period at Merawi station were 78% and 75% on daily time series. Similarly, during the validation period R^2 and ENS on daily and monthly time step were 74%, and 73%. The result obtained from the SWAT model fulfilled the requirements suggested by Santhi *et al.* (2001) for R^2 >0.6 and ENS >0.5 so that the model can be applied to the Gilgel Abbay catchment to simulate the flow and to develop model parameters.

7.2 Recommendation

The SEBS model application to estimate actual ET and eventually, to evaluate its spatial and seasonal variability over the Gilgelabay catchment were fulfilled for the selected days in the wet season. The comparison of these results with the SWAT model estimates and MODIS ET showed some what good performance. However, the estimations for the dry season days were overestimated and a bit exaggerated compared to the wet season estimates. Thus, for future detailed study has to be taken in order:

- To achieve a more accurate estimation of sensible heat flux and actual ET field experiment like using scintilometer and eddy correlation will be an advantageous.
- The availability of continuous record of hydrological and meteorological data makes it possible in the near future to carry out a complete water balance and modeling in the study area whereby it can offer the possibility of validation of the remote sensing result.
- In this study only Thirteen years data (1998 - 2010) were used for calibration and validation process of SWAT model. However, it is recommended to use a longer time series data for the calibration and validations of the models. Moreover, during the selection of data years for the study, it is more convenient to consider longer time series data in order to select the more consistent data years for the study.
- The range of DEM grid cell sizes applied in this study was 90 by 90m resolution. Therefore the model performance can be checked for those finer resolution DEMs in the future.
- In this study the SWAT model is calibrated only using flow data and for the future calibrating the model using other water balance components such as ET, Soil moisture etc can be vital to characterize the catchment very well.

References

1. Abdo, K. S.Fiseha, B. M.Rientjes, T. H. M.Gieske, A. S. M.Haile, A. T. (2009). Assessment of climate change impacts on the hydrology of Gilgelabay catchment in Lake Tana basin, Ethiopia. Journal Hydrological processes: an international journal, 23(6), 3661-3669.
2. Ahmed A (2012) Satellite based evapotraspiration estimation and runoff simulation: a topmodel application to the Gilegel Abbay catchment, Ethiopia. MSc, University of Twente
3. Anderson, M. C., J. M. Norman, G. R. Diak, W. P. Kustas and J. R. Mecikalski, 1997. A two-source time-integrated model for estimating surface fluxes using thermal infrared remote sensing. *Remote Sensing of Environment*. 60, 195-216
4. Bastiaanssen WGM, Menenti M, Feddes RA et al (1998) A remote sensing surface energy balance algorithm for land (SEBAL). 1. Formulation. Journal of Hydrology 212–213: 198-212 DOI 10.1016/s0022-1694(98)00253-4
5. BCEOM (1999), Abay River Basin integrated master plan, main report, MoWR, AddisAbaba, Ethiopia
6. Brutsaert, W., 1982. *Evaporation into the atmosphere.* D. Reidel, 299pp.
7. Brutsaert W (1986) Catchment-scale evaporation and the atmospheric boundary layer Water Resour Res 22: 39S-45S DOI 10.1029/WR022i09Sp0039S
8. Brutsaert W (1999) Aspects of bulk atmospheric boundary layer similarity under free-convective conditions. Rev Geophys 37: 439-451 DOI 10.1029/1999rg900013
9. Brutsaert, W (2005) Hydrology: An introduction Cambridge: Cambridge University Press.
10. Carlson TN, Ripley DA (1997) On the relation between NDVI, fractional vegetation cover, and leaf area index. Remote Sensing of Environment 62: 241-252 DOI 10.1016/s0034-4257(97)00104-1
11. Chehbouni A, Lo Seen D, Njoku EG et al (1997) Estimation of sensible heat flux over sparsely vegetated surfaces. Journal of Hydrology 188–189: 855-868 DOI 10.1016/s0022-1694(96)03174-5
12. Chow, V. T., D. R. Maidment, and L. W. Mays, 1988. *Applied hydrology.* McGraw Hill, Newyork .
13. Cleugh HA, Leuning R, Mu Q et al (2007) Regional evaporation estimates from flux tower and MODIS satellite data. Remote Sensing of Environment 106: 285-304 DOI 10.1016/j.rse.2006.07.007
14. Conway D (1997) A water balance model of the Upper Blue Nile in Ethiopia. Hydrological Sciences Journal 42: 265-286 DOI 10.1080/02626669709492024
15. Courault *et al*. (2005) Use of remote sensing for evapotranspiration monitoring over land surfaces Estimation from Remotely Sensed Data. Hydrological Sciences Journal 25: 295-316 DOI
16. Conway. D. (2000). "The Climate and Hydrology of the Upper Blue Nile River." The Geographical Journal 166(1): 49-62.
17. Davin E, Stöckli R, Jaeger E et al (2011) COSMO-CLM: a new version of the COSMO-CLM model coupled to the Community Land Model. Climate Dynamics 37: 1889-1907 DOI 10.1007/s00382-011-1019-z

18. de Jong K (2009) Aguila Documentation. Release 1.1.0, Utrecth, The Netherlands.
19. Demissie GA (2010) Integrated Sediment Transport Modeling using SWAT-MOHID Models in the Lake Tana Subbasin, Upper Blue Nile, Ethiopia MSc, UNESCO-IHE
20. Dingman, S.L. (2002), Physical Hydrology (2nd ed.), Prentice Hall Inc., USA ERA Interim. URL:http://data-portal.ecmwf.int/data/d/interim_daily/ (2012). Cited May 20 2012Geospatial Data Abstraction Library. URL:http://gdal.org/ (2012). Cited March 10 2012
21. Gumindoga, Webster , Hydrologic impact of Landuse change in the upper Gilgelabay River Basin2010,ITC,Netherlands
22. Jia L, Su Z, van den Hurk B et al (2003) Estimation of sensible heat flux using the Surface Energy Balance System (SEBS) and ATSR measurements. Physics and Chemistry of the Earth, Parts A/B/C 28: 75-88 DOI 10.1016/s1474-7065(03)00009-3
23. Jia L, Xi G, Liu S et al (2009) Regional estimation of daily to annual regional evapotranspiration with MODIS data in the Yellow River Delta wetland. Hydrol Earth Syst Sci 13: 1775-1787 DOI 10.5194/hess-13-1775-2009
24. Justice CO, Townshend JRG, Vermote EF et al (2002) An overview of MODIS Land data processing and product status. Remote Sensing of Environment 83: 3-15 DOI 10.1016/s0034-4257(02)00084-6
25. Kalma J, McVicar T, McCabe M (2008) Estimating Land Surface Evaporation: A Review of Methods Using Remotely Sensed Surface Temperature Data. Surveys in Geophysics 29: 421-469 DOI 10.1007/s10712-008-9037-z
26. Kebede S, Travi Y, Alemayehu T et al (2006) Water balance of Lake Tana and its sensitivity to fluctuations in rainfall, Blue Nile basin, Ethiopia. Journal of Hydrology 316: 233-247 DOI 10.1016/j.jhydrol.2005.05.011
27. Kustas, W.P. and Daughtry, C.S.T., 1989. Estimation of the soil heat flux/net radiation ratio from spectral data. *Agric. Forest. Meteorol.,* 49, 205–223.
28. Kustas WP, Norman JM (1996) Use of remote sensing for evapotranspiration monitoring over land surfaces. Hydrological Sciences Journal 41: 495-516 DOI 10.1080/02626669609491522
29. Kustas WP, Pinker RT, Schmugge TJ et al (1994) Daytime net radiation estimated for a semiarid rangeland basin from remotely sensed data. Agricultural and Forest Meteorology 71: 337-357 DOI 10.1016/0168-1923(94)90019-1
30. LA Gibson*1,4, C Jarmain2, Z Su3 and FE Eckardt4(2013) Estimating evapotranspiration using remote sensing and the Surface Energy Balance System – A South African perspective
31. Lal P. Muthuwatta (2010) Estimating the spatial variability of water consumption in the Karkheh river basin, Iran - using MODIS data. AQUA mundi (2010) - Am02015: 115 - 122
32. Lhomme JP, Chehbouni A, Monteny B (2000) Sensible Heat Flux-Radiometric Surface Temperature Relationship Over Sparse Vegetation: Parameterizing B-1. Boundary-Layer Meteorology 97: 431-457 DOI 10.1023/a:1002786402695
33. Liang S (2001) Narrowband to broadband conversions of land surface albedo I: Algorithms. Remote Sensing of Environment 76: 213-238 DOI 10.1016/s0034-4257(00)00205-4
34. Li Z-L, Tang R, Wan Z et al (2009) A Review of Current Methodologies for Regional Evapotranspiration Estimation from Remotely Sensed Data. Sensors 9: 3801-3853

35. Mauser W, Schädlich S (1998) Modelling the spatial distribution of evapotranspiration on different scales using remote sensing data. Journal of Hydrology 212–213: 250-267 DOI 10.1016/s0022-1694(98)00228-5
36. Melesse AM, Oberg J, NangiaA V, Beeri O and Baumgartner D (2006) Spatiotemporal dynamics of evapotranspiration at the Glacial Ridge prairie restoration in northwestern Minnesota. *Hydrol. Process.* 20 1451-1464.
37. Mohamed YA, Savenije HHG, Bastiaanssen WGM et al (2005) New lessons on the Sudd hydrology learned from remote sensing and climate modeling. Hydrol Earth Syst Sci Discuss 2: 1503-1535 DOI 10.5194/hessd-2-1503-2005
38. Monteith, J.L., 1973. *Principles of environmental physics*. Edward Arnold Press. 241 pp.
39. Mu Qz, Heinsch Fa, Zhom and Running SW (2007) Development of a global evapotranspiration algorithm based on MODIS and global meteorology data. *Remote Sens. Environ.* 111 519-536.
40. Mu Q, Zhao M, Running SW (2011) Improvements to a MODIS global terrestrial evapotranspiration algorithm. Remote Sensing of Environment 115: 1781-1800 DOI 10.1016/j.rse.2011.02.019
41. Mutiga JK, Su Z, Woldai T (2010) Using satellite remote sensing to assess evapotranspiration: Case study of the upper Ewaso Ng'iro North Basin, Kenya. International Journal of Applied Earth Observation and Geoinformation 12, Supplement 1: S100-S108 DOI 10.1016/j.jag.2009.09.012
42. Neitsch (a), S.L., J.G. Arnold, J.R. Kiniry, J.R. Williams, K.W. King , 2002. Soil and Water Assessment Tool (SWAT) Theoretical Documentation, Version 2000,Grassland Soil and Water Research Laboratory, Blackland Research Center, Texas Agricultural Experiment Station, Texas Water Resources Institute, Texas Water Resources Institute, College Station, Texas, 506pp.
43. Paulos, S., 1998. Establishing water release rules for Koka Reservoir for wet seasons. M.Sc. Thesis, Addis Ababa University, Ethiopia.
44. Peters, S. W. M., 1995. Energy- and water-balance modeling of a semi arid area using remote sensing. PhD Thesis, Vrije Universiteit, Amsterdam, 256pp
45. Refsgaard, J.C. and B. Storm (1996), Construction, calibration and validation of hydrological models, in: Bayesian estimation of parameters in a regional hydrological model, In: Engeland, K. and L. Gottschalk (2002), Hydrology and Earth System Sciences 6(5), 883–898.
46. Santhi, C., J.G. Arnold, J.R. Williams, W.A. Dugas, R. Srinivasan, and L.M.Hauck,October 2001. Validation of the SWAT Model on a Large River Basin with Point andNonpoint Sources, Journal of the American Water Resources Association, Vol. 37,No. 5, 1169-1188pp
47. Setegn SG, Srinivasan R, Dargahi B (2008) Hydrological Modelling in the Lake Tana Basin, Ethiopia Using SWAT Model. The Open Hydrology Journal 2: 49-62
48. Shaka, A. K. (2008). Assessment of climate change impacts on the hydrology of gilgel abbay catchment in lake tana basin, ethiopia. ITC, Enschede.
49. Shan X, van de Velde R, Wen J et al (2008) Regional Evapotranspiration over the arid inland heihe river basin in northwest China, Dragon 1 Programme Final Results, Beijing,China.

50. Sintondji C., October 2005: Modelling the Rainfall-Runoff Process in the Upper Queme catchment (Terou in Benin Republic) in a Context of Global Change:Extrapolation from the Local to the Regional Scale. PhD Dissertation, 78-82pp
51. SMEC. (2007). Hydrological study of the Tana and Beles sub basin –Interception report. SMEC International pty Ltd, Addis Ababa, Ethiopia.
52. Su Z (2002) The Surface Energy Balance System (SEBS) for estimation of turbulent heat fluxes. Hydrol Earth Syst Sci 6: 85-100 DOI 10.5194/hess-6-85-2002
53. Su H, Overgaard McCabe MF, Wood EF et al (2006) Modeling Evapotranspiration during SMACEX: Comparing Two Approaches for Local- and Regional-Scale Prediction. Journal of Hydrometeorology 6: 910-922 DOI 10.1175/jhm466.1
54. Sun Z, Gebremichael M, Ardö J et al (2011) Mapping daily evapotranspiration and dryness index in the East African highlands using MODIS and SEVIRI data. Hydrol Earth Syst Sci 15: 163-170 DOI 10.5194/hess-15-163-2011
55. Tadesse Alemayhu (2012), Evaluation of Actual Evapotranspiration Using Remote Sensing products and Its Comparison with Estimates from other Models: a Case Study of the Lake Tana Basin, MSc Thesis UNESCO-IHE, Delft, Netherlands.
56. Terra: The EOS Flagship. URL:http://terra.nasa.gov/ (2012). Cited April, 15 2012 Global Terrestrial Evapotranspiration Data Set.URL:http://www.ntsg.umt.edu/project/ mod16 (2012). Cited May 10 2012 OpenEV software library and application. URL:http://openev.sourceforge.net/ (2012). Cited April 05 2012
57. Tessema, S.M. (2006), Assessment of temporal hydrological variations due to land use changes using remote sensing/GIS: a case study of Lake Tana Basin, Master Thesis, KTH, Sweden.
58. Timmermans J, van der Tol C, Verhoef A et al (2011) Quantifying the uncertainty in estimates of surface- atmosphere fluxes through joint evaluation of the SEBS and SCOPE models. Hydrol Earth Syst Sci Discuss 8: 2861-2893 DOI 10.5194/hessd-8-2861-2011
59. Valor, E. and V. Caselles, 1996. Mapping land surface emissivity from NDVI: Application to European, African, and South American Areas. *Remote Sensing of Environment*. 57(3): 167-184.
60. Van Dam O (2000) Modelling incoming potential radiation on a land surface with PCRaster: Potrad5.Mod manual. PhD, Utrecht University
61. van der Kwast J, Timmermans W, Gieske A et al (2009) Evaluation of the Surface Energy Balance System (SEBS) applied to ASTER imagery with flux-measurements at the SPARC 2004 site (Barrax, Spain). Hydrol Earth Syst Sci 13: 1337-1347 DOI 10.5194/hess-13-1337-2009
62. van der Kwast J, Timmermans W, Gieske A et al (2010) Evaluation of the Surface Energy Balance System (SEBS) applied to ASTER imagery with flux-measurements at the SPARC 2004 site (Barrax, Spain). Hydrol Earth Syst Sci Discuss 6: 1165-1196 DOI 10.5194/hessd-6-1165-2009
63. Verhoef, A. and G. McNaughton, 1997. A parameterization of momentum roughness length and displacement height for a wide range of canopy densities. *Hydrology and Earth System Sciences.* 1(1): 81-91.

Appendices

Appendix 1 - Python script for converting MODIS HDF data to raster and PCRaster formats

```
usr/bin/env python
# -*- coding: utf-8 -*-
# Import modules
import sys
import os, glob
import numpy as np
import PCRaster as pcr
# This script converts MODIS HDF images to GeoTiFF then to PCRaster maps
path=os.getcwd() # dir_path = "D:\"
clone = pcr.readmap(os.path.join(path,"clone.map"))# clone map of the Lake Tana basin
def find_nearest(datelist,date):
""" a function to to look for the closest date
for MOD13A1 and MOD09A1 in accordnace with the daily MOD11A1 """
idx=(np.abs(datelist-date)).argmin()
return datelist[idx] # the closet date to the value from the dateCodeList
def translate_tif2map(filename,OutputFilename):
""" This converts GeoTiff formatted files to PCRaster
readable map format"""
cmd = "gdal_translate -of PCRaster -ot Float32 %s %s" %(filename, outputFilename)
return os.system(cmd)
def translate_hdf2tif(fileName,outputFilename):
cmd = "gdal_translate -of GTiff -a_srs SR-ORG: 6842 :HDF4_EOS:EOS_GRID:%s %s"
%(fileName,outputFilename
return os.system(cmd)
def reproject_sin2utm(filename, outputFilename):
cmd = "gdalwarp -s_srs SR-ORG:6842 EPSG:32637 -t_srs PROJCS[\"WGS 84 / UTM zone
37N\",GEOGCS[\"WGS %s %s" %(filename, outputFilename)
return os.system(cmd)
def ScaleCorrection(filename, scale):

""" This corrects the scale in MODIS data
in PCRaster format"""
pcr.setclone(filename)
modisProduct = pcr.readmap(filename)
CorrectionFactor =pcr.scalar(scale)
CorrectedProduct = modisProduct * CorrectionFactor
return CorrectedProduct
def resample_1000(filename,outputfileName, clone):
""" This resamples MOD09A1 and MOD13A1
to 1000 meters"""
cmd = "resample --clone clone.map %s %s " % (filename,outputfileName)
return os.system(cmd)
def studyarea(outputFilename_covered,outputName):
""" Cropping the study area
based on the clone map"""
cmd = "pcrcalc %s = clone.map * %s" % (outputFilename_covered, outputfileName)
return os.system(cmd)
def VegetationCover(map):
""" calculates the fractional vegetation cover using NDVI values
based on Carlson and Ripley (1997)"""
```

```
NDVI = pcr.readmap(map)
NDVImin = pcr.mapminimum(map)
NDVImax = pcr.mapmaximum(map)
VegCover = ((NDVI - NDVImin)/(NDVImax - NDVImin))**2
return VegCover
def broadbandalbedo(band):
""" Calculates the broadband albedo using land surface refelectance map
based on Liang (2000) """

# coefficients list
C = [0.160,0.291,0.243,0.116,0.112,0.081]
D = pcr.scalar(0.0015)
albedo = band[0]* pcr.scalar(C[0]) + band[1] * pcr.scalar(C[1]) + band[2] * pcr.scalar(C[2]) + band[3]*
pcr.scalar(C[3]) + band[4] * pcr.scalar(C[4])+ band[6] * pcr.scalar(C[5])- D
return albedo
def emissivity(inputmap):
""" calculates the broadband surface emissivity using vegetation cover map
based on Valor and Caselles (1996)"""
fullVeg_Cover = pcr.scalar(0.985)# emissivity for full vegetation cover
baresoil = pcr.scalar(0.96) # emissivity for bare soil
totalarea = pcr.scalar(1.0)
Emissivity = fullVeg_Cover*inputmap + baresoil*(totalarea-inputmap)
return Emissivity
# Conversion for MOD11A1
dateCodeList = [] # list the year and date
for filename in glob.glob(os.path.join(path, 'MOD11A1*.hdf')): # Location of MOD11A1
if filename[-23]!= '7': # Tile location h21v7
continue
# read the aquisition date and year from filename of LST
dateCode = filename[-36:-29]
dateCodeList.append(int(dateCode))
fileName= filename + ":MODIS_Grid_Daily_1km_LST:LST_Day_1km"
# define the directory for the output GeoTiff images using the datecode
if not os.path.exists(os.path.join(path,dateCode)):
os.makedirs(os.path.join(path,dateCode))
# define the output filename directory path
outputFilename = os.path.join(path,dateCode,"LST_Day_1km.tif")
# HDF to GeoTiff with SR-ORG projection 6842

translate_hdf2tif(fileName, outputFilename)
# Conversion for MOD09A1
for filename in glob.glob(os.path.join(path, 'MOD09A1*.hdf')): # Location of MOD09A1
if filename[-23]!= '7': # Tile location h21v7
continue
# read the aquisition date and year from filename of reflectance
dateCode = filename[-36:-29]
# Checking if the directory is already generated by LST dateCode
if os.path.exists(os.path.join(path,dateCode)):
for band in range(1,8): # reflectance band
fileName = filename + ":MOD_Grid_500m_Surface_Reflectance:sur_refl_b0%s" % band
# Define output file name directory path using date code and band number
outputFilename = os.path.join(path,dateCode,"sur_refl_b0%s_0.tif") % str(band)
# HDF 2 GeoTiff with SR-ORG projection 6842
translate_hdf2tif(fileName, outputFilename)
else:
```

```
""" when the LST date of MOD11A1 does not match with reflectance date
Define output file name using the nearest date from MOD11A1
date code list and band number"""
for band in range(1,8):
# Looking for the nearest date to avilable MOD11A1 date list
newDateCode = find_nearest(np.array(dateCodeList),int(dateCode))
dateCodeDiff = abs(newDateCode - int(dateCode))
fileName = filename + ":MOD_Grid_500m_Surface_Reflectance:sur_refl_b0%s" % band
if dateCodeDiff <= 8:
outputFilename = os.path.join(path,str(newDateCode),"sur_refl_b0%s_%s.tif") % (str(band),str(dateCodeDiff))
# HDF to GeoTiff format with SR-ORG projection 6842
translate_hdf2tif(fileName, outputFilename)

# Conversion for MOD13A1
for filename in glob.glob(os.path.join(path, 'MOD13A1*.hdf')): # Location of MOD13A1
if filename[-23]!= '7':
continue
dateCode = filename[-36:-29]
fileName = filename + ":MODIS_Grid_16DAY_500m_VI:\"500m 16 days NDVI\""
if os.path.exists(os.path.join(path,dateCode)):
outputFilename = os.path.join(path,dateCode,"NDVI_0.tif")
# HDF to GeoTiff format with SR-ORG projection 6842
translate_hdf2tif(fileName, outputFilename)
else:
newDateCode = find_nearest(np.array(dateCodeList),int(dateCode))
dateCodeDiff = abs(newDateCode - int(dateCode))
if dateCodeDiff <= 16:
outputFilename = os.path.join(path,str(newDateCode),"NDVI_%s.tif") %str(dateCodeDiff)
# HDF to GeoTiff format with SR-ORG projection 6842
translate_hdf2tif(fileName, outputFilename)
# Reprojection from SR-ORG projection 6842 to WGS 1984 UTM
for dateCode in dateCodeList: # the folder with date and year of image acquisition
# Location of MOD09A1 in GeoTiff format
for filename in glob.glob(os.path.join(path, str(dateCode),'sur_refl_b0*.tif')):
dateDiff= filename[-6:-4]
bandNumber = filename[-7]
# Define the output file name using the difference with LST acquisition date
outputName = "Reprojected_sur_refl_b0%s%s.tif" %(str(bandNumber),dateDiff)
# define output filename directory path
outputFilename = os.path.join(path,str(dateCode),outputName)
# SR-ORG projection 6842 to WGS 1984 UTM

reproject_sin2utm(filename,outputFilename)
# Location of the reprojected MOD09 GeoTiff images
for filename in glob.glob(os.path.join(path, str(dateCode),'Reprojected_sur_refl_b0*.tif')):
dateDiff= filename[-6:-4]
bandNumber = filename[-7]
# Define the output file name using the difference with LST date
outputName = "sur_refl_b0%s%s.map" %(str(bandNumber),dateDiff)
# define output filename directory path
outputFilename = os.path.join(path,str(dateCode),outputName)
# GeoTiff to PCRaster map
translate_tif2map(filename, outputFilename)
# Location of MOD11A1 in GeoTiff format
for filename in glob.glob(os.path.join(path,str(dateCode),"LST_Day_1km.tif")):
```

```
# Define output file name directory path
outputFilename = os.path.join(path,str(dateCode),"Reprojected_LST_Day_1km.tif")
# SR-ORG projection 6842 to WGS 1984 UTM
reproject_sin2utm(filename,outputFilename)
for filename in glob.glob(os.path.join(path, str(dateCode),"Reprojected_LST_Day_1km.tif")):
outputFilename = os.path.join(path, str(dateCode),"LST_Day_1km.map")
#GeoTiff to PCRaster map
translate_tif2map(filename, outputFilename)
#Location of MOD13A1 in GeoTiff format
for filename in glob.glob(os.path.join(path, str(dateCode),'NDVI*.tif')):
b = filename.index('_') # Index number before the date difference
a= filename.index('.') # Index number after date difference
dateDiff= filename[b+1:a]
# Define the output file name using the date difference with LST date
outputName = "ReprojectedNDVI_%s.tif" % dateDiff

# define output filename directory path
outputFilename = os.path.join(path,str(dateCode),outputName)
reproject_sin2utm(filename,outputFilename) # reprojection from sinsodial to UTM in GTIFF format for MOD09A1
for filename in glob.glob(os.path.join(path, str(dateCode),'ReprojectedNDVI*.tif')):
b = filename.index('_') # Index number before the date difference
a= filename.index('.') # Index number after date difference
dateDiff= filename[b+1:a]
outputName = "NDVI_%s.map" % dateDiff
outputFilename = os.path.join(path,str(dateCode),outputName)
#GeoTiff to PCRaster map
translate_tif2map(filename, outputFilename)
# Land surface correction and resampling
for filename in glob.glob(os.path.join(path, str(dateCode),'LST_Day_1km.map')):
scale = 0.02 # The scale factor for MOD11A1
outputName = "Corrected_LST.map"
outputFilename = os.path.join(path,str(dateCode),outputName)
LSTCorrected = ScaleCorrection(filename, scale)
# The new corrected LST map
pcr.report(LSTCorrected,outputFilename)
for filename in glob.glob(os.path.join(path, str(dateCode),'Corrected_LST.map')):
outputName = "Resampled_LST.map"
outputfileName = os.path.join(path,str(dateCode),outputName)
# resmapling to 1000 meters
resample_1000(filename,outputfileName, clone)
outputName = "Tanacovered_LST.map"
outputFilename_covered = os.path.join(path,str(dateCode),outputName)
studyarea(outputFilename_covered,outputName)
for filename in glob.glob(os.path.join(path, str(dateCode),"NDVI_*.map")):

scale = 0.0001# The scale factor for MOD11A1
NDVICorrected = ScaleCorrection(filename, scale)
b = filename.index('_') # Index number before the date difference
a= filename.index('.') # Index number after date difference
dateDiff= filename[b+1:a]
outputName = "Corrected_NDVI_%s.map" % dateDiff
outputfileName = os.path.join(path,str(dateCode),outputName)
pcr.report(NDVICorrected,outputfileName)# The new corrected NDVI map
for filename in glob.glob(os.path.join(path, str(dateCode),'Corrected_NDVI_*.map')):
outputName = "Resampled_NDVI_%s.map" %dateDiff
```

```
outputfileName = os.path.join(path,str(dateCode),outputName)
# resmapling to 1000 meters
resample_1000(filename,outputfileName, clone)
outputName = "Tanacovered_NDVI_%s.map" % dateDiff
outputFilename_covered = os.path.join(path,str(dateCode),outputName)
studyarea(outputFilename_covered,outputName)
for filename in glob.glob(os.path.join(path, str(dateCode),'Tanacovered_NDVI_*.map')):
pcr.setclone(filename)
NDVI = pcr.readmap(filename)
NDVICorrectedMap = pcr.ifthenelse(pcr.pcrle(NDVI,pcr.scalar(0.01)),pcr.scalar(0.01),NDVI)
outputName = "Tanacovered_NDVI_%s.map" % dateDiff
outputFilename_covered = os.path.join(path,str(dateCode),outputName)
pcr.report(NDVICorrectedMap, outputFilename_covered)
outputName = "VegetationCover_%s.map" % dateDiff
outputFilename = os.path.join(path,str(dateCode),outputName)
FractionCover = VegetationCover(outputFilename_covered)
pcr.report(FractionCover,outputFilename)
pcr.setclone(outputFilename)

fractionCover =os.path.join(path,str(dateCode),outputName)
BroadbandEmissivity = emissivity(fractionCover)
outputName = "Broadband_surfaceEmissivity_%s.map" %dateDiff
outputFilename = os.path.join(path,str(dateCode),outputName)# output directory
pcr.report(BroadbandEmissivity, outputFilename)
# reflectance correction and resampling
for filename in glob.glob(os.path.join(path, str(dateCode),'sur_refl_b0*.map')):
dateDiff = filename[-5]
bandNumber = filename[-7]
scale = 0.0001
ReflectanceCorrected = ScaleCorrection(filename, scale)
outputName = "Corrected_sur_refl_b0%s_%s.map" %(bandNumber, dateDiff)
outputfileName = os.path.join(path,str(dateCode),outputName)
pcr.report(ReflectanceCorrected,outputfileName)
dateDiffList = [ ]
dateDiffset = [ ]
for filename in glob.glob(os.path.join(path, str(dateCode),'Corrected_sur_refl_b0*.map')):
print filename
dateDiff = filename[-5]
dateDiffList.append(int(dateDiff))
bandNumber = filename[-7]
outputName = "Resampled_sur_refl_b0%s_%s.map" %(bandNumber,dateDiff)
outputfileName = os.path.join(path,str(dateCode),outputName)
print outputfileName
# resmapling to 1000 meters
resample_1000(filename,outputfileName, clone)
dateDiffset = set(dateDiffList)
print dateDiffset

# Broadband albedo calculation
for dateDiff in dateDiffset:
print dateDiff
band = [ ]
for filename in glob.glob(os.path.join(path, str(dateCode),'Resampled_sur_refl_b0*.map')):
pcr.setclone(filename)
diff = int(filename[-5])
```

```
if dateDiff == diff:
bandNumber = filename
band.append(bandNumber)
BroadbandAlbedo = broadbandalbedo(band)
outputName = "Broadband_albedo_%s.map" %dateDiff
outputFilename = os.path.join(path,str(dateCode),outputName)# output directory
pcr.report(BroadbandAlbedo, outputFilename)
outputName = "Gabaycovered_Broadband_albedo_%s.map" %dateDiff
outputFilename_covered = os.path.join(path,str(dateCode),outputName)
studyarea(outputFilename_covered,outputName)
```

Appendix 2: Python script for running the SEBS model

```
#!/usr/bin/env python
# -*- coding: latin-1 -*-
from PCRaster import *
from time import *
import string
# General functions
def assertWithinRange(map, Lower, Upper):
  """ Checks the range of maps
  map Input PCRaster map"""
  Minimum = cellvalue(mapminimum(map), 0, 0)
  Maximum = cellvalue(mapmaximum(map), 0, 0)
  assert Minimum[0] >= Lower and Maximum[0] <= Upper
def writeVar(varName, varContent):
  """Writes the value of a variable to a file
  varName string name of variable
  varContent value of variable"""
    varContent = str(varContent)
  checkFile.write(varName+" = "+varContent+"\n")
  return
def writeLoc(varName, map):
  """Writes values of a variable at a specific location to a file
  varName string name of variable
  map name of map"""
     findLoc = cellvalue(map, rowy, colx)
  map = findLoc[0]
  writeVar(varName, map)
  return
def median(map):
  """Function to calculate median of a map
  map Input PCRaster map"""
  OrderMap = order(map)
  Mid = roundoff(mean(OrderMap))
  MidMap = ifthenelse(OrderMap == Mid, map, 0)
  Median = cellvalue(mapmaximum(MidMap), 0, 0)
  assert Median[0] > 0.0
  return Median[0]
def mean(map):
  """Calculates the mean value of a PCRaster map
  map Input PCRaster map"""

  Total = cellvalue(maptotal(map), 0, 0)
  NumCells = cellvalue(maparea(map) / cellarea(), 0, 0)
  assert NumCells[0] != 0
  mean = Total[0] / NumCells[0]
  return mean

# SEBS functions
def Rswd(DEM, Lat, Trans, DOY, Time):
  """ Potential Radiation Equator model
  (c) O. van Dam, UU, Tropenbos-Guyana
  Version 5, June 2000
  NOTE: Copyright: This program is free to use provided·
       you refer to the manualfor citation.
```

```
    Do not distribute without prior approval of the author.
    Manual and additional info: O.vanDam@geog.uu.nl

  -------------------------------------------------------
              Model for calculation
           incoming potential light energy
  -------------------------------------------------------
    DEM Input Digital Elevation Model (spatial)
  Lat Latitude in decimal degrees (non-spatial)
  Trans Transmissivity tau (Gates, 1980) (non-spatial)
  DOY Day of Year (non-spatial)
  Time Time in hours (non-spatial)"""
     # constants
  pi      = 3.1415         # pi
  Sc      = 1367.0         # Solar constant (Gates, 1980) [W/m2]

  SlopMap = scalar(atan(slope(DEM)))
  AspMap  = scalar(aspect(DEM)) # aspect [deg]
  AtmPcor = ((288.0-0.0065*DEM)/288.0)**5.256 # atmospheric pressure correction [-]
  # Solar geometry
  # ----------------------------
  # SolDec  :declination sun per day  between +23 & -23 [deg]
  # HourAng :hour angle [-] of sun during day
  # SolAlt  :solar altitude [deg], height of sun above horizon
  SolDec  = -23.4*cos(360.0*(DOY+10.0)/365.0)
  HourAng = 15.0*(Time-12.01)
  SolAlt  = scalar(asin(scalar(sin(Lat)*sin(SolDec)+cos(Lat)*cos(SolDec)*cos(HourAng))))
  # Solar azimuth
  # ----------------------------
  # SolAzi  :angle solar beams to N-S axes earth [deg]
  SolAzi = scalar(acos((sin(SolDec)*cos(Lat)-cos(SolDec)*sin(Lat)*cos(HourAng))/cos(SolAlt)))
  SolAzi = ifthenelse(Time <= 12.0, SolAzi, 360.0 - SolAzi)
  # Additonal extra correction by R.Sluiter, Aug '99
  SolAzi = ifthenelse(SolAzi > 89.994 and SolAzi < 90.0, 90.0, SolAzi)
  SolAzi = ifthenelse(SolAzi > 269.994 and SolAzi < 270.0, 270.0, SolAzi)
  # Surface azimuth
  # ----------------------------
  # cosIncident :cosine of angle of incident; angle solar beams to angle surface
  cosIncident = sin(SolAlt)*cos(SlopMap)+cos(SolAlt)*sin(SlopMap)*cos(SolAzi-AspMap)

  # Critical angle sun
  # ----------------------------
  # HoriAng  :tan maximum angle over DEM in direction sun, 0 if negÂ·
  # CritSun  :tan of maximum angle in direction solar beams
  # Shade    :cell in sun 1, in shade 0
  HoriAng   = horizontan(DEM,directional(SolAzi))
  HoriAng   = ifthenelse(HoriAng < 0.0, scalar(0.0), HoriAng)
  CritSun   = ifthenelse(SolAlt > 90.0, scalar(0.0), scalar(atan(HoriAng)))
  Shade   = ifthenelse(SolAlt > CritSun, scalar(1), scalar(0))
    # Radiation outer atmosphere
  # ----------------------------
  OpCorr = Trans**((sqrt(1229.0+(614.0*sin(SolAlt))**2.0)-614.0*sin(SolAlt))*AtmPcor)     # correction for air
masses [-]Â·
  Sout   = Sc*(1.0+0.034*cos(360.0*DOY/365.0)) # radiation outer atmosphere [W/m2]
  Snor   = Sout*OpCorr                  # rad on surface normal to the beam [W/m2]
```

```
  # Radiation at DEM
  # ----------------------------
  # Sdir   :direct sunlight on a horizontal surface [W/m2] if no shade
  # Sdiff  :diffuse light [W/m2] for shade and no shade
  # Stot   :total incomming light Sdir+Sdiff [W/m2] at Hour
  # PotRad :avg of Stot(Hour) and Stot(Hour-HourStep)
  Sdir   = ifthenelse(Snor*cosIncident*Shade < 0.0, 0.0, Snor*cosIncident*Shade)
  Sdiff  = ifthenelse(Sout*(0.271-0.294*OpCorr)*sin(SolAlt) < 0.0, 0.0, Sout*(0.271-0.294*OpCorr)*sin(SolAlt))
  #Rswd  = Sdir + Sdiff                                  # Rad [W/m2]
  Rswd = Snor
  return Rswd
def LAINDVI(NDVI):
  """ Calculates initial Leaf Area Index from NDVI (Su, 1996). Output is non-spatial
    NDVI Input Normalized Difference Vegetation Index Map (scalar, ratio between 0 and 1)"""
  nd_max = cellvalue(mapmaximum(NDVI), 0, 0)
  nd_min = cellvalue(mapminimum(NDVI), 0, 0)
  nd_mid = median(NDVI)
  nd_df = nd_max[0] - nd_min[0]
  if nd_df == 0.0:
    nd_df == 1.0
  LAI = sqrt(nd_mid * (1.0 + nd_mid) / (1.0E-6 + 1.0 - nd_mid))
  if LAI > 6.0:
    LAI == 6.0
  return LAI, nd_max[0], nd_min[0], nd_mid, nd_df

def u_pbl(LAINDVI,z_pbl,z_ms,u_s):
  """Calculates Planetary Boundary Layer wind speed [m s-1] from NDVI
    NDVI Input PCRaster NDVI map (scalar, ratio between 0 and 1)"""
    nd_mid = LAINDVI[3]
  nd_max = LAINDVI[1]
  nd_min = LAINDVI[2]
  nd_df = LAINDVI[4]
  z0m = 0.005 + 0.5 * (nd_mid/nd_max) ** 2.5   #van der Kwast 2009 (p.103)
  assert z0m >= 0.0
  fc = ((nd_mid - nd_min) / nd_df) ** 2.0    # fractional vegetation cover == Wfol (-)
  assert fc >= 0.0
  h = z0m / 0.136                    # total height of vegetation (m)
  d = 2.0/3.0 * h                            # zero plane displacement (m)
  u_c = ln((z_pbl - d) / z0m) / ln((z_ms - d) / z0m)
  u_pbl = u_s * u_c
  return u_pbl, z0m, d, fc, h
# FUNCTIONS FOR DETERMINATION OF ROUGHNESS LENGTH FOR HEAT TRANSFER
def FKB_1(u_zref, zref, h, LAI, Wfol, Ta, pa):
  """Initial determination of roughness length for heat transfer (non-spatial)
  KB-1 function according to Massman, 1999
  Convention of variable names:
  f_z = f(z)
  d2h = d/h
    u_zref Input wind speed at reference height [m s-1]
  zref Input reference height [m]
  h Input canopy height [m]
  LAI Input canopy total Leaf Area Index [-]
  Wfol Input Fractional canopy cover [-]
  Ta Input ambient temperature [degrees Celsius]
```

```
  pa Input ambient air pressure [Pa]"""
  # Constants
  C_d = 0.2   # foliage drag coefficient
  C_t = 0.01  # heat transfer coefficient
  k = 0.41    # Von Karman constant
  Pr = 0.7    # Prandtl number
  hs = 0.009  # height of soil roughness obstacles (0.009-0.024)

  # Calculations
  Wsoil = 1.0 - Wfol
  if Wfol == 0.0: # for bare soil take soil roughness
    h = hs
  assert Wfol >= 0.0 and Wfol <= 1.0 and Wsoil >= 0.0 and Wsoil <= 1.0
  z0 = 0.136 * h   # Brutsaert (1982)
  u_h0 = u_zref * ln(2.446) / ln ((zref - 0.667 * h) / z0) # wind speed at canopy height -u(h)
  u_h0 = cellvalue(u_h0, 0, 0)
  u_h0 = u_h0[0]
  assert u_h0 >= 0.0
  # -ve sign missed
  ust2u_h = 0.32 - 0.264/exp(15.1 * C_d * LAI) # Su et al 2001(p.4)
  #ust2u_h = 0.32 - 0.264/exp(15.1 * C_d * LAI)
  ustarh = ust2u_h * u_h0
  #nu0 = 1.327E-5 * (101325.0 / pa) * (Ta / 273.15 + 1.0) ** 1.81 # kinematic viscosity van der Kwast 2009 (p.102)
  # 1 cancelled based on van der kwast(2009)
  nu0 = 1.327E-5 * (101325.0/ pa) * (Ta / 273.15) ** 1.81
  n_h = C_d * LAI / (2.0 * ust2u_h ** 2.0) # within canopy wind speed extension van der Kwast 2009 (p.103)
  # First term
  if n_h <> 0.0:
    F1st = (k * C_d / (4.0 * C_t * ust2u_h * (1.0 - exp(pcrumin(n_h)/2.0)))) * Wfol ** 2.0 # van der Kwast 2009
(p.102)
  else:
    F1st = 0.0
  # Second term
  S2nd = k * ust2u_h * 0.136 * Pr ** (2.0/3.0) * sqrt(ustarh * h / nu0) * Wfol ** 2.0 * Wsoil ** 2.0 # multiply by 2
# van der Kwast 2009 (p.102)
  # Third term
  T3rd = (2.46 * (u_zref * k / ln(zref/hs) * hs / nu0) ** 0.25 - ln(7.4)) * Wsoil ** 2.0 # van der Kwast 2009 (p.102)

  return F1st + S2nd + T3rd

def z0h(KB_1, z0m):
  """Calculates the scalar roughness height for heat transfer (z0h)
  KB_1 Input KB_1 values
  z0m Input scalar roughness height for momentum"""
    z0h = z0m / exp(KB_1)
  return z0h
def GKB_1(u_zref, zref, h, LAI, Wfol, Ta, pa):
  """Same as FKB_1, but then for spatial in- and output"""
    # Constants
  C_d = 0.2   # foliage drag coefficient
  C_t = 0.05  # heat transfer coefficient
  k = 0.41    # Von Karman constant
  Pr = 0.7    # Prandtl number
  hs = 0.009  # height of soil roughness obstacles (0.009-0.024)
    # Calculations
```

```
  Wsoil = 1.0 - Wfol
  h = ifthenelse(Wfol == 0.0, hs, h)
    z0 = 0.136 * h   # Brutsaert (1982)
  u_h0 = u_zref * ln(2.446) / ln ((zref - 0.667 * h)/z0) # wind speed at canopy height
  ust2u_h = 0.32 - 0.264 / exp(15.1 * C_d * LAI) # friction velocity t
  #ust2u_h = 0.32 - 0.264 / exp(15.1 * C_d * LAI)
  ustarh = ust2u_h * u_h0
  # 1 cancelled update 23-05-12
  #nu0 = 1.327E-5 * (101325.0/pa) * (Ta / 273.15 + 1.0) ** 1.81 # kinematic viscosity
  nu0 = 1.327E-5 * (p_s/pa) * (Ta / 273.15) ** 1.81 # van der Kwast 2009 (p.102)
  n_h = C_d * LAI / (2.0 * ust2u_h ** 2.0)
  # First term
  F1st = ifthenelse(pcrne(n_h, 0.0), k * C_d / (4.0 * C_t * ust2u_h * (1.0 - exp(pcrumin(n_h)/2.0))) * Wfol ** 2.0,
0.0)
  # Second term
  S2nd =  k * ust2u_h * 0.136 * Pr ** (2.0/3.0) * sqrt(ustarh * h / nu0) * Wfol ** 2.0 * Wsoil ** 2.0
  # Third term
  T3rd = (2.46 * (u_zref * k / ln(zref/hs) * hs / nu0) ** 0.25 - ln(7.4)) * Wsoil ** 2.0

  return F1st + S2nd + T3rd
def Rn(Alfa, Rswd, Eair, t_s, ems, T):
#def Rn(Alfa, Rswd, Eair, t_s, Eground):
  """ Calculation of surface net radiation [W m-2]
  Alfa Input albedo map [-]
  Rswd Input downward solar radiation [W m-2], PCRaster map from POTRAD
  Eair Input emissivity air [-]
  Eground Input PCRaster emissivity map [-]
  t_s Input PBL temperature map [K]..see Brutsaret 1975
  T Surface Kinetic Temperature [K]"""
    print "Calculating Net Radiation map..."
  # constants
  sigma = 5.678E-8   #Stefan Boltzmann's constant (W m-2 K-4)
    # calculations of net available energy- update 21-05-12
  Rn = (1.0 - Alfa) * Rswd + 5.678 * ems * (Eair * (t_pbl/100.0)**4.0 - (T/100.0)**4.0)
  #Rn = (1.0 - Alfa) * Rswd + sigma * (Eair * t_pbl **4.0 - ems* T **4.0) # atmospheric emissivity (Brutsaret,
1975)+ van der Kwast(2009) p-88
  return Rn
def G0(Rn, cover):
  """Calculates Soil Heat Flux [W m-2]
  Rn Input Surface Net Radiation [W m-2]
  cover Input fractional canopy cover [-]"""
    print "Calculating soil heat flux map..."
  # constants:
  Gamma_c = 0.05   # ratio of G0 to Rn for full vegetation canopy (Monteith, 1973)
  Gamma_s = 0.315  # ratio of G0 to Rn for bare soil (Kustas & Daughtry, 1989)
    # calculation
  G0 = Rn * (Gamma_c + (1.0 - cover) * (Gamma_s - Gamma_c))
  return G0
def FRUstar(z_pbl,hst):
  """Iteration to calculate RUstar
  z_pbl Input PBL depth [m]
  hst Input height of the ASL [m]"""
    print "Starting iterations to derive stability parameters..."
    RUstar = ku / zdm
  RH = CH * RUstar / zdh
```

```
    RH0 = RH
    Reps = 10.0
    Isteps = 0
    RHA = RH
    RHB = RH
    RH0A = RH0
    RH0B = RH0
    RUstarA = RUstar
    RUstarB = RUstar
    IstepsA = Isteps
    IstepsB = Isteps
    RepsA = Reps
    RepsB = Reps
    itNr = 100.0
    itThreshold = 0.01
        while RepsA > itThreshold and IstepsA < itNr:
      RLA = CL * RUstarA ** 3.0 / RHA
      tempBw = Bw(z_pbl, RLA, z0m)
      RUstarA = ku / (zdm - tempBw)
      tempCw = Cw(z_pbl, RLA, z0m, z0h)
      RHA = CH * RUstarA / (zdh - tempCw)
      RepsA = mapmaximum(abs(RH0A - RHA))
      difa = abs(RH0A - RHA)
      min = mapminimum(difa)
      meandif = mean(difa)
      RH0A = RHA
      IstepsA = IstepsA + 1
      percentage = (IstepsA/itNr)*100
      print "Iteration A:", int(percentage), "% completed\r",
    print
      while RepsB > itThreshold and IstepsB < itNr:
      RLB = CL * RUstarB ** 3.0 / RHB
      tempPSIm_y1 = PSIm_y(zd0/ RLB)
      tempPSIm_y2 = PSIm_y(z0m / RLB)
      RUstarB = ku / (zdm - tempPSIm_y1 + tempPSIm_y2)
      tempPSIh_y1 = PSIh_y(zd0 / RLB)
      tempPSIh_y2 = PSIh_y(z0h / RLB)
      RHB = CH * RUstarB / (zdh - tempPSIh_y1 + tempPSIh_y2)
      RepsB = mapmaximum(abs(RH0B - RHB))
      difb = abs(RH0B - RHB)
      meandif = mean(difb)
      min = mapminimum(difb)
      RH0B = RHB
      IstepsB =  IstepsB + 1
      percentage = (IstepsB/itNr)*100
      print "Iteration B:", int(percentage), "% completed\r",
    print
    RUstar = ifthenelse(z_pbl >= hst, RUstarA, RUstarB)
    RL = ifthenelse(z_pbl >= hst, RLA, RLB)
    dif = ifthenelse(z_pbl >= hst, difa, difb)
    return RUstar, RL
# MOS STABILITY CORRECTION FUNCTIONS
def PSIma(f, g):
    a = 0.33
    b = 0.41
```

```
  pi = 3.141592654
  tangens = scalar(atan((2.0 * g - 1.0) / sqrt(3.0))) * pi /180
  tangens = ifthenelse(tangens > pi/2.0, tangens - 2.0 * pi, tangens)
  PSIma = ln(a + f) - 3.0 * b * f ** (1.0 / 3.0) + b * a ** (1.0 / 3.0) / 2.0 * ln((1 + g) ** 2.0 / (1.0 - g + sqr(g))) +
sqrt(3.0) * b * a ** (1.0 / 3.0) * tangens
  return PSIma
  def PSIm_y(Y):
  # Integrated stability correction function for momentum
  # Inputs
  # Y = -z/L, where z is the height, L the Obukhov length
  # test values
    # Constants (Brutsaert, 1999)
  a = 0.33
  b = 0.41
  m = 1.0
  pi= 3.141592654
    # Calculation
  #//HK 040902
  Y = abs(Y) #abs(Y)
  x = (Y/a) ** (1.0/3.0)
  PSI0 = pcrumin(ln(a)) + sqrt(3.0) * b * a ** (1.0 / 3.0) * pi / 6.0
  b_3 = b ** -3.0
  PSIm_y = ifthenelse(Y <= b_3, PSIma(Y, x) + PSI0, PSIma(b_3, ((b_3/a)**(1.0/3.0))) + PSI0)
  #PSIm_y = ifthenelse(Y <= b_3, PSIma(Y, x) + PSI0, (1.0 / (PSIma(b_3, ((b_3/a)**(1.0/3.0))))) + PSI0)
  return PSIm_y
 def PSIh_y(Y):
  # Integrated stability correction function for heat
  # Inputs
  # Y = -z/L, z is the height, L the Obukhov length
  # constants (Brutsaert, 1999)
  c = 0.33
  d = 0.057
  n = 0.78
  # Calculation
  Y =  abs(Y)
  PSIh_y = (1.0 - d) / n * ln((c + Y ** n) / c)
  return PSIh_y
# BAS STABILITY CORRECTION FUNCTIONS
def Bw(hi, L, z0):
  # constants (Brutsaert, 1999)
  alfa = 0.12
  beta = 125.0
    # calculations
  B0 = (alfa / beta) * hi
  B1 = -1.0 *z0 / L
  B11 = -alfa * hi / L
  B21 = hi / (beta * z0)
  B22 = -beta * z0 / L
  tempB11 = PSIm_y(B11)
  tempB1 = PSIm_y(B1)
  B = ifthenelse(z0 < B0, -1.0 * ln(alfa) + PSIm_y(B11) - PSIm_y(B1), ln(B21) + PSIm_y(B22) - PSIm_y(B1)) #
possibility 1
  Bw = ifthenelse(B < 0.0, 0.0, B) # This results from unfortunate parameter combination!
  return Bw
```

```
def Cw(hi, L, z0, z0h):
  alfa = 0.12
  beta = 125.0
  C0 = (alfa / beta) * hi
  C1 = pcrumin(z0h) / L
  C11 = -alfa * hi / L
  C21 = hi / (beta * z0)
  C22 = -beta * z0 / L
  C = ifthenelse(z0 < C0, pcrumin(ln(alfa)) + PSIh_y(C11) - PSIh_y(C1), ln(C21) + PSIh_y(C22) - PSIh_y(C1))
  Cw = ifthenelse(C < 0.0, 0.0, C) # This results from unfortunate parameter combination!
  return Cw
def esat(t):
  """Calculation of saturated vapour pressure [Pa]
    t Input temperature in degrees Celsius"""
  # constants
  e0 = 611.0  # saturated water vapour pressure at 273.15K
  A = 17.27 # 7.5 changed to 17.27
  B = 237.3
    # Calculation
  esat = e0 * exp((A * t) / (B + t))
  return esat
#---------------------------------------------------------------------------
# INPUT
# Validation pixel
#rowy = 0                                    # row number of validation pixel
#colx = 0                                    # column number of validation pixel
#checkFile = file("check.txt", "w")  # name of validation textfile
# Define inputs
# maps
DEM = readmap('dem.map')          # Digital Elevation Model [m]
nd = readmap('ndvi.map') # NDVI map [-]
T = readmap('tkin.map') # Surface temperature [Kelvin]
albedo = readmap('albedo.map') # Albedo map [-]
ems = readmap('emissivity.map') # emissivity [-]
# parameters
Trans = readmap("transmissivity.map")
Lat = 11.6
DOY = 98.0
Time = 10.92
z_pbl = 1000.00
alt_ms = 2.0
ht_c = readmap("height.map")
u_s = readmap("windspeed.map")
t_s = readmap("temperature.map")
p_s = readmap("pressure.map")
hr_s = readmap("rh.map")
z_ms = alt_ms
print "Initializing SEBS.",
# Initialize model starttime for calculation runtime
starttime = time()
# Check input data
nd = ifthenelse(pcror(pcrlt(nd,0.0),pcrgt(nd,1.0)), 1.0, nd) # Convert waterbodies to 1.0 --> soilflux is minimal
assertWithinRange(nd, 0.0, 1.0)
assert cellvalue(mapminimum(DEM), 0, 0) >= 0.0
assert cellvalue(mapminimum(T), 0, 0) >= 0.0
```

```
assert DOY >= 0.0 and DOY <= 366
assert Time >= 0.0 and Time <= 24.0
assert alt_ms >= 0.0
assert cellvalue(mapminimum(u_s), 0, 0) >= 0.0
#assert cellvalue(mapminimum(hr_s), 0, 0) >= 0.0 and cellvalue(mapmaximum(hr_s), 0, 0) <= 1.0
assert z_pbl >= 0.0
albedo = ifthenelse(pcror(pcrlt(albedo,0.0),pcrgt(albedo,1.0)), 0.0, albedo)
assertWithinRange(albedo, 0.0, 1.0)
ems = ifthenelse(pcror(pcrlt(ems,0.0), pcrgt(ems,1.0)), 0.0, ems)
assertWithinRange(ems, 0.0, 1.0)
print "\b.",
# INITIALIZE MODEL
# Calculating initial LAI
LAINDVI = LAINDVI(nd)
LAI = LAINDVI[0]
assert(LAI >= 0.0 and LAI <= 6.0)
print "\b.",
report(LAI, "LAI_I.map")
nd_max = LAINDVI[1]
nd_min = LAINDVI[2]
nd_mid = LAINDVI[3]
nd_df = LAINDVI[4]
print "\b.",
# Calculate initial PBL parameters
Fu_pbl = u_pbl(LAINDVI,z_pbl,z_ms,u_s)
u_pbl = Fu_pbl[0]
#u_pbl = cellvalue(u_pbl, 1, 1)
#u_pbl = u_pbl[0]
assert cellvalue(mapminimum(u_pbl), 0, 0) >= 0.0
report(u_pbl, "u_pbl.map")
print "\b.",
z0m = Fu_pbl[1]
d = Fu_pbl[2]
fc = Fu_pbl[3]
h = Fu_pbl[4]
# Calculating initial KB-1 and z0h
avu_pbl = mean(u_pbl)
KB_1 = FKB_1(avu_pbl, z_pbl, mean(ht_c), LAI, fc, mean(t_s), mean(p_s))
report(KB_1,"kb1.map")
KB_1 = cellvalue(KB_1, 0, 0)
KB_1 = KB_1[0]
print "\b.",
z0h = cellvalue(z0h(KB_1, z0m), 0, 0)
z0h = z0h[0]
print "\b."
# Calculating initial temperatures and pressures"
t_c = ln((z_pbl - d) / z0h) / ln((alt_ms - d) / z0h)
t_s = t_s + 273.15 # reference height temperature in degree Kelvin
report(t_s, "t_s.map")
t_pbl_A = T * (1.0 - t_c) + t_s * t_c # look for the source
report(t_pbl_A, "t_pbl_A.map")
p_s_A = p_s
z_pbl_A = z_pbl
p_pbl_A = 101325 * ((293 - 0.0065*(DEM + z_pbl_A)) / 293) ** 5.26
T0 = T
```

```
T_0pbl = 0.5 * (T0 + t_pbl_A)   # mean  temperature
Tcn = T_0pbl - 273.15    # mean PBL temperature converted to degrees Celcius
report(Tcn,"tcn1.map")
esat = 611.0 * exp(17.27 * Tcn / (Tcn + 237.3)) # saturated vapor pressure
report(esat, "esat.map")
hr_pbl = hr_s # relative humidity fraction
eact = hr_pbl * mean(esat) # actual vapour pressure ## taking the average value of esat affect the calculation
report(eact,"eact.map")
q_pbl_A = (5.0 / 8.0) * (eact / p_pbl_A) # mean specific humidity at PBL
z_pbl = z_pbl_A
ps = p_s_A
Ta = T_0pbl - 273.15
t_pbl = t_pbl_A
# LAI based on van der Kwast (2009)
LAI = sqrt(nd * (1.0 + nd)/ (1.0 - nd))
#LAI = sqrt(nd * (1.0 + nd)/ (1.0 + 1.0E-6 - nd))# slightly different from the thesis
report(LAI, "LAI.map")
LAI = ifthenelse(LAI > 6.0, 6.0, LAI)
assertWithinRange(LAI, 0.0, 6.0)
fc = ((nd - nd_min) / nd_df) ** 2.0
report(fc, "fc.map")
assertWithinRange(fc, 0.0, 1.0)
p_pbl = p_pbl_A# pressure at the top of ASL
report(p_pbl, "p.map")
q_pbl = q_pbl_A # averaged specific humidity at top of ASL
z0m = 0.005 + 0.5 * (nd / nd_max) ** 2.5
report(z0m, "z0m.map")
h = z0m / 0.136
report(h, "hc.map")
h = ht_c
z0m = h * 0.136
report(z0m, "z0m_lit.map")
# zero dispalacement height updated 22-05-12
#d = z0m * 4.9
d = (2.0/3.0) * h
KB_1 = GKB_1(u_pbl, z_pbl, h, LAI, fc, Ta, p_pbl)
report(KB_1, "kb_1.map")
z0h = z0m / exp(KB_1)
report(z0h,'z0h.map')
Tsk = T0
Theta_s = T0 *(101325/p_s)**0.286    # potential surface temperature
#Theta_s = T0
report(Theta_s, "t0.map")
#Theta_v = Tsk * (1.0 + 0.61 * q_pbl)          # surface virtual temperature
Theta_v = Theta_s * (1.0 + 0.61 * q_pbl)
Theta_a = t_pbl * (p_s/p_pbl)**0.286  # sea level pressure overestimate the value
#Theta_a = t_pbl * (101325/p_pbl) ** 0.286
report(Theta_a, "theta.map")
T0ta = (Theta_s - Theta_a)# potential temperature difference at the surface and top ASL
report(T0ta, "thetadif.map")
Rv = 461.05                                   # specific gas constant water vapour (J kg-1 K-1)
Rd = 287.04                                   # specific gas constant dry air (J kg-1 K-1)
Cp = 1005.0                        # specific heat (J kg-1 K-1)
# eact can be calculated directly check
eact = p_pbl * q_pbl * (Rv / Rd)      # actual vapour pressure
```

```
rhoa = ps / (Rd * Theta_v)              # surface air density (kg m-3)
rhoam = (ps / (Rd * Tsk)) * (1.0 - 0.378 * eact / ps) # moist air density (kg m-3)
report(rhoam,"rhoam.map")
rhoacp = rhoa * Cp                # specific air heat capacity (J K-1 m-3)
report(rhoacp,"rhoacp.map")
alfa = 0.12
beta = 125.0
g = 9.81
k = 0.4
hst = max((alfa * z_pbl), (beta * z0m)) # height of ASL (m)
report(hst, "asl_height.map")
zd0 = z_pbl - d
report(zd0, "zd0.map")
ku = k * u_pbl
report(ku,"ku.map")
zdm = ln(zd0/z0m) # momentum transfer
zdh = ln(zd0/z0h) # heat transfer
CH = T0ta * k * rhoacp
report(CH, "ch.map")
CL = pcrumin(rhoam) * Cp * Theta_v / (k * g) # check this again
report(CL,"cl.map")
# Calculate energy balance
print "Calculating Energy Balance terms..."
Rswd = Rswd(DEM, Lat, Trans, DOY, Time)
report (Rswd, "rswd.map")
Eair = 9.2 * (t_pbl/1000.0) ** 2.0 # Brutsaret(1975)
Rn = Rn(albedo, Rswd, Eair, t_s, ems, T)
report(Rn, "rn.map")
G0 = G0(Rn, fc)
report(G0,"g.map")
R_G = Rn - G0
# Dry-limit heat flux
print "Calculating Dry Limit..."
H_d = R_G
report(H_d, "h_d.map")
FRUstar = FRUstar(z_pbl,  hst)
RUstar = FRUstar[0]
RL = FRUstar[1]
print "Calculating Wet Limit..."
# For completely wet areas
# Wet-limit stability length
L_e = 2.430E+06   # Latent heat of vapourization (J kg-1) (Brutsaert, 1982)
L_w =(RUstar ** 3.0) * rhoam / (0.61 * k * g * R_G / L_e)
C_wet = ifthenelse(z_pbl >= hst, Cw(z_pbl, L_w, z0m, z0h), PSIh_y((z_pbl/L_w)))
# Wet-limit external resistance
re_w = (zdh - C_wet) / (k * RUstar)
report(re_w, "rew.map")
re_w = ifthenelse(re_w <= 0.0, zdh / (k * RUstar), re_w)
# Wet-limit heat flux
slopef = 17.502 * 240.97 * esat / (Ta + 240.97) ** 2.0
# Gamma changed from 67 to 55
gamma = 0.000665 * p_s  # psychrometric constant (Pa 0c-1) Us
report(gamma, "gamma.map")
H_w = (R_G - (rhoacp / re_w) * ((esat - eact) / gamma)) / (1.0 + slopef / gamma)
report(H_w, "H_w.map")
```

```
#H_w = ifthenelse(H_w >= 230.0,230,H_w)
#H_w = ifthenelse(H_w < 0,0, H_w)
#report(H_w, "hwet.map")
LEwet = Rn - G0 - H_w
report(LEwet, "lewet.map")
# Sensible Heat flux
print "Calculating sensible heat flux..."
C_i = ifthenelse(z_pbl >= hst, Cw(z_pbl, RL, z0m, z0h), PSIh_y(pcrumin(z_pbl)/RL))
# external resistance
re_i = (zdh - C_i) / (k * RUstar)
report (re_i, "re_i.map")
H_i = rhoacp * T0ta / re_i ### check from here it is low
report(H_i, "h_i.map")
H_i = ifthenelse(H_i > H_d, H_d, H_i)
report(H_i, "h_id.map")
H_i = ifthenelse(H_i < H_w, H_w, H_i)
report(H_i, "h.map")
# Calculate evaporation variables
print "Calculating relative evaporation and evaporative fraction..."
# Calculate relative evaporation
ev_r = 1.0 - (H_i - H_w) / (H_d - H_w) # set water and wet surfaces to 1.0
report(ev_r, "evapr.map")
# Calculate evaporative fraction
Evapfr = ev_r * (1.0 - H_w / H_d)
report(Evapfr, "evapfr.map")

# Calculate latent energy flux
print "Calculating Latent Energy Flux..."
labdaE = Evapfr * (Rn - G0)
labdaE2 = Rn - G0 - H_i
report(labdaE2, "le1.map")
#assert(labdaE == labdaE2) # Check on closure of energy balance components!
report(labdaE, "le.map")

# Calculate evapotranspiration flux
print "Calculating Evapotranspiration Flux..."
rhow = 998.0 # density of water [kg m-3]
E = labdaE / (L_e * rhow) #[m/s]
report(E, "etm.map")
Eday = E * 3600.0 *24 * 1000.0 # mm/day for data assimilation with sm model
report(Eday, "et.map")
#checkFile.close( )
endtime = time( )
deltaTime = endtime - starttime
print
print "================================================="
print "The model has been running for %5.2f seconds." % deltaTime
print
print "Credits:"
print "Bob Su (ITC)"
print "Ambro Gieske (ITC)"
print "Wim Timmermans (ITC)"
print "Victor Jetten (UU)"
print "Steven de Jong (UU)"
print "Li Jia (WUR)"
print "Kor de Jong (UU)"
```

Appendix 3: Weather Generator Parameter

Weather generator (WGEN) parameters used by SWAT model

Legend of the parameters used in the weather generators	
Symbol	Descriptions
TMPMX	Average or mean daily maximum air temperature for month (ºC).
TMPMN	Average or mean daily minimum air temperature for month (ºC).
TMPSTDMX	Standard deviation for daily maximum air temperature in month(ºC).
TMPSTDMN	Standard deviation for daily minimum air temperature in month(ºC).
PCPMM	Average or mean total monthly precipitation (mm H2O).
PCPSTD	Standard deviation for daily precipitation in month (mm H2O/day).
PCPSKW	Skew coefficient for daily precipitation in month.
PR_W1	Probability of a wet day following a dry day in the month.
PR_W2	Probability of a wet day following a wet day in the month.
PCPD	Average number of days of precipitation in month.
RAINHHMX	Monthly maximum half-hour Rain
SOLARAV	Average daily solar radiation for month (MJ/m2/day).
DEWPT	Average daily dew point temperature in month (ºC).
WNDAV	Average daily wind speed in month (m/s).